UNCLASSIFIED

SECURITY CLASSIFICATION OF THIS PAGE

REPORT DOCUMENTATION PAGE

1a. REPORT SECURITY CLASSIFICATION Unclassified	1b. RESTRICTIVE MARKINGS None
2a. SECURITY CLASSIFICATION AUTHORITY	3. DISTRIBUTION/AVAILABILITY OF REPORT Approved for public release; distribution is unlimited.
2b. DECLASSIFICATION/DOWNGRADING SCHEDULE	
4. PERFORMING ORGANIZATION REPORT NUMBER(S) NORDA Report 108	5. MONITORING ORGANIZATION REPORT NUMBER(S) NORDA Report 108
6. NAME OF PERFORMING ORGANIZATION Naval Ocean Research and Development Activity	7a. NAME OF MONITORING ORGANIZATION Naval Ocean Research and Development Activity
6c. ADDRESS *(City, State, and ZIP Code)* Ocean Science Directorate NSTL, Mississippi 39529-5004	7b. ADDRESS *(City, State, and ZIP Code)* Ocean Science Directorate NSTL, Mississippi 39529-5004
8a. NAME OF FUNDING/SPONSORING ORGANIZATION Naval Ocean Research and Development Activity 8b. OFFICE SYMBOL *(If applicable)*	9. PROCUREMENT INSTRUMENT IDENTIFICATION NUMBER
8c. ADDRESS *(City, State, and ZIP Code)* Ocean Science Directorate NSTL, Mississippi 39529-5004	10. SOURCE OF FUNDING NOS. PROGRAM ELEMENT NO. / PROJECT NO. / TASK NO. / WORK UNIT NO.
11. TITLE *(Include Security Classification)* The NORDA/FNOC Polar Ice Predicton System (PIPS)—Arctic: A Technical Description	
12. PERSONAL AUTHOR(S) Ruth Preller	
13a. TYPE OF REPORT Final	13b. TIME COVERED From _____ To _____
14. DATE OF REPORT *(Yr., Mo., Day)* May 1985	15. PAGE COUNT 63
16. SUPPLEMENTARY NOTATION	
17. COSATI CODES FIELD / GROUP / SUB. GR.	18. SUBJECT TERMS *(Continue on reverse if necessary and identify by block number)* sea ice, atmospheric prediction, environmental parameters

19. ABSTRACT *(Continue on reverse if necessary and identify by block number)*

The hydrodynamic/thermodynamic sea ice model designed by W. D. Hibler of the Cold Regions Research and Engineering Laboratory (CRREL) was modified to run operationally at the Fleet Numerical Oceanography Center (FNOC). Changes were made to adapt the model to the Cyber 205 system and to allow easy interfacing between the model and the data base needed to drive the model, the Navy Operational Global Atmospheric Prediction System (NOGAPS).

The Polar Ice Prediction System (PIPS) contains the most recently updated thermodynamic version of the model. Improved numerics have been included in the model relaxation routine, which increases the model efficiency by a factor of three.

20. DISTRIBUTION/AVAILABILITY OF ABSTRACT UNCLASSIFIED/UNLIMITED ☐ SAME AS RPT. ■ DTIC USERS ☐	21. ABSTRACT SECURITY CLASSIFICATION Unclassified
22a. NAME OF RESPONSIBLE INDIVIDUAL Ruth Preller	22b. TELEPHONE NUMBER *(Include Area Code)* (601) 688-5444 / 22c. OFFICE SYMBOL Code 322

DD FORM 1473, 83 APR EDITION OF 1 JAN 73 IS OBSOLETE.

UNCLASSIFIED

SECURITY CLASSIFICATION OF THIS PAGE

Naval Ocean Research and Development Activity
NSTL, Mississippi 39529 NORDA Report 108 May 1985

The NORDA/FNOC Polar Ice Prediction System (PIPS)—Arctic: A Technical Description

Final Report

Ruth H. Preller
Ocean Sensing and Prediction Division
Ocean Science Directorate

Foreword

The time evolution of environmental parameters in the ocean has an important impact on the performance of weapons systems, acoustic surveillance capabilities, search and rescue planning, and other aspects of Naval Operations. In the Arctic and Antarctic, in particular, the knowledge of ice thickness distribution, concentration, and strength is essential for the operation of ships. Obtaining this information on a daily basis is a virtually impossible task. However, with the use of numerical sea ice models, ice characterstics can be forecast with great accuracy on a daily basis. The Hibler ice model has been adapted by the Naval Ocean Research and Development Activity to run in such a forecast mode at the Fleet Numerical Oceanography Center, predicting ice drift, thickness, concentration, strength, and growth.

R. P. Onorati, Captain, USN
Commanding Officer, NORDA

Executive summary

The hydrodynamic/thermodynamic sea ice model designed by W. D. Hibler of the Cold Regions Research and Engineering Laboratory (CRREL) was modified to run operationally at the Fleet Numerical Oceanography Center (FNOC). Changes were made to adapt the model to the Cyber 205 system and to allow easy interfacing between the model and the data base needed to drive the model, the Navy Operational Global Atmospheric Prediction System (NOGAPS).

The Polar Ice Prediction System (PIPS) contains the most recently updated thermodynamic version of the model. Improved numerics have been included in the model relaxation routine, which increases the model efficiency by a factor of three.

A long-term simulation of the ice model was run using the NOGAPS forcing fields from 18 January 1983 to 18 January 1984. The model was run for three years and used the 1983 data repeatedly. This repetition allows the model to "spin up" from its initial conditions, a 3.3 m thick layer of ice, to an appropriate ice thickness for 1983. Results from the third year of integration are compared to previous model results and observations.

Acknowledgments

This work was supported by the Naval Air Systems Command under program element 63207N, a part of the Automated Environmental Prediction System (AEPS). The author would like to acknowledge valuable assistance provided by Dr. William B. Hibler III (CRREL), Ms. Pam Posey of Berkley Associates, and Dr. Alex Warn-Varnas (NORDA).

The NORDA/FNOC Polar Ice Prediction System (PIPS)—Arctic: A Technical Description

1. Introduction

Previous operational Arctic sea ice forecasts have been produced at Fleet Numerical Oceanography Center (FNOC) using empirical models of interaction between the ocean, sea ice, and winds. The first model used, the Skiles model (Skiles, 1968), related ice drift to geostrophic wind and mean upper ocean currents. The results obtained from this model suggest that a number of errors exist in the code or procedures. Subsequently, the Skiles model was replaced by the Thorndike and Colony (1982) model. This model is a linear free-drift model that has an updated definition for ice drift based on numerous observations of ice drift, geostrophic wind, and mean currents. However, these models have serious deficiencies. They do not take into account the important effects of the ice thickness, concentration, and growth on ice drift. The amount of ice growth or melt and ice strength is greatly dependent upon the thickness and concentration of ice. The new model chosen for Arctic sea ice forecasts, the dynamic/thermodynamic sea ice model developed by W. D. Hibler of Cold Regions Research and Engineering Laboratory (CRREL), couples the ice movement and growth to the ice thickness and concentration. This model is similar to that used by Hibler (1979) with the addition of a thermodynamic treatment similar to that used by Semtner (1976).

The main objective of the Naval Ocean Research and Development Activity's (NORDA) FY 84 Arctic sea ice forecasting effort was to adapt the Hibler ice model for operational use at FNOC. Specifically, the latest version of the model was placed on the Cyber 205 with the most recent improvements to the thermodynamic portion of the model and to the numerics. A full year of Navy Operational Global Atmospheric Prediction System (NOGAPS) analysis fields was obtained and used to drive the model to equilibrium solutions. These solutions were then examined and verified with previous model climatological studies (Hibler 1979, 1980) and data. The new sea ice forecasting system developed by NORDA Code 322 will be referred to as the Polar Ice Prediction System (PIPS). PIPS is a component of the Navy's Automated Environmental Prediction System (AEPS).

2. Model description

The coupled dynamic/thermodynamic sea ice model may be broken down into five main components: the momentum balance, ice rheology, ice thickness distribution, ice strength, and a thermodynamic heat budget. The momentum balance used to describe the ice drift is given by

$$m \frac{D\vec{u}}{Dt} = m f k \times \vec{u} + \vec{\tau}_a + \vec{\tau}_w - mg \, grad \, H + \vec{F} \, ,$$

where m is the ice mass per unit area, $\vec{u}$ is the ice velocity, f is the Coriolis parameter, τ_a and τ_w are the forces due to air and water stresses, g is the acceleration of gravity, H is the sea surface dynamic height, and F is the force due to variation in the internal ice stress. The ice is considered to move in a two-dimensional field with forcing applied through simple planetary boundary layers. In general, the wind stress forcing dominates the ocean current forcing, particularly on a short time scale (days). On the long time scale (annual), ocean currents may be responsible for as much as 25% of the ice drift (Hibler and Tucker, 1979).

The air and water stresses are defined using constant turning angles

$$\tau_a = \varrho_a C_a |\vec{U}_g| (\vec{U}_g \cos\phi + k \times \vec{U}_g \sin\phi)$$

$$\tau_w = \varrho_w C_w |\vec{U}_w - \vec{u}| [(\vec{U}_w - \vec{u}) \cos\theta + k \times (\vec{U}_w - \vec{u}) \sin\theta]$$

where $\vec{u}$ is the ice drift velocity, $\vec{U}_g$ is the geostrophic wind, $\vec{U}_w$ is the geostrophic ocean current, C_a and C_w are the air and water drag coefficients, ϱ_a and ϱ_w are the air and water densities and ϕ and θ are the air and water turning angles. In the PIPS model, surface winds in the form of marine wind fields, A29 and A30, are used so that $\vec{U}_g$ is replaced by $\vec{U}_s$ (the surface or marine winds) and ϕ is set equal to zero. For a more detailed discussion of the dynamical portion of the model and the spatial finite-differencing code, see Hibler (1979).

The ice rheology, a viscous-plastic constitutive law, relates the ice stress to ice deformation and strength with the following equation:

$$\sigma_{ij} = 2\eta\,(\epsilon_{ij}, P)\,\epsilon_{ij} + [\zeta\,(\epsilon_{ij}, P) - \eta\,(\epsilon_{ij}, P)]\,\epsilon_{kk}\,\delta_{ij} - P\delta_{ij}/2,$$

where σ_{ij} is the two-dimensional stress tensor, ϵ_{ij} is the strain tensor, P/2 is a pressure or strength term, and ζ and η are nonlinear bulk and shear viscosities. Ice flows plastically for normal strain rates and deforms in a linear viscous manner for small strain rates.

The ice thickness distribution takes into account the ice thickness evolution as a result of dynamic and thermodynamic effects. The PIPS model uses a two-level approach with ice broken up into two categories, thick and thin; the division between the two is 0.5 m. The compactness, A, is the area within a grid cell covered by thick ice, while $(1-A)$ is the area covered by thin ice.

The thickness and compactness equations are

$$\frac{\partial h}{\partial t} = -\frac{\partial(uh)}{\partial x} - \frac{\partial(vh)}{\partial y} + S_h + diffusion$$

$$\frac{\partial A}{\partial t} = -\frac{\partial(uA)}{\partial x} - \frac{\partial(vA)}{\partial y} + S_A + diffusion\,,$$

where S_h and S_A are thermodynamic terms defined by

$$S_h = f\left(\frac{h}{A}\right)A + (1 - A)\,f\,(0)$$

$$S_A = \begin{cases} \dfrac{f\,(0)}{h_o}\,(1-A) & \text{if } f\,(0) > 0 \\ 0 & \text{if } f\,(0) < 0 \end{cases}$$

$$+ \begin{cases} 0 & \text{if } S_h > 0 \\ \left(\dfrac{A}{2h}\right) S_h & \text{if } S_h < 0 \end{cases}$$

with $f(h)$ as the growth rate of ice of thickness h and h_o a fixed division between thick and thin ice (0.5 m).

The ice strength is treated as a function of the ice thickness distribution and is given by the equation

$$P = P^*\,h\,exp\,[-C(1-A)],$$

where P^* and C are fixed empirical constants, h is the ice thickness and A is the compactness.

The thermodynamic portion of the code specifies the growth and decay rates of ice thickness. Vertical growth rates for each ice category (thick or thin ice) are determined by heat budget considerations at the top and bottom surface of the ice and by adding the heat absorbed by leads via lateral mixing. Similar to the formulation of Semtner (1976), heat is transferred through the ice by assuming a linear temperature profile along with a constant ice conductivity. When open water is losing heat to the atmosphere, the heat budget growth rates are taken to be vertical growth. When open water absorbs heat, the heat mixes underneath the floes to decrease the vertical growth rate. Any remaining heat either causes lateral melting or raises the temperature of the mixed layer. In the presence of an ice cover, the mixed layer temperature is always set equal to freezing. Thus, the excess heat absorbed by the leads is used for lateral melting until the ice disappears. Also, during growth conditions, ice is not allowed to form until the mixed layer reaches the freezing temperature of sea water.

The Hibler model treats the effects of snow cover differently than they are treated in the Semtner (1976) model. Following Bryan et al. (1975) and Manabe et al. (1979), the effects of snow cover are treated in such a way that the ice surface albedo is that of snow when the calculated surface temperature is below freezing and that of snow free ice when the surface temperature is at the melting point. Thus, the upward heat flow, I_h, through ice of thickness h is

$$I_h = (K/h)\,(T_w - T_o)\,,$$

where K is the ice conductivity, T_w is the water temperature and T_o is the surface temperature of the ice.

The surface heat budget, after Parkinson and Washington (1979) and Manabe et al. (1979),is given by

$$(1 - \alpha)\,F_s + F_L + D_1\,|\vec{U}g|\,(T_a - T_o) + D_2\,|\vec{U}g|\,[q_a\,(T_a) - q_s\,(T_o)] - D_3\,T_o^4 + (K/H)\,(T_w - T_o) = 0\,,$$

where α is the surface albedo (0.75 for snow cover or 0.616 for snow-free ice), T_o is the surface temperature of ice, T_a is the air temperature, T_w is the water temperature, $\vec{U}_g$ is the geostrophic wind, q_a is the specific humidity of air, q_s is the specific humidity of the ice surface, F_s is the incoming short wave radiation, F_L is the incoming long wave radiation, D_1 is the bulk sensible heat transfer coefficient, D_2 is the bulk latent heat transfer coefficient (water or ice), and D_3 is the Stephan-Boltzman

constant times the surface emissivity. This surface heat budget defines a surface temperature for the ice, which balances the heat budget. This temperature then determines the conduction of heat through the ice and the growth rate. If the derived temperature is above freezing, it is set back to the freezing point. Surface and bottom ablation rates are then determined by the imbalances in the surface heat budget and by conduction of heat into the mixed layer. Heat transfer from the deep, warmer, ocean water can either be treated as a constant or as a variable heat flux into the mixed layer. For a detailed discussion of the thermodynamic portion of the model and the numerical schemes, see Hibler (1980).

3. The grid

The operational sea ice model was designed to exist on a subsection of the FNOC Northern Hemisphere polar stereographic grid. In the original testing of this model on the Cyber 205 system, a model domain with similar boundaries to those used by Hibler (1979, 1980) was used for comparison. After such comparisons revealed that the model was functioning correctly, a larger domain that included the Barents, Greenland and Norwegian Seas was used. Figure 1 shows the boundaries of both models on the FNOC polar stereographic grid. The ice model grid was designed by determining an average map factor for the model region. This map factor was used to estimate equal grid distances between all FNOC polar stereographic grid points within the ice model domain. The ice model grid was then defined at equally spaced intervals between FNOC polar stereographic grid points. As a result, the ice model dimensions are 47 x 25 with a resolution of 127 km.

All boundaries of the sea ice model are solid except for the Fram Strait in the central Arctic model and the southern boundary of the Greenland and Norwegian Seas (Figs. 2 and 3). These regions contain "outflow" grid cells. Ice can be transferred into these grid cells only by advection and, once there, flows out of the basin.

4. Forcing

Three basic forcing components are necessary to drive the sea ice model: wind stress, geostrophic ocean currents, and atmospheric thermodynamic variables that include deep oceanic heat fluxes used to determine the heat budget. For the PIPS operational model, all forcing fields were obtained from the NOGAPS model, except for the marine winds, geostrophic ocean currents and oceanic heat fluxes. Initially, the geostrophic ocean currents used to drive the ice model were the Skiles currents shown in Figure 4. These currents came from the U. S. Navy Hydrographic Office (1958) and were derived by using a geostrophic approximation based on sparse data gathered over a long period. Though readily available at FNOC, these currents do not agree well with the observed Arctic currents. Inaccuracies exist in the Greenland-Norwegian Seas as well as the Laptev, Kara, and East Siberian Seas. They show no northward-moving Norwegian Current, no southward-moving east Greenland Current, and currents with magnitudes far too large in the Laptev, Kara, and East Siberian Seas. Thus, a new data set of geostrophic ocean currents was obtained from a combined ice-ocean model (Hibler and Bryan, 1984). Twelve monthly mean ocean current fields, as well as an annual average, were made available. Figures 5a-c show the annual mean currents and a representative winter (March) and summer (September) current field. The general circulation depicted by these currents, a large anticyclonic gyre and a cross-polar current, agree with observation. A later section will show the importance of using the correct currents to accurately predict ice edge. For the central Arctic basin, the ocean currents have been shown to be important on long time scales (Thorndike and Colony, 1982) but not on the time scale of a forecast. However, time variability of ocean currents can be important on short time scales (weeks) in regions of the marginal ice zone. Obtaining time-varying currents from observations in this region is virtually an impossible task. At present, an Arctic ocean model that can predict these currents does not exist. For this reason, the PIPS model uses the monthly varying Hibler-Bryan ocean currents.

Winds for the PIPS model are obtained from FNOC marine boundary layer wind fields A29 and A30. These winds, though actually located at 19.5 m height, are used as surface winds in these tests. The Hibler model was originally designed to use geostrophic winds. As a result the model included the appropriate angle to adjust geostrophic winds to surface winds. This turning angle was removed and the drag coefficient increased from 0.0012 (McPhee, 1980) to 0.0027 (McPhee, 1979) to allow for the use of surface winds.

Six additional forcing fields are necessary to drive the thermodynamic portion of the code.

A07—Surface air temperature

A01—Surface pressure

A12—Surface vapor pressure (Fields A01 and A12 are used to calculate specific humidity at the ice surface)

A11—Incoming solar radiation (short wave)

A16—Sensible heat flux

A18—Total heat flux (Fields A11, A16, and A18 are used to determine longwave radiation)

In all of the "spin up" experiments used to test the PIPS model, a time step of 24 hours was used. All input

forcing was updated every 24 hours except for the geostrophic ocean currents and deep ocean heat fluxes, which were updated every month. All FNOC forcing fields are spatially interpolated from the 63 x 63 Northern Hemisphere polar stereographic grid to the PIPS grid. Additional parameters used in all model integrations are given in Table 1.

Table 1. Parameters used in the numerical simulation

Parameter	Definition	Value
C_a	Drag coefficient of air	0.0027
C_w	Drag coefficient of water	0.0055
C	Empirical constant in the strength equation	20
e	Ratio of the principal axis of the elliptic yield equation	2
f	Coriolis parameter	1.46×10^{-4} sec^{-1}
h_0	Thickness limit between thick and thin ice	0.5 m
ϱ_i	Density of ice	0.91×10^3 kg m^{-3}
ϱ_a	Density of air	1.3 kg m^{-3}
P*	Pressure constant	2.75×10^4 N m^{-2}
$\Delta x = \Delta y$	Horizontal grid spacing	127 km
Δt	Time step	1 day
ζmax	Nonlinear bulk viscosity	$(P/4) \times 10^9$ kg s^{-1}
ηMAX	Nonlinear shear viscosity	ζmax/e^2
ϕ	Turning angle of air	0°
θ	Turning angle of water	25°
H_i	Initialization ice thickness	3.3 m

5. Initial conditions

PIPS will contain three methods of initialization. The first method is used for spin up of the model to a cyclic equilibrium state, with thickness, ice growth, and velocity characteristics taking on similar values on corresponding days of successive years. In this case, the ice drift velocities are set equal to zero, while the thickness is defined as a constant value of 3.3 m (3.0×10^3 kg m$^{-2}/\varrho_I$) and the compactness defined as 1.0 at all grid points. From these initial conditions, it takes approximately three years of integration for the model to reach an equilibrium state.

The second method is to initialize from previous model derived fields. To do this, it is necessary to have the ice drift fields, the thickness fields, the concentration fields, the lateral melt, and the ice temperature. For the PIPS model, initialization is done in two ways. The model either initializes from its own forecast fields or, if those are not available, from model-derived monthly mean climatology fields. This climatology is the result of three years of integration using the 1983 NOGAPS atmospheric forcing and the Hibler-Bryan ocean currents and oceanic heat fluxes.

The third method would be to initialize the model by using the Naval Polar Oceanographic Center's (NPOC) weekly analysis of concentration and, to some extent, thickness. These fields, though not yet available, are in the process of being digitized and will be incorporated into the model forecasts when available.

6. Example output from PIPS

The results of three different experiments will be presented in this section. In each experiment, the PIPS model was forced by NOGAPS fields from 18 January 1983 to 18 January 1984. This same year of forcing was used repeatedly in every year of model integration. The first two experiments used the Skiles ocean currents, and a constant oceanic heat flux of 2 watts m^{-2}, while the third experiment used the monthly mean Hibler-Bryan ocean currents and oceanic heat fluxes.

The Hibler model is used to predict the following information for the Arctic: ice drift velocity, ice thickness, ice compactness (concentration), growth of thick and thin ice, ice strength (pressure), and areas of convergence and divergence. Model results will be presented in terms of contour or vector plots of these fields.

The first experiment was performed on the central Arctic basin (Fig. 2) and used to verify that the model had been correctly implemented on the FNOC system. Model results show the strong dependence of the ice drift velocity upon wind forcing. Vector plots of the annual average of the wind (Fig. 6a) and of the ice drift velocity (Fig. 6b) from the third year of integration show the pattern of ice drift to be turned slightly to the right of the wind as expected. The pattern of ice thickness contours (Fig. 6c) shows a maximum buildup of ice north of the Canadian Archipelago and a secondary maximum along the northeastern coast of Greenland. This is in good agreement with observations (Fig. 7) but is slightly different from previous climatological results obtained by Hibler (1979, 1980). Hibler's results show the thickest ice north of Greenland (Fig. 8a), while PIPS results show the thickest ice north

of the Canadian Archipelago (Fig. 8b). The difference in these results is due to the different wind forcing for each case. The 1983 marine winds show a small anticyclonic circulation over the location of the Beaufort gyre. As a result, the ice is forced to pile up farther west along the Canadian coast than was in the case produced by Hibler's climatological forcing.

The ice thickness contours also revealed regions of thin ice in the Kara, Laptev, and Chukchi Seas. Model results show these to be areas of divergence (Fig. 9a) and growth of ice on open water (Fig. 9b). It will be shown later that this tendency toward creating regions of open water is somewhat exaggerated in these areas because incorrect ocean currents exist in the Skiles data set.

Figure 9c shows the annual average total ice growth for the third year of integration. The regions of strong divergence and open water are also the areas of most total growth of ice. The total ice growth values along the Siberian coast (≈ 7 m) are twice those of Hibler's previous results. These differences are also due to the inaccuracies in ocean currents that were used. A region of average annual ice melt exists in the west Chukchi-East Siberian Seas.

Annual average ice compactness, the percentage of a grid cell covered by thick ice, is shown in Figure 9d. The central Arctic, Canadian Archipelago, and northern coast of Greenland are areas of high concentration, while areas of low concentration correspond to the areas of thin ice (Fig. 6c). Annually averaged ice strength, or pressure, is given in Figure 9e. Areas of highest strength correspond to the regions of thickest ice.

Additional checks were made on the FNOC model results to determine whether the model was spinning up properly. Figure 10a shows a time series of ice thickness transects from Hibler's climatological study. This figure shows how the ice thickness field develops in time from its initial condition of 3.3 m of ice everywhere in the basin. The results show that the model is basically "spun up" by year three, with only small differences showing between years three and five. Based on these results, the FNOC model was integrated through the third year and assumed steady. Figure 10b shows results of similar transects from the first three years of integration of the FNOC model. While Hibler's results show one peak in ice thickness developing, the PIPS model shows two. This corresponds to the two regions of thick ice in the Canadian Archipelago and the northern Greenland border. Figures 11 and 12 show the seasonal variability in ice thickness of transects 1 and 2 shown in Figure 2. In both locations ice thicknesses are much larger in the winter (March) than in summer (September), where ice almost totally disappeared in the Kara, Laptev, and East Siberian Seas. Based on the results of the three-year simulation, we concluded that the FNOC version of the Hibler sea ice model was giving numerically and physically acceptable results.

For the final version of the FNOC operational sea ice forecast model, PIPS, we chose to extend the model boundaries to include the Barents Sea and most of the Greenland-Norwegian Sea. The final version of the PIPS model also used both the Hibler-Bryan ocean currents and oceanic heat fluxes.

The importance of using correct ocean currents can be seen in this comparison of two model results, one using the Skiles currents, the other the Hibler-Bryan currents, and both using constant heat fluxes of 2 watts m^{-2}. Figure 13 shows the ice edge extent as analyzed by the Navy-NOAA Joint Ice Center for 2 August 1983. Figure 14 shows the results of the PIPS model for 4 August 1983 using the Skiles currents, while Figure 15 shows the 4 August 1983 PIPS results using the Hibler-Bryan currents. Note in the case using the Skiles currents, the ice edge extends too far south in the east Greenland Sea and covers the northern part of Iceland. Use of the Hibler-Bryan currents improves the accuracy of the ice edge extent.

Since the operational version of the model includes marginal ice zone regions, an adjustment was made to the treatment of the deep oceanic heat flux into the mixed layer. In the original version of the model, Hibler set the oceanic heat flux equal to a constant value of 2 watts m^{-2} at every time step. This estimate is accurate for oceanic heat flux in the Central Arctic (Maykut and Untersteiner, 1969). However, in the marginal ice zone both temporal and spatial variability of the heat fluxes are important. Thus, monthly mean heat flux fields from the Hibler-Bryan model were included. These fields (Figs. 16 a and b) show the high variability of the heat flux from winter to summer in the marginal ice zone. They also indicate that the oceanic heat flux within the central Arctic is very small when compared to the oceanic heat flux in the Greenland-Norwegian Seas. This difference is due to the large amounts of heat brought into the Greenland-Norwegian Seas by the Norwegian Current. The Hibler-Bryan model (1984) has shown that oceanic heat flux can melt as much as 12.5 m of ice per year in the east Greenland Sea (Fig. 17). The importance of including the deep oceanic heat flux will be shown in a later section.

The results of the final version of the PIPS model using the Hibler-Bryan currents and heat fluxes are presented in terms of annually averaged fields and monthly mean fields from the third year of integration. Five resultant model fields are shown for each month/year: wind ($msec^{-1}$), ice drift ($msec^{-1}$), ice thickness (m), ice compactness (%; 1. = 100%), and total ice growth (m). The annually averaged figures also show growth of thick and

thin ice (m) separately and ice strength or pressure (Nt m^{-2}) and ice divergence (sec^{-1}).

The first set of figures, 18 a-i, the annual averages, show that ocean currents do have an effect on the long-term-model results in the central Arctic, as well as in the marginal ice zone. On comparing ice drift velocity from this case to the case using the Skiles currents (Fig. 4), it is apparent that a larger anticyclonic circulation dominates the western half of the Arctic in the case using the Hibler-Bryan currents. The velocities are generally stronger in the East Siberian and Laptev Seas. These currents agree closely with the mean drift in the Arctic (Gordienko, 1958, Fig. 19).

The ice thickness field also shows the effects of the change of currents on the central Arctic. A more spatially regular increase in ice thickness from the East Siberian and Laptev Seas toward the Canadian coast appears in the PIPS version of the model. The relative maximum of thickness northwest of the Chukchi Sea disappears with the use of the Hibler-Bryan currents. There is also somewhat thicker ice (1 m vs. 0-0.5 m) and less divergence and growth (6 m vs. 8 m) of ice in the Kara, Laptev and East Siberian Seas. The patterns of ice compactness and pressure are similar to those of thickness.

The ice growth fields presented here show the cumulative growth of ice over a period of a year based strictly on growth rates, not including the effects of lateral melt. These figures are, then, somewhat deceptive in areas like the East Greenland-Norwegian Seas where growth rates indicate that small amounts of ice should grow here, particularly in winter. The ice never accumulates because it is immediately removed by lateral melt. The figures show that most regions of thin ice growth are the marginal ice zones. Thick ice growth exists in most parts of the Arctic, with the exception of the east Greenland and Norwegian Seas and the Canadian and north Greenland coasts. These regions are dominated by negative thick ice growth (i.e., melting of thick ice).

The divergence fields show that most of the regions that become ice-free are areas of divergence. Areas of convergence exist north of Iceland near the Greenland coast. This area of convergence, also an area often covered with thin ice, is a likely region for ridge formation.

The second set of figures, 20a-g and 21a-g, show sample monthly mean fields from March and September along with two sample NPOC analyses for each month. The first analysis figure is for the eastern Arctic; the second is for the western Arctic in March and September of 1983. March results represent winter conditions, and September results are typical of summer.

For the entire 12-month period, wind and ice drift velocity fields show that the ice drift vectors appear turned slightly to the right of the wind vectors as expected. Solutions also show a large amount of monthly variability. Large variability was also found on the daily time scale with the ice drift responding immediately to the changing winds.

Ice thickness and compactness patterns for the 12-month period changed very little in the central Arctic along the northern Canadian and Greenland coasts. A great deal of seasonal variability exists, however, in parts of the Laptev, Kara, East Siberian and Chukchi Seas, which become areas of open water in summer and ice covered in winter. The maximum ice thickness (≈ 6 m) remains along the Canadian and north Greenland coasts throughout the year. The greatest change in the ice thickness occurs in the marginal ice zones. Ice reaches its maximum thickness and extent during the months of March and April. The retreat of the ice edge is a maximum during the months of August and September. These basic tendencies agree with both NPOC climatology and the analyses. Model results and the NPOC analyses differ in a few areas, however. The first is the Chukchi Sea in which the ice edge retreats too far north in the summer. Possible explanations are the lack of the effect of flow through the Bering Strait (model grid spacing prevents adequate treatment of this strait) and the wind forcing pushing ice out of the Chukchi Sea during these months. The other region of disagreement between model and analysis is the east Greenland-Norwegian Seas in the winter months. The model tends to grow too much ice in this location in the winter months. Similar results were obtained by Tucker (1982) in a study of the Greenland Sea using the Hibler model. Reasons for this accelerated growth rate are unknown at this time. The model also tends to grow too much ice in a small area just southwest of Spitzbergen. This tendency is probably due to the inability of the model's grid resolution to accurately define Spitzbergen.

Growth fields show a general tendency of positive growth in winter negative growth (melt) in summer. In the east Greenland-Norwegian Seas, negative growth of ice begins as early as March, which indicates that the combination of oceanic and atmospheric heating is strong enough at this time to melt ice. Positive growth of ice resumes in this region in September.

The importance of including accurate oceanic heat fluxes is shown in the following three figures. In each case, monthly varying ocean currents were used, but the heat flux was held at a constant 2 watts m^{-2}. Figure 22 is the annually averaged ice thickness, while Figures 23 and 24 are the ice thickness for March and September respectively. Comparing these solutions to those of Figures 18c, 20c, and 21c shows that including the correct oceanic heat fluxes decreases the amount of ice in the east Greenland sea and greatly improves the ice edge location.

7. Summary and conclusions

PIPS, the FNOC version of the Hibler ice model, is available for operational use at FNOC. The model has been spun up to a steady cyclic climatological state using the thermodynamic forcing from NOGAPS, the marine winds, and the Hibler-Bryan ocean currents and deep oceanic heat fluxes. These results are in good agreement with those obtained by Hibler (1979, 1980) and with NPOC analysis of ice edge location.

As a forecast tool, PIPS will be forced by NOGAPS and, thus, will be limited in the extent of its forecast time to that of NOGAPS, 120 hours. Beyond that, the predictions can be made only as persistence forecasts or climatological forecasts with the use of climatological forcing. The model will be able to predict ice drift, ice thickness, ice compactness, ice growth, ice strength and regions of convergence and divergence. In the coming fiscal year the model will be initialized and updated by the weekly compactness and thickness analysis made available from NPOC.

8. References

Bryan, K., S. Manabe, and R. L. Pacanowski (1975). A Global Ocean-Atmosphere Climate Model, Part II The Oceanic Circulation. *Journal of Physical Oceanography*, v. 5, pp. 30-46.

Gordienko, P. (1958). Arctic Ice Drift. Proceedings, *Conference on Arctic Sea Ice*, Publication 598, National Academy of Sciences and National Research Council, Washington, D.C., pp. 210-220.

Hibler, W. D. (1979). A Dynamic Thermodynamic Sea Ice Model. *Journal of Physical Oceanography*, v. 9, pp. 815-846.

Hibler, W. D. (1980). Modeling a Variable Thickness Sea Ice Cover. *Monthly Weather Review*, v. 108, n. 12, pp. 1944-1973.

Hibler, W. D. and T. Tucker (1979). Some Results of a Linear-Viscous Model of the Arctic Ice Cover. *Journal of Glaciology*, v. 22, n. 87, pp. 293-304.

Hibler, W. D. and K. Bryan (1984). Ocean Circulation: Its Effects on Seasonal Sea-Ice Simulations. *Science*, v. 224, n. 4648, pp. 489-491.

Manabe, S., K. Bryan, and M. J. Spelman (1979). A Global Ocean-Atmosphere Climate Model with Seasonal Variation for Future Studies of Climate Sensitivity. *Dynamics of the Atmosphere and the Ocean*, v. 3, pp. 393-426.

Maykut, G. A. and N. Untersteiner (1969). *Numerical Prediction of the Thermodynamic Response of Arctic Sea Ice to Environmental Changes*. Rand Corporation, Santa Monica, California, Memo. Rm-6093-PR, 173 pp.

McPhee, M. G. (1979). The Effect of the Oceanic Boundary Layer on the Mean Drift of Pack Ice: Application of a Simple Model. *Journal of Physical Oceanography*, v. 9, pp. 388-400.

McPhee, M. G. (1980). An Analysis of Pack Ice Drift in Summer. In: *Sea Ice Processes and Models* (R. S. Pritchard, Ed.) University of Washington Press, pp. 62-75.

Parkinson C. L. and W. M. Washington (1979). A Large-Scale Numerical Model of Sea Ice. *Journal of Geophysical Research*, v. 84, pp. 311-337.

Semtner, A. J., Jr. (1976). A Model for the Thermodynamic Growth of Sea Ice in Numerical Investigations of Climate. *Journal of Physical Oceanography*, v. 6, pp. 379-389.

Skiles, F. L. (1968). *Empirical Wind Drift of Sea Ice*. Arctic Drifting Stations, the Arctic Institute of North America.

Thorndike, A. S. and R. Colony (1982). Sea Ice Motion in Response to Geostrophic Winds. *Journal of Geophysical Research*, v. 87, n. C7, pp. 5845-5892.

Tucker, W. B, III (1982). *Application of a Numerical Sea Ice Model to the East Greenland Area*. CRREL Report 82-16, 44 pp.

U. S. Navy Hydrographic Office (1958). *Oceanographic Atlas of the Polar Sea, Part II Arctic*. Hydrographic Office, Publication 705, Washington D.C.

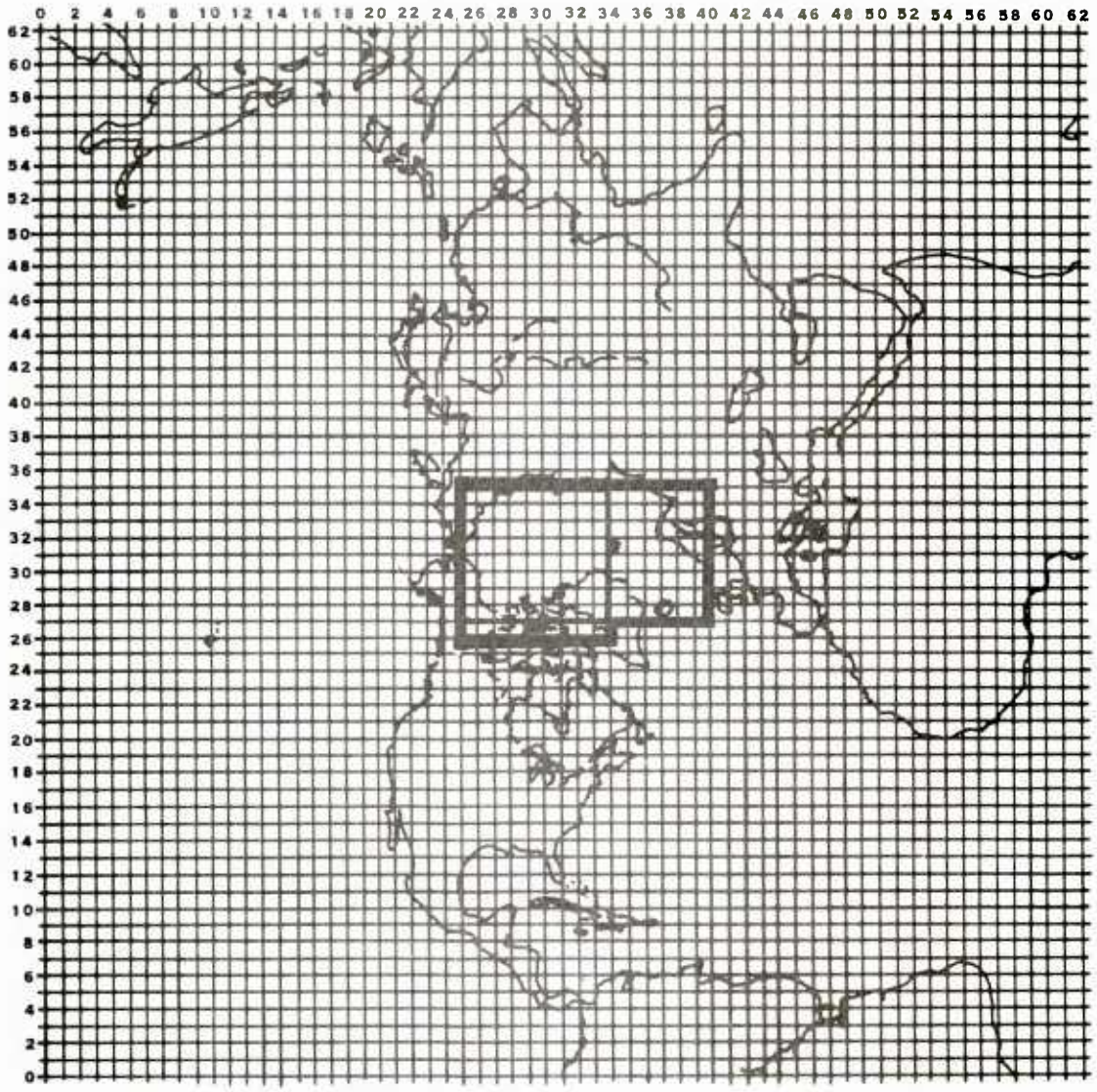

Figure 1. Standard FNOC 63 x 63 Northern Hemisphere polar stereographic grid. Solid line boundaries show the regions used for the central Arctic and PIPS domain.

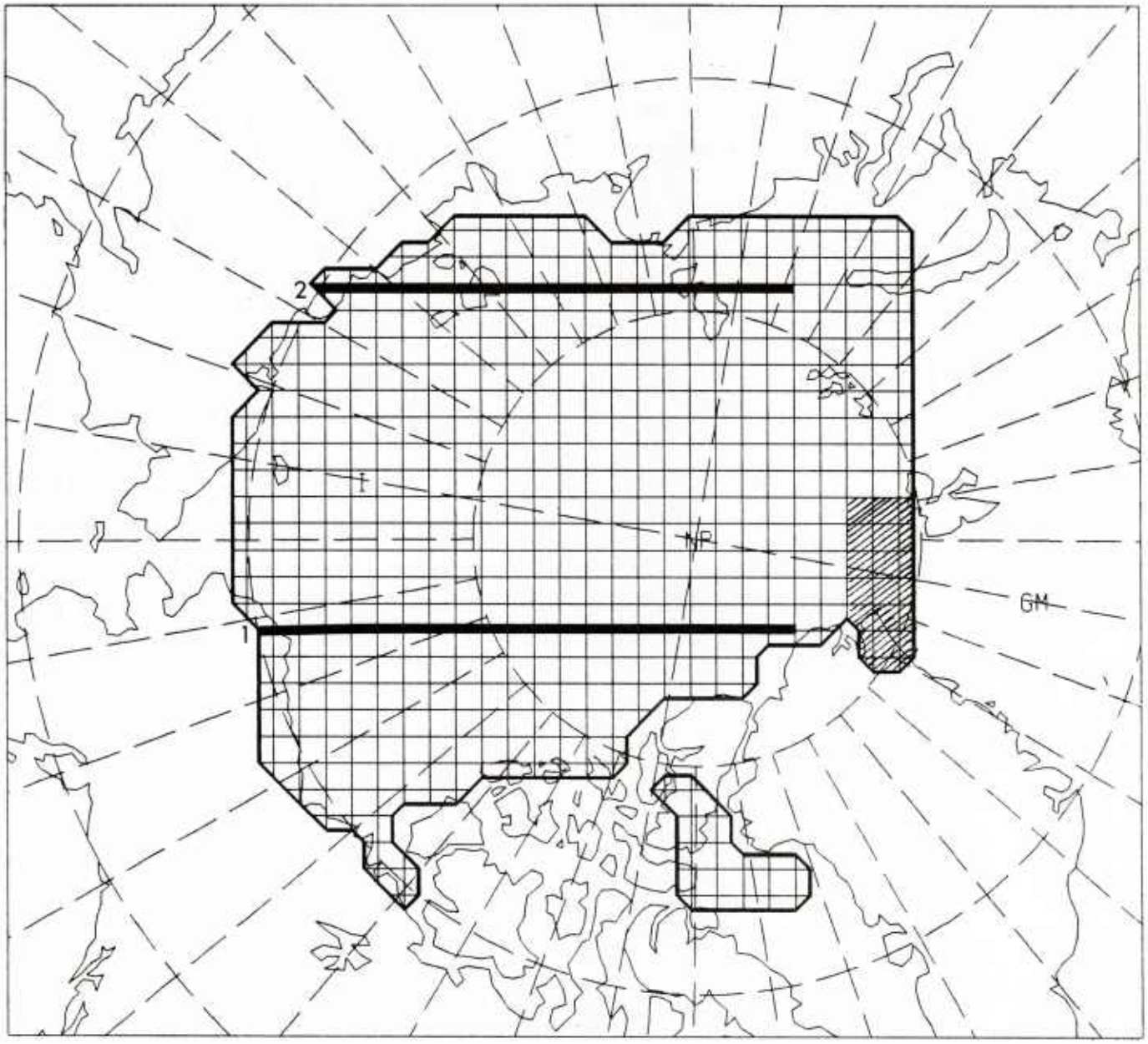

Figure 2. Model grid for the central Arctic ice model domain. Hatched grid spaces are outflow grid cells. Two transect lines labeled 1 and 2 are also drawn on the grid.

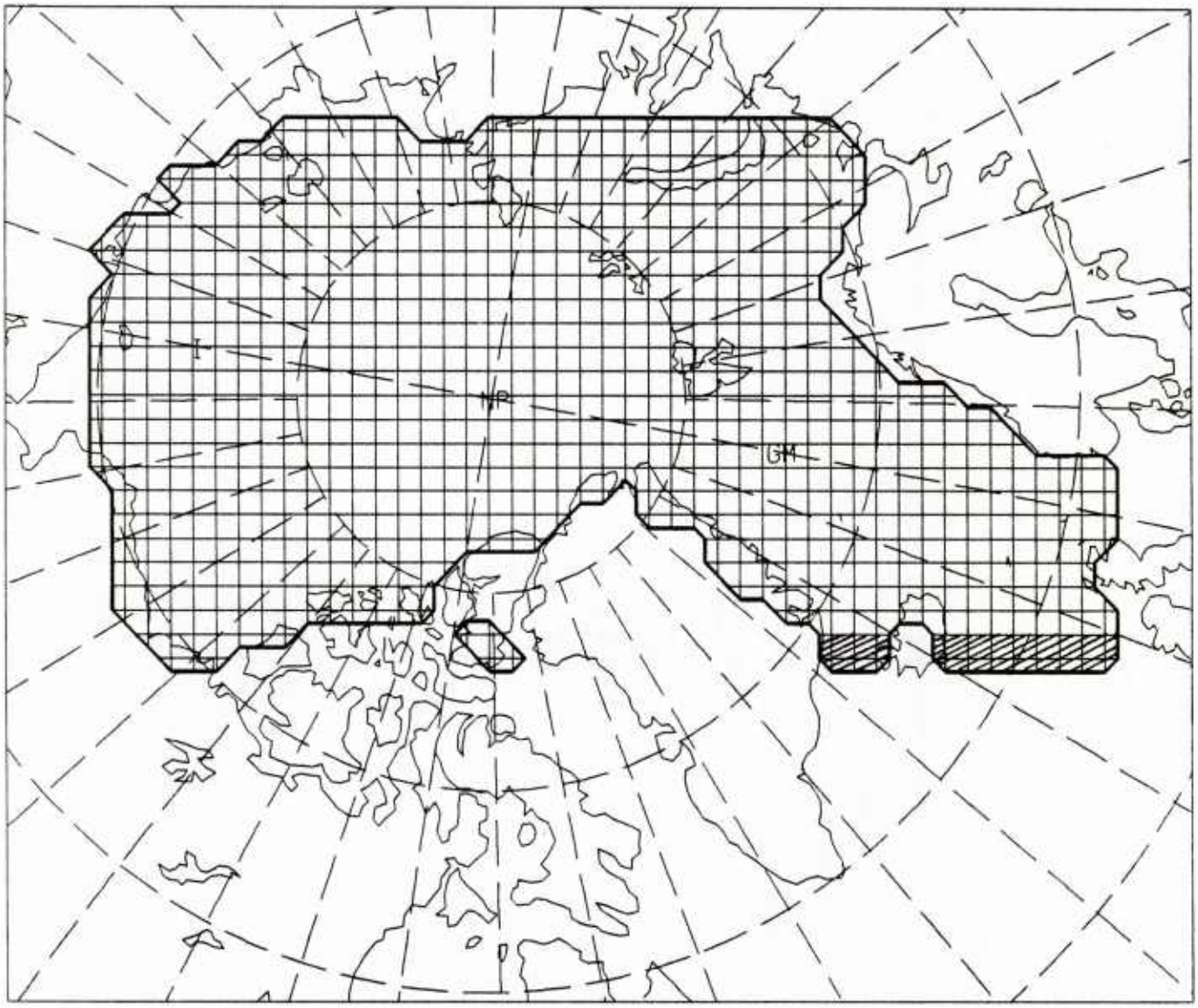

Figure 3. Model grid for the PIPS ice model domain. Hatched grid spaces are outflow grid cells.

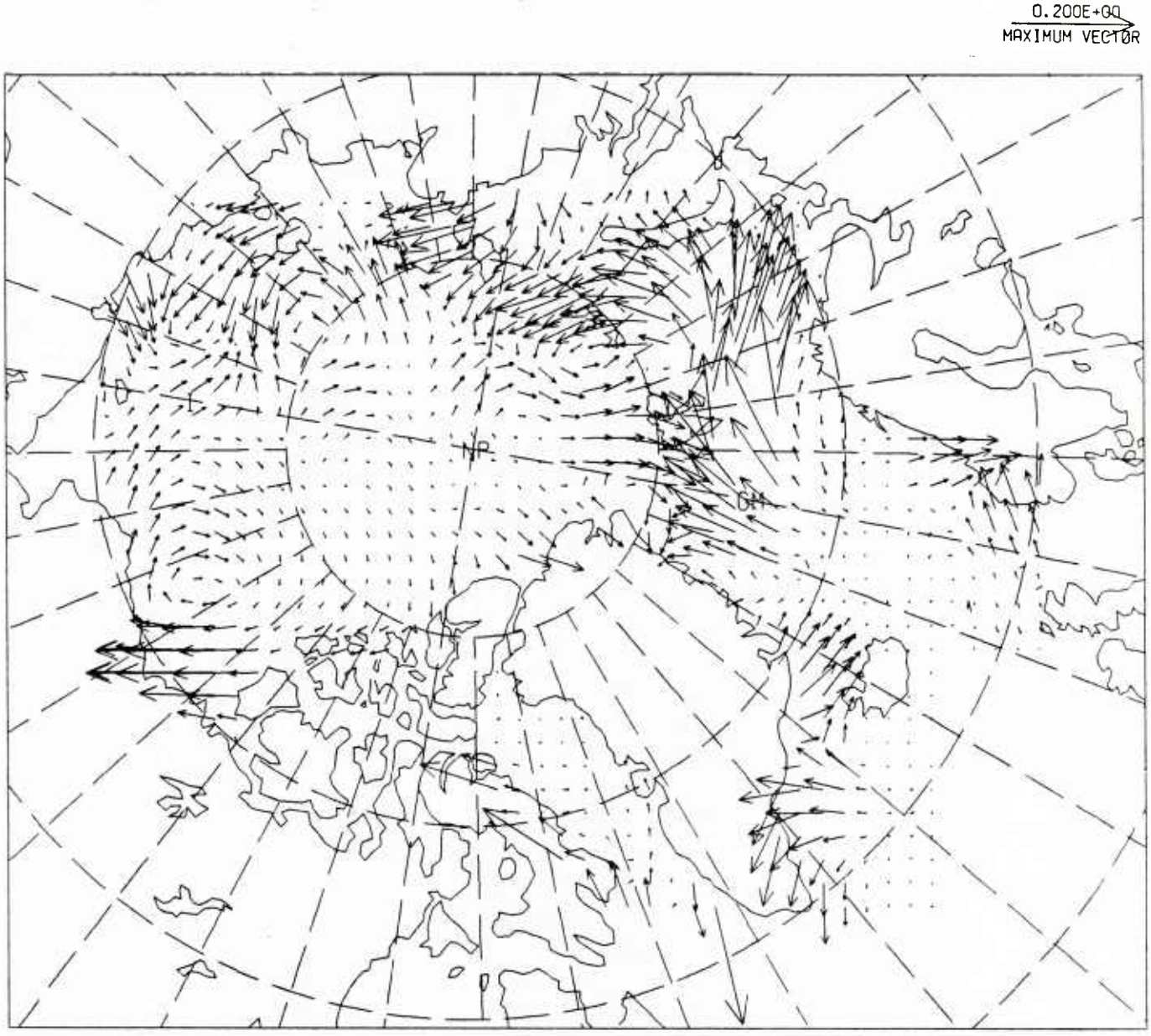

Figure 4. Skiles ocean currents. Maximum vector is 0.2 m/sec.

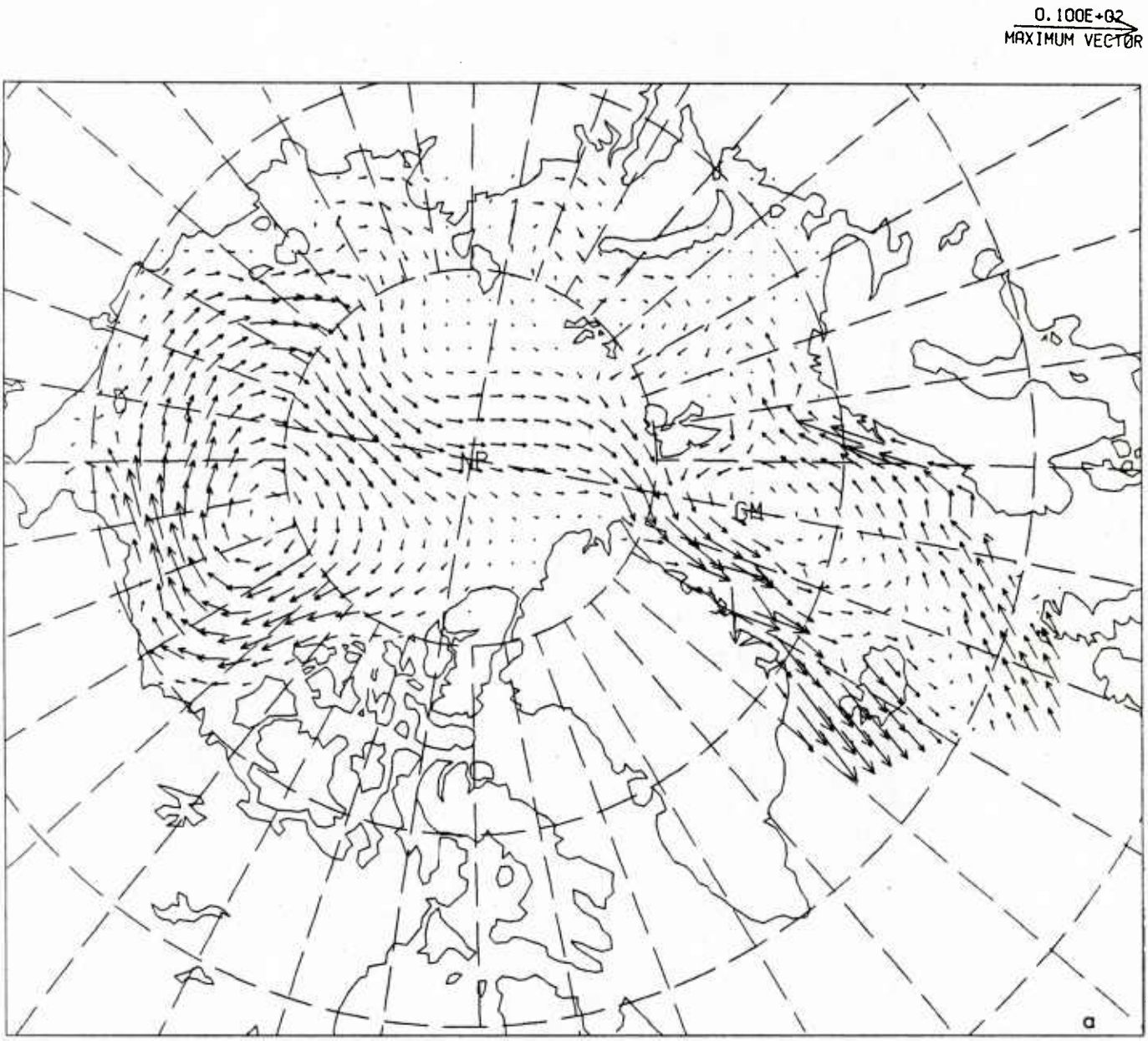

Figure 5a. Annual averaged Hibler-Bryan ocean currents. Maximum vector is 0.1 m/sec.

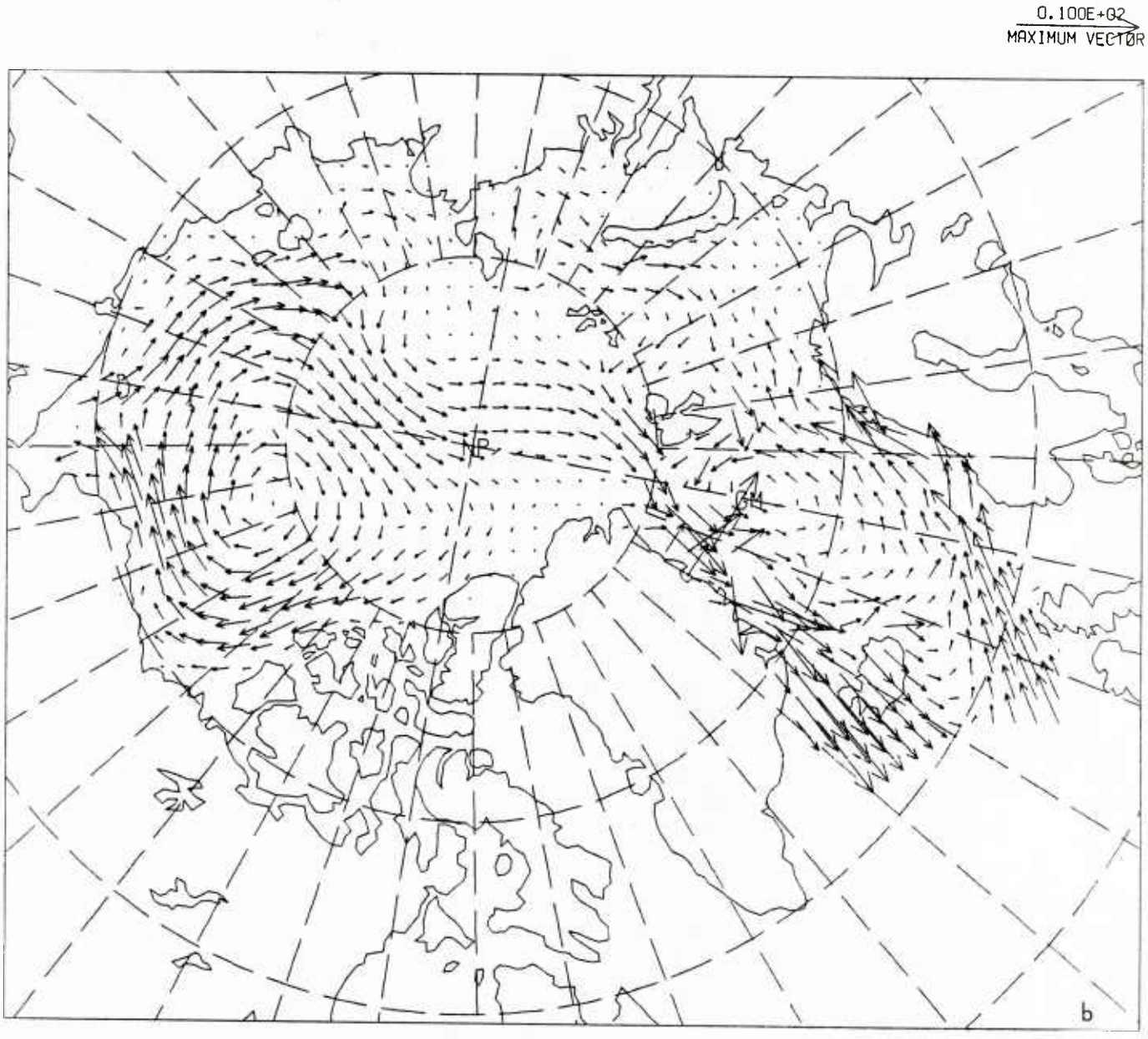

Figure 5b. April monthly mean Hibler-Bryan ocean currents. Maximum vector is 0.1 m/sec.

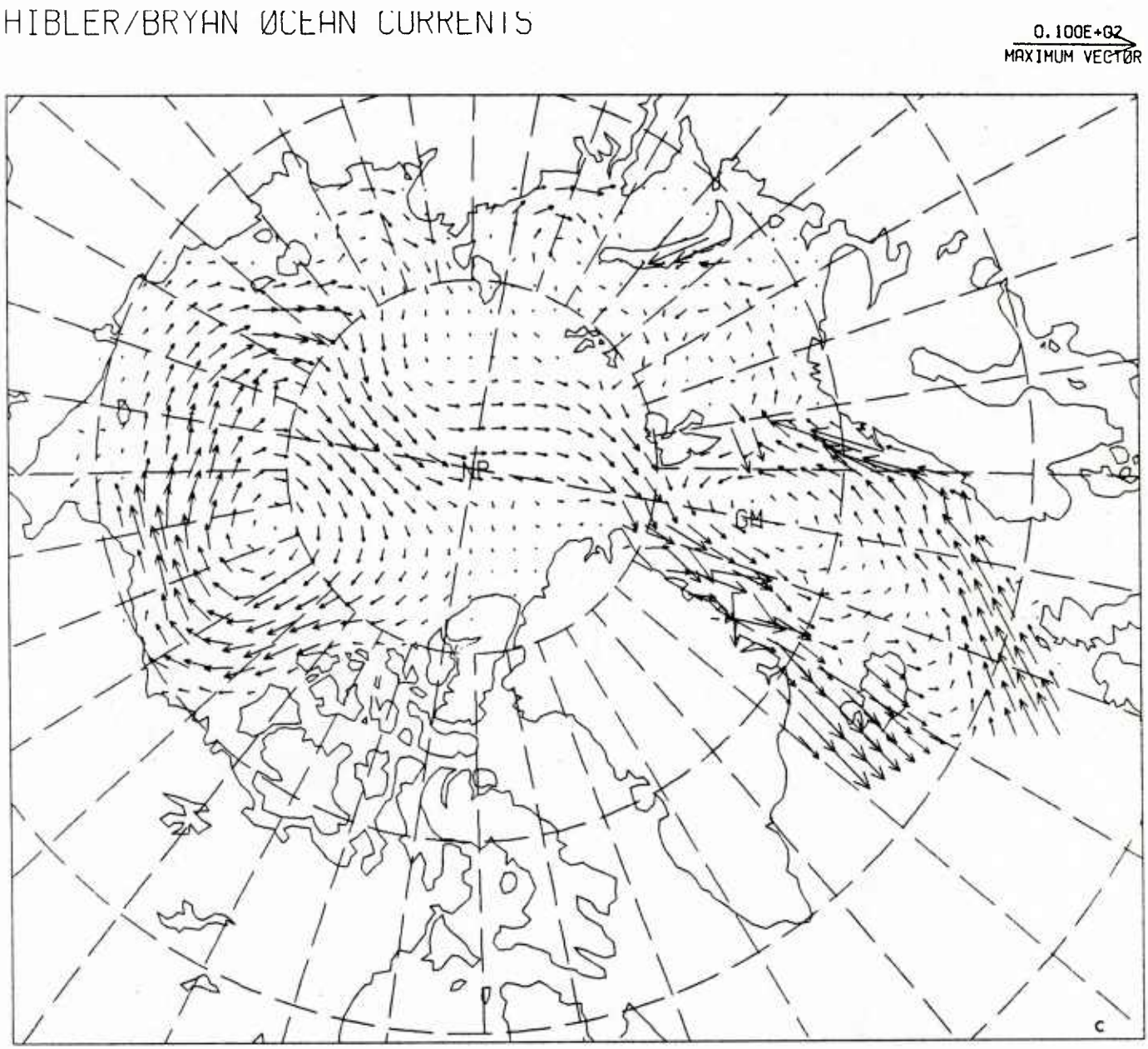

Figure 5c. September monthly mean Hibler-Bryan ocean currents. Maximum vector is 0.1 m/sec.

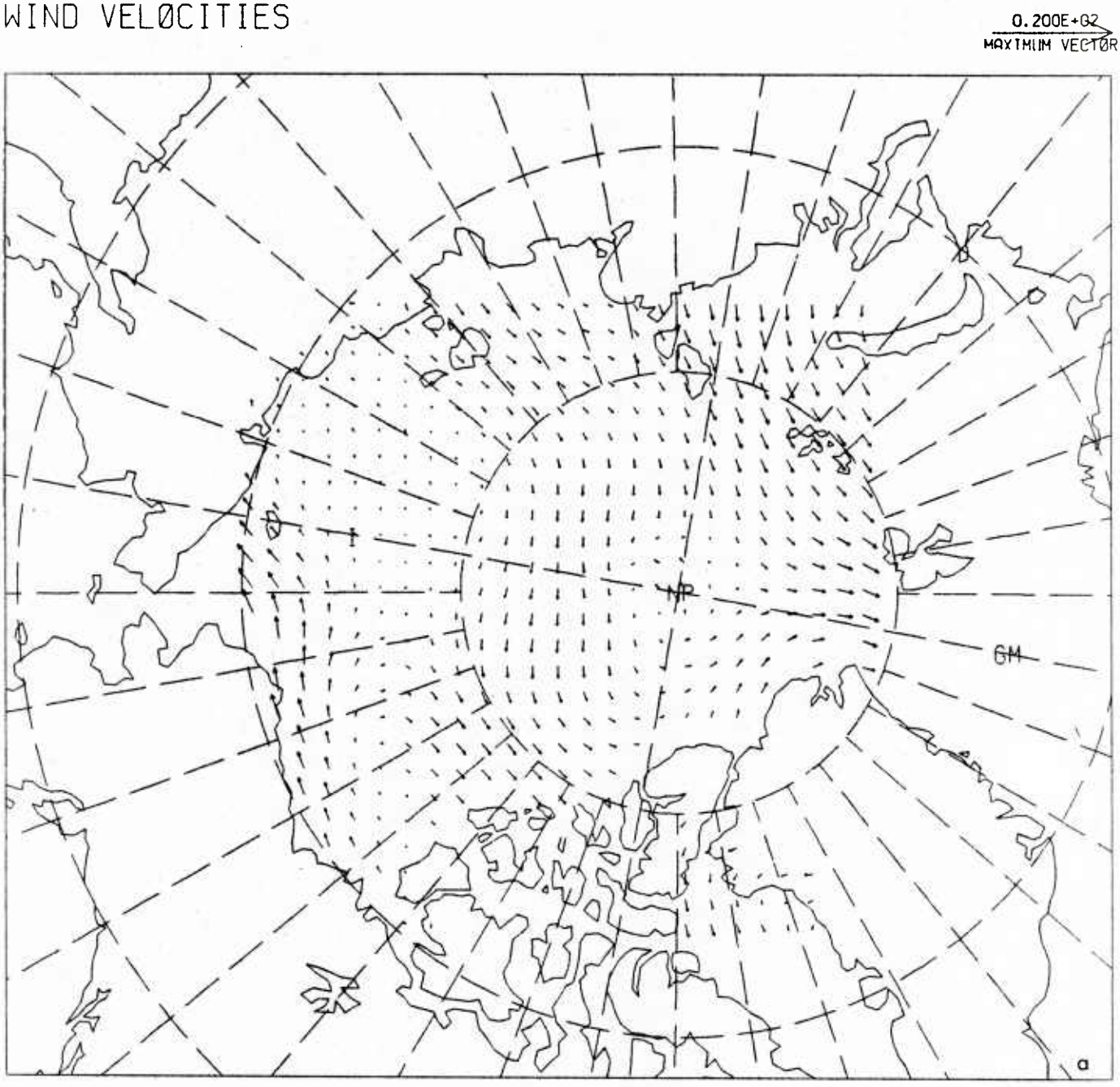

Figure 6a. Third-year averaged solutions for the central Arctic case, wind velocities—maximum vector is 20 m/sec.

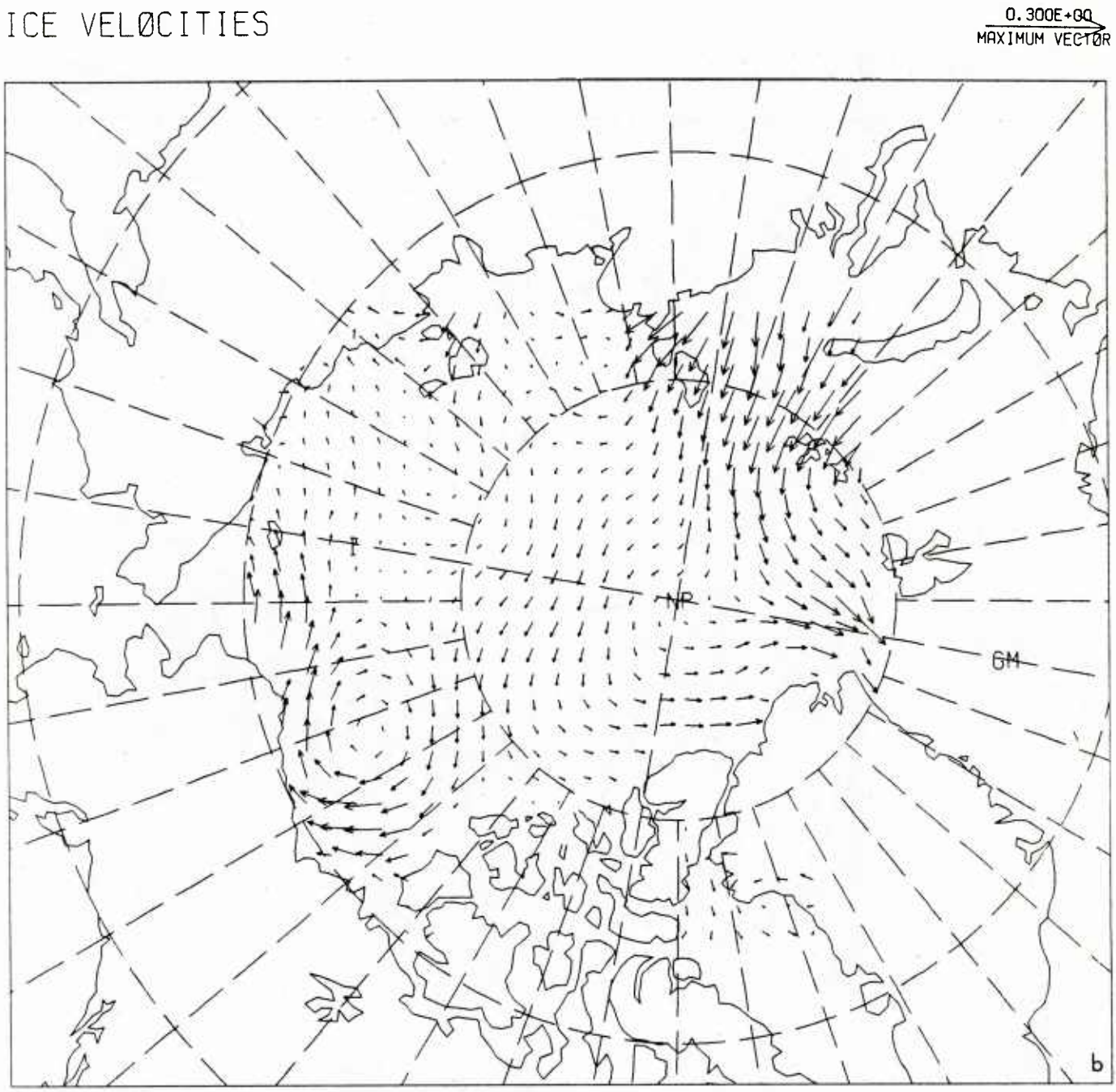

Figure 6b. Third-year averaged solutions for the central Arctic case, ice drift velocities—maximum vector is 0.3 m/sec.

ICE THICKNESS

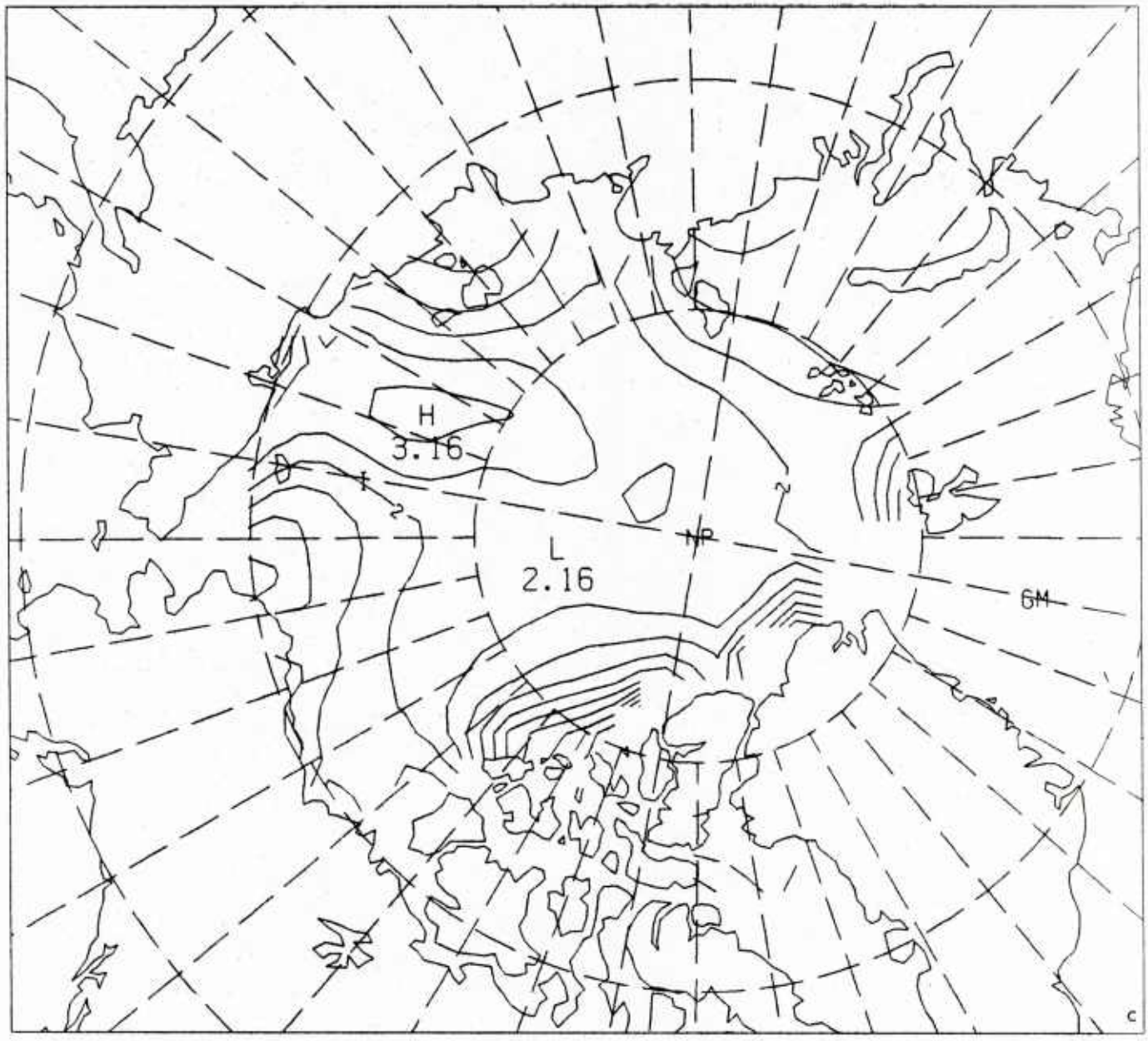

Figure 6c. Third-year averaged solutions for the central Arctic case, ice thickness—contours go from 0 to 10 m by 0.5 m.

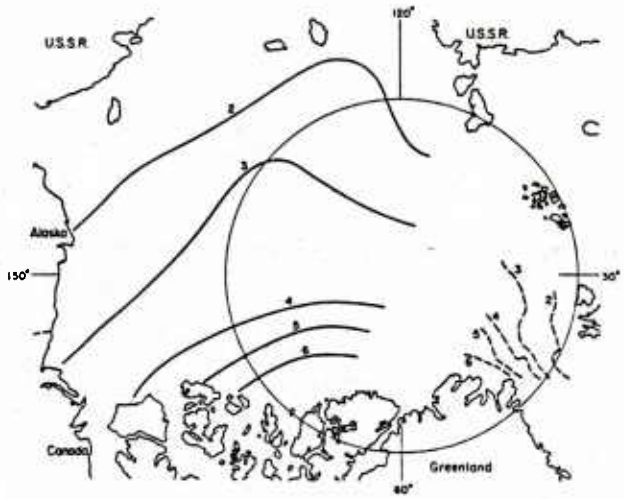

Figure 7. Approximate contours (m) of observed ice thickness obtained from submarine sonar data (Le Schack, private communication). Solid contours were obtained by Le Schack from both summer (1960, 1962) and winter data (1960). Dashed contours are April 1977 data.

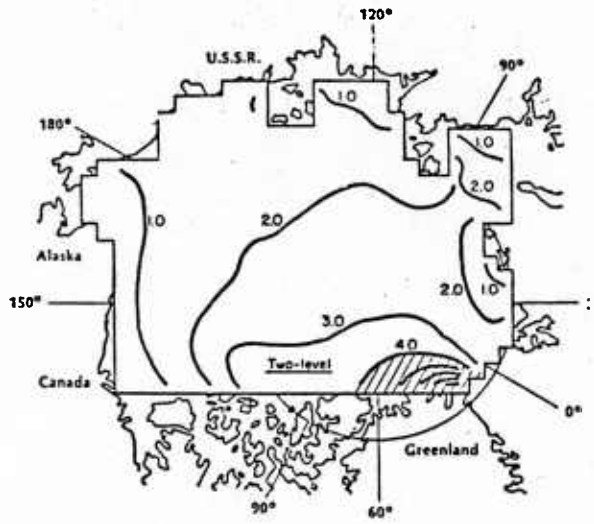

Figure 8a. December average thickness from the Hibler ice model.

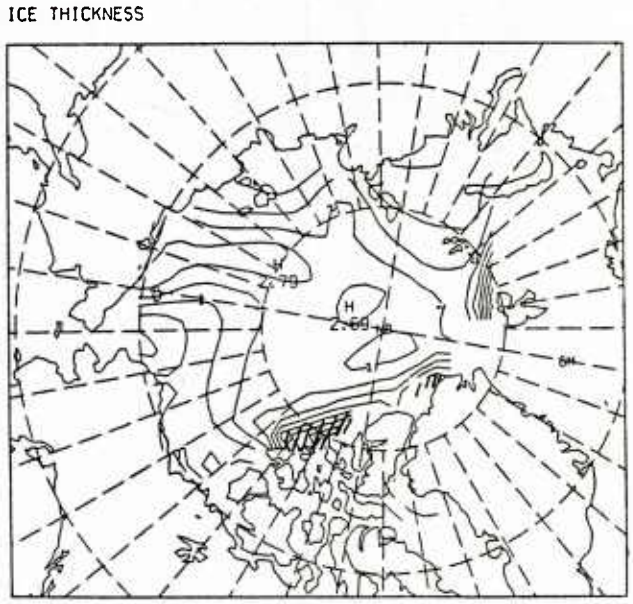

Figure 8b. December average thickness from the FNOC version of the Hibler model.

ICE DIVERGENCE

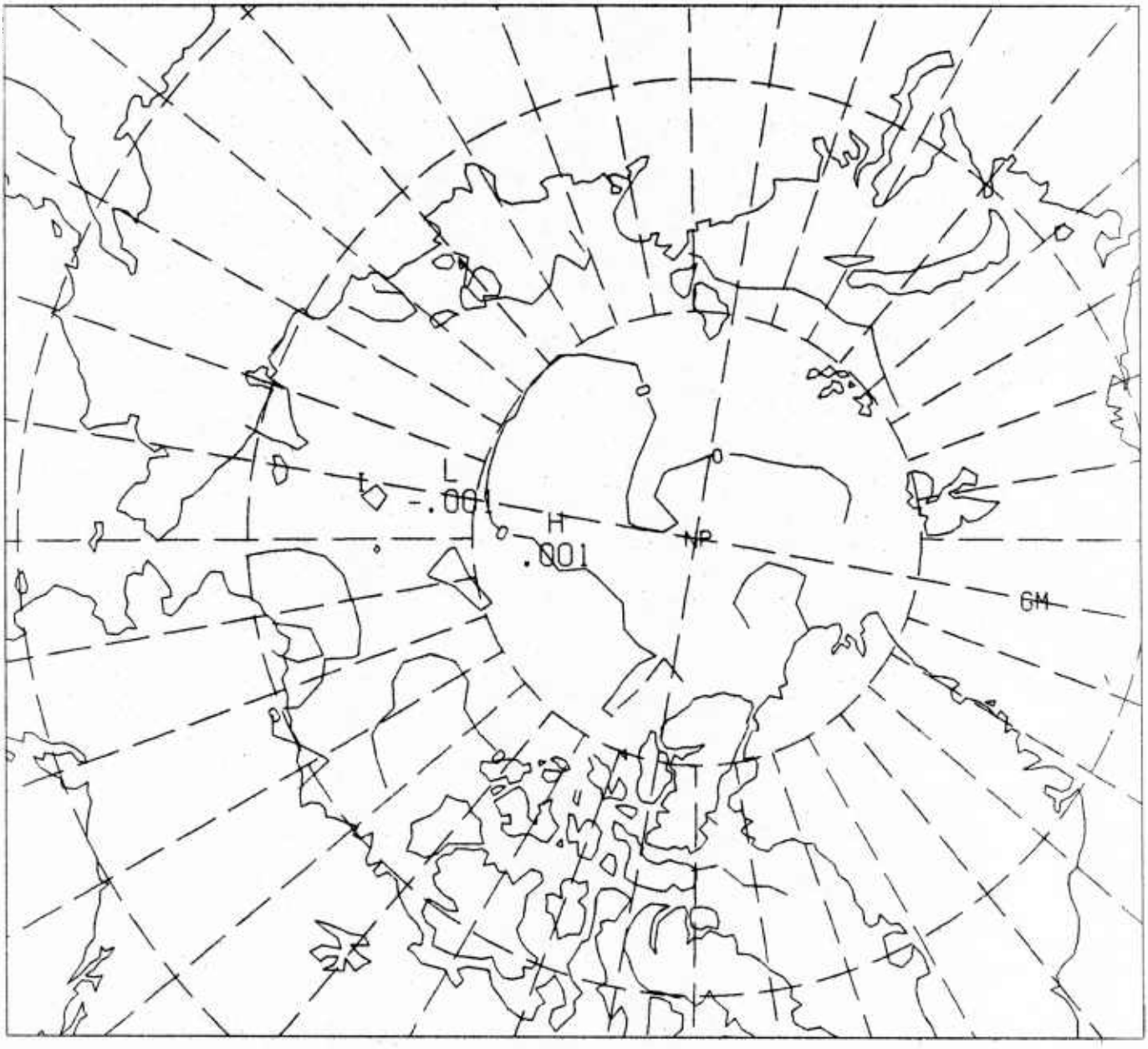

Figure 9a. Third-year averaged solutions for the central Arctic model, ice divergence (x 10^4) in sec^{-1}—contours go from −2 to 9 by intervals of 2.

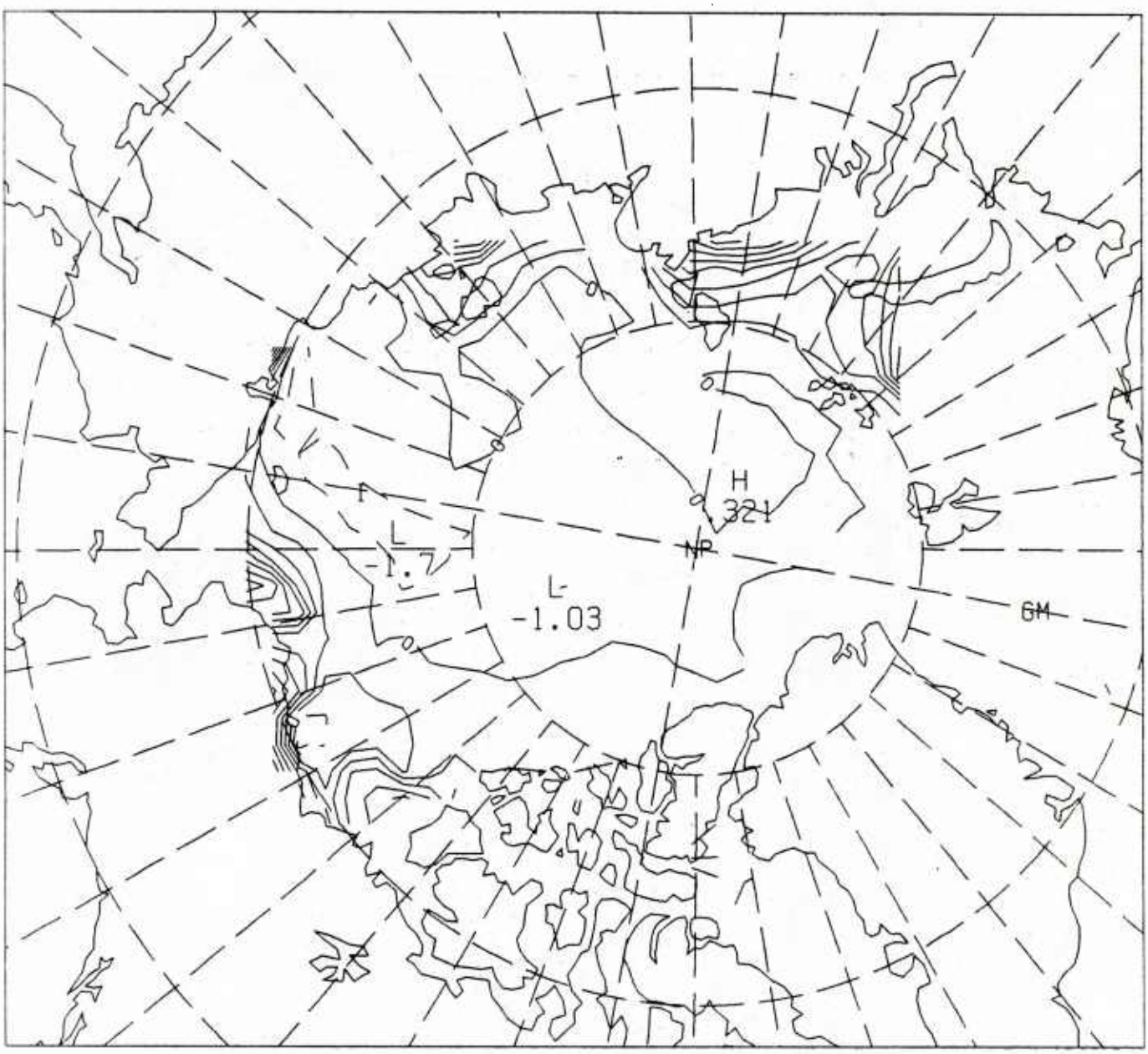

Figure 9b. Third-year averaged solutions for the central Arctic model, growth of thin ice or ice on open water (without the effects of lateral melt)—contours go from −2 m to 6 m at intervals of 1 m.

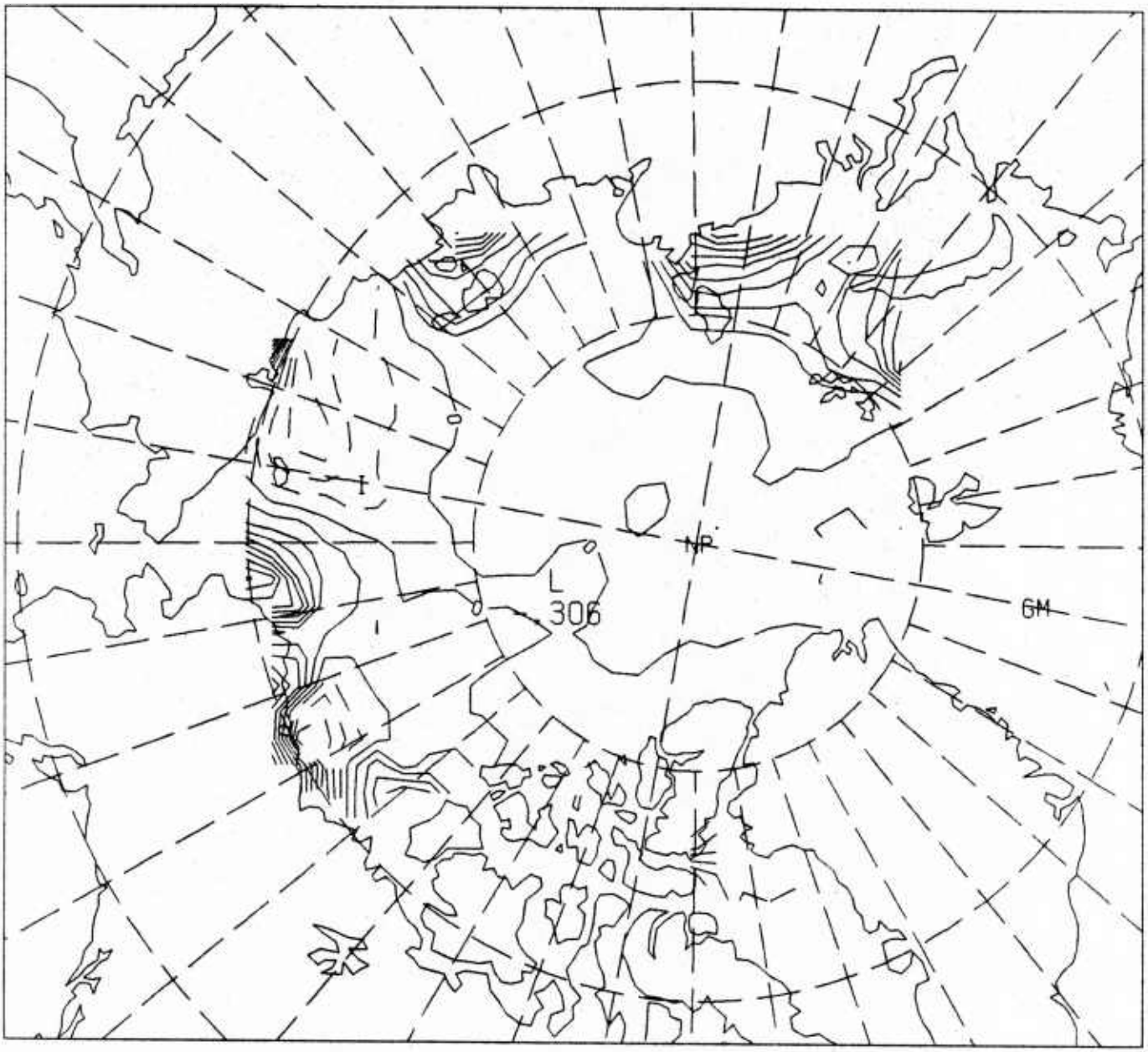

Figure 9c. Third-year averaged solutions for the central Arctic model, total ice growth—contours go −5 m to 10 m by 1 m.

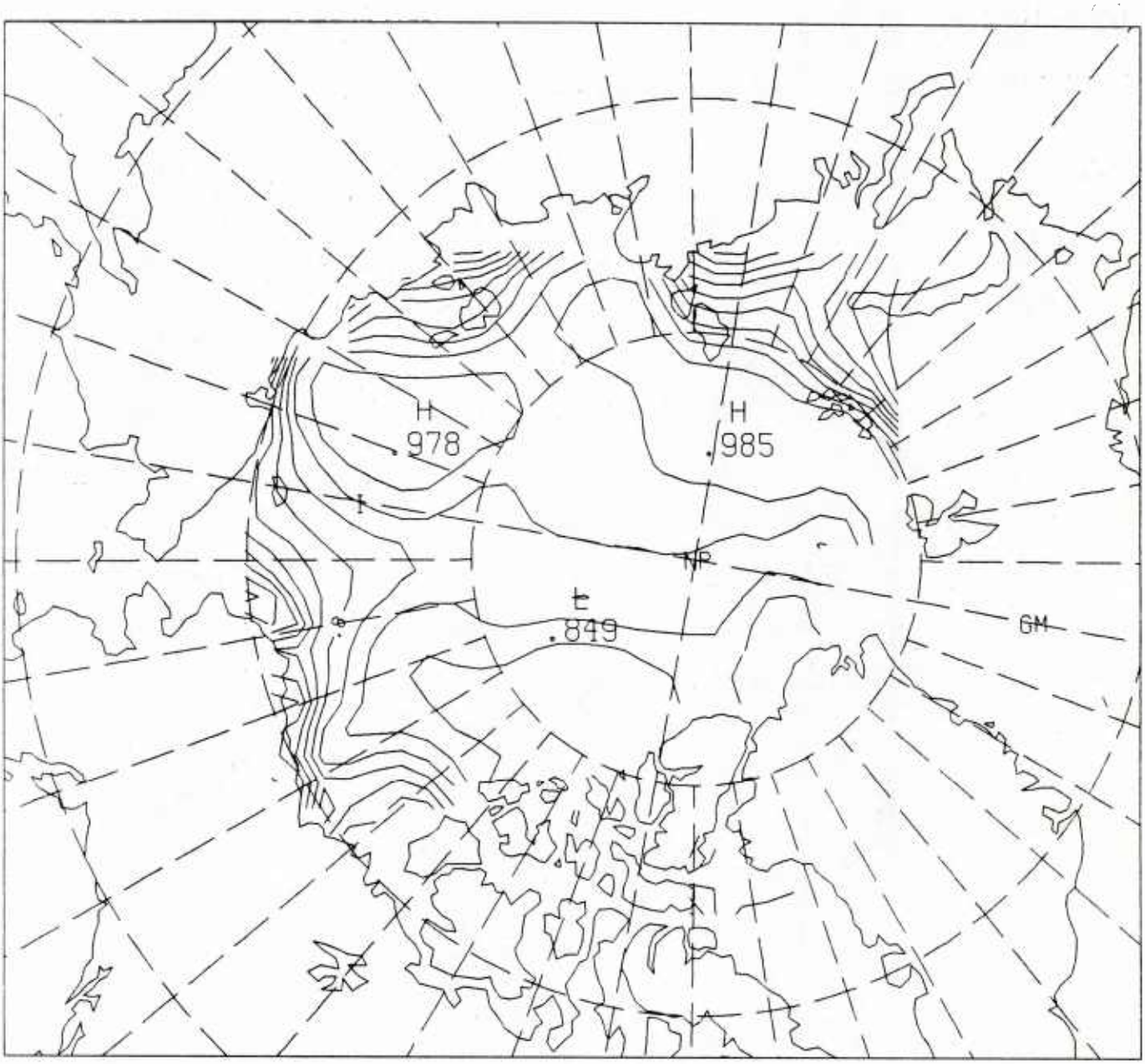

Figure 9d. Third-year averaged solutions for the central Arctic model, percentage of ice concentration at intervals of 5%.

ICE STRENGTH

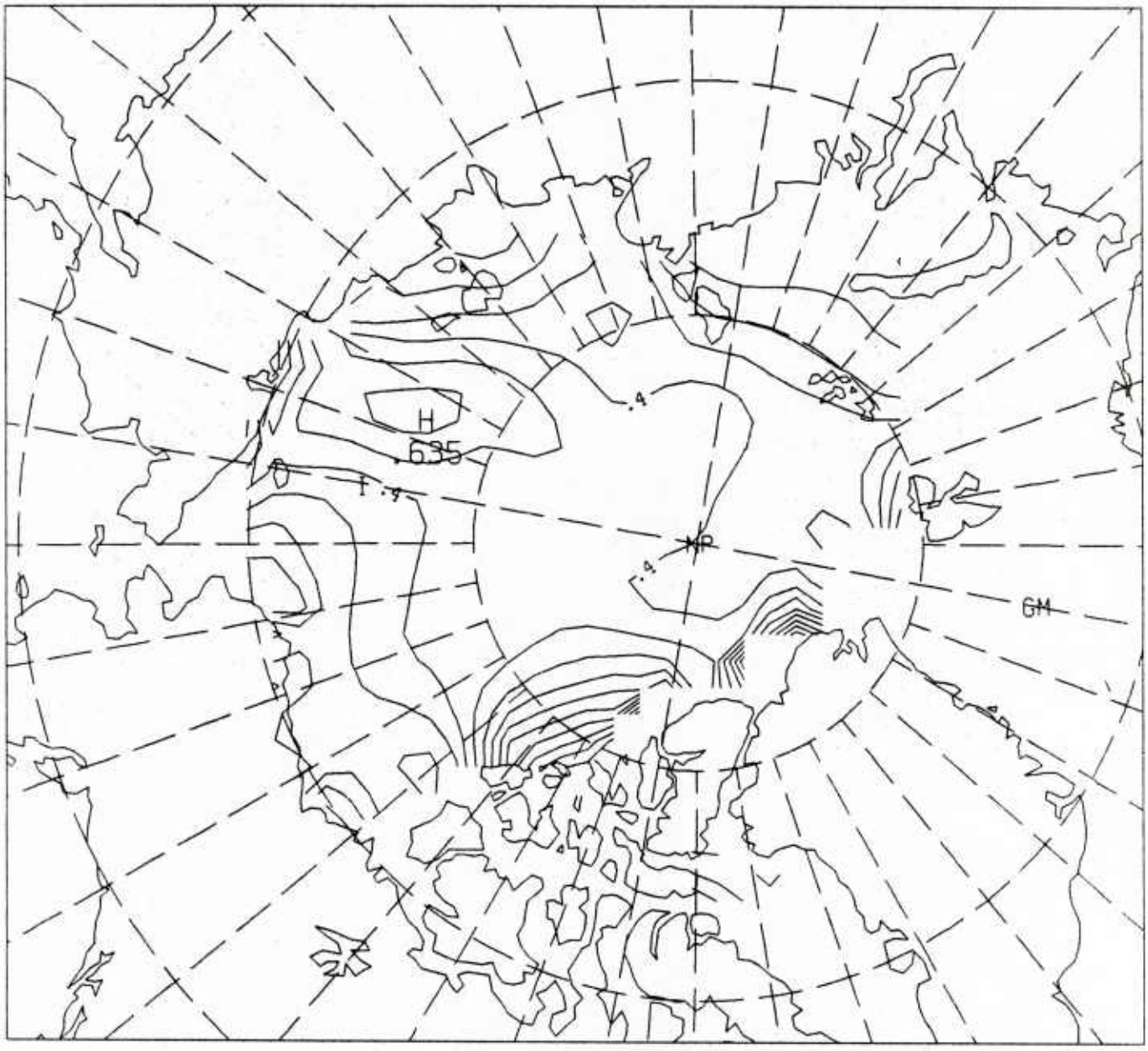

Figure 9e. Third-year averaged solutions for the central Arctic model, ice strength or pressure in Nt m^{-2} contours go from 0 to 2 (x 10^{-5}) at intervals of 0.1.

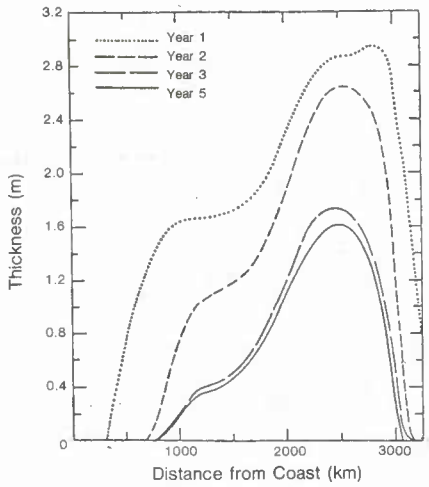

Figure 10a. Evolution of ice thickness from the Hibler model for mid-September.

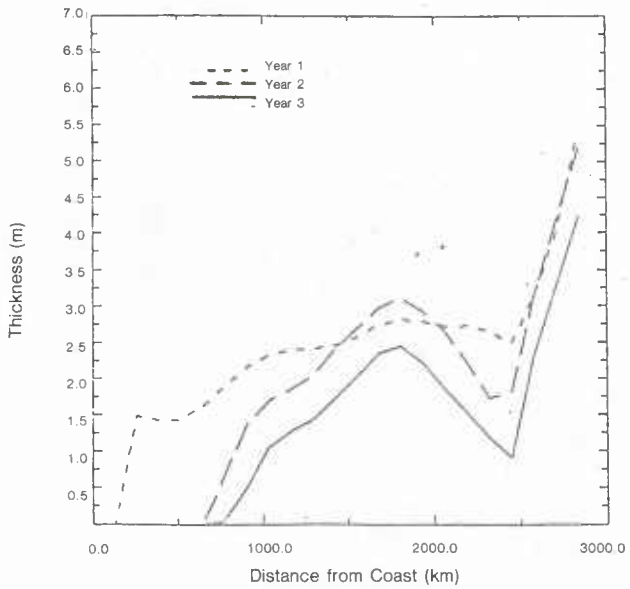

Figure 10b. Evolution of ice thickness from the central Arctic model from September 8, transect 1. Note transect 1 (see Fig. 2) corresponds closely to the transect used by Hibler.

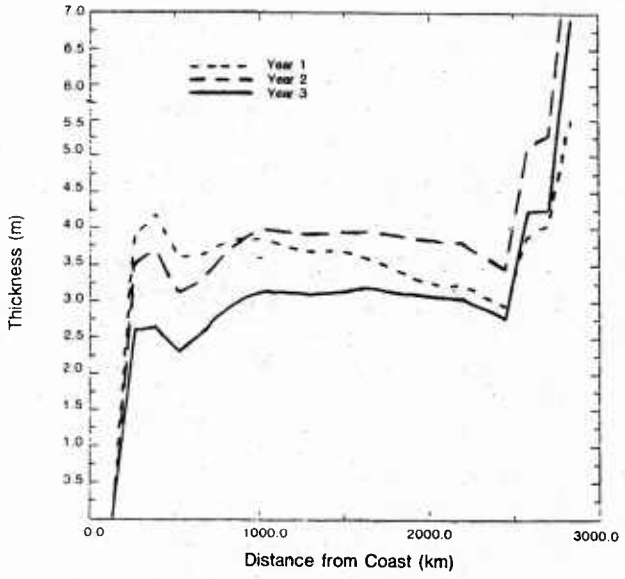

Figure 11a. Evolution of ice thickness from the central Arctic model in March along transect 1.

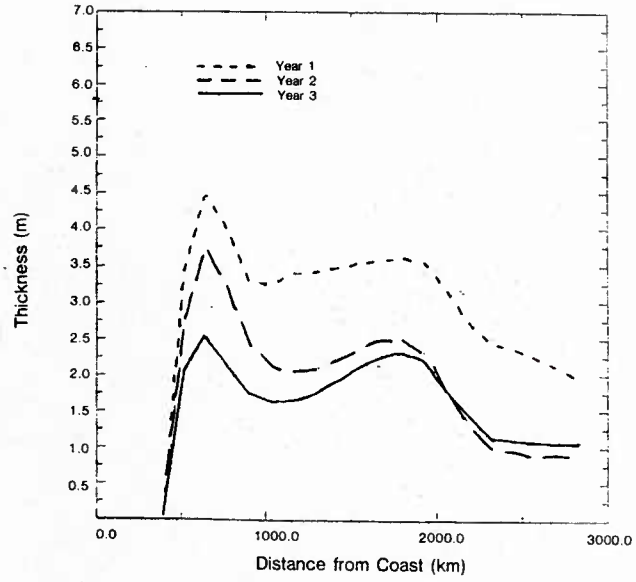

Figure 11b. Evolution of ice thickness from the central Arctic model in March along transect 2.

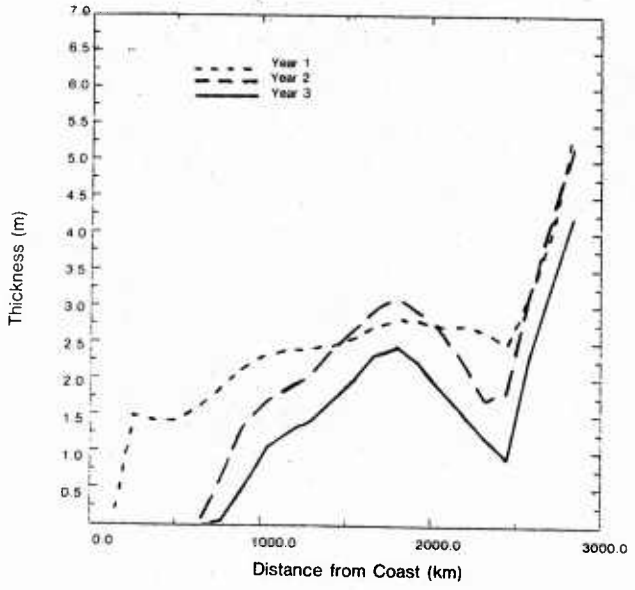

Figure 12a. Evolution of ice thickness from the central Arctic model in September from transect 1.

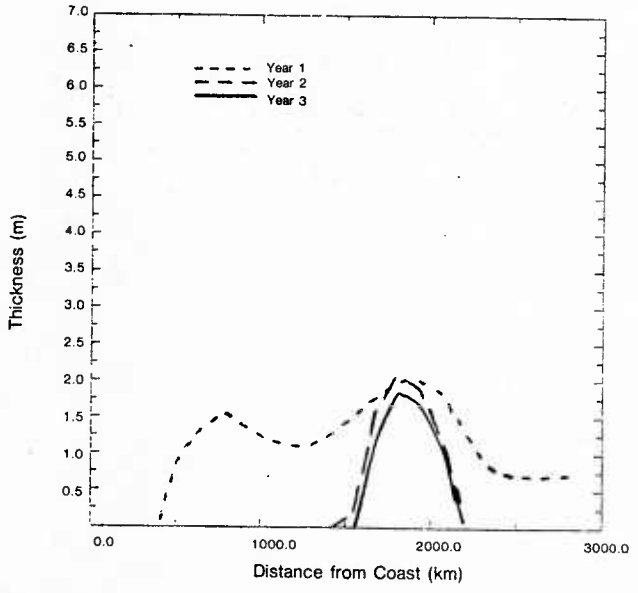

Figure 12b. Evolution of ice thickness from the central Arctic model in September from transect 2.

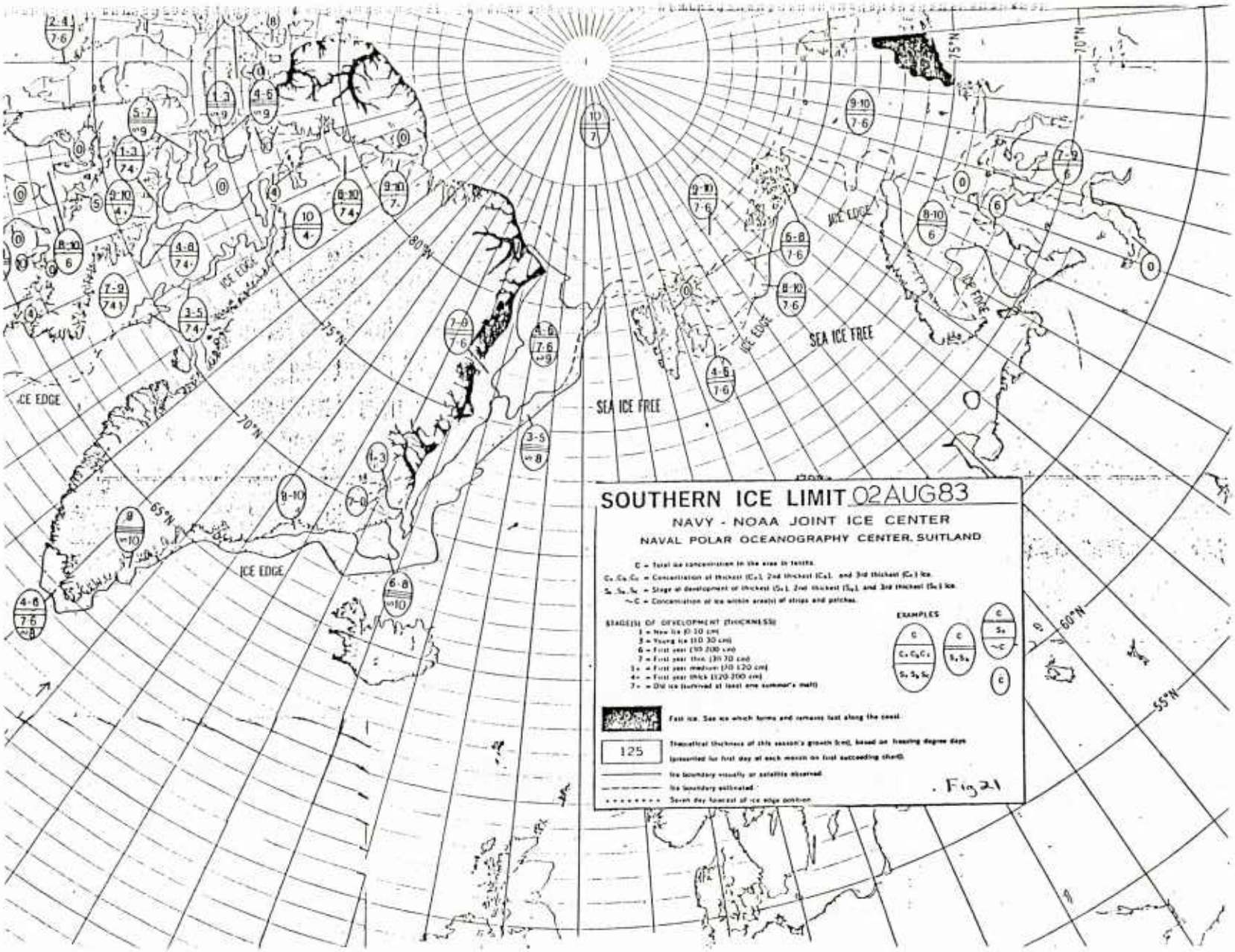

Figure 13. NPOC southern ice edge limit for August 2, 1983.

ICE THICKNESS

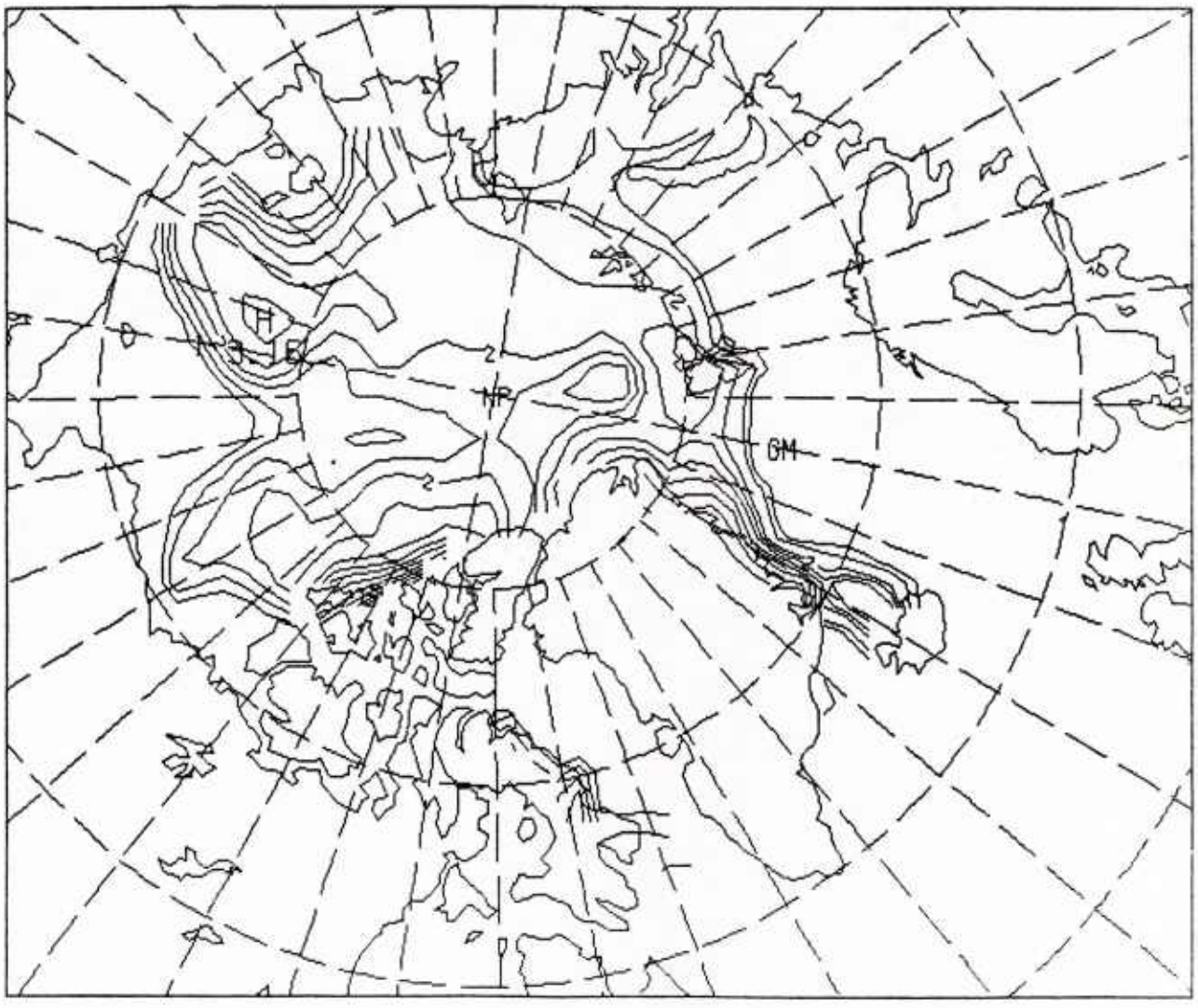

Figure 14. Ice model thickness contours (m) for the PIPS model using the Skiles ocean currents August 4, 1983. Contours go from 0-10 m by 0.5 m.

ICE THICKNESS

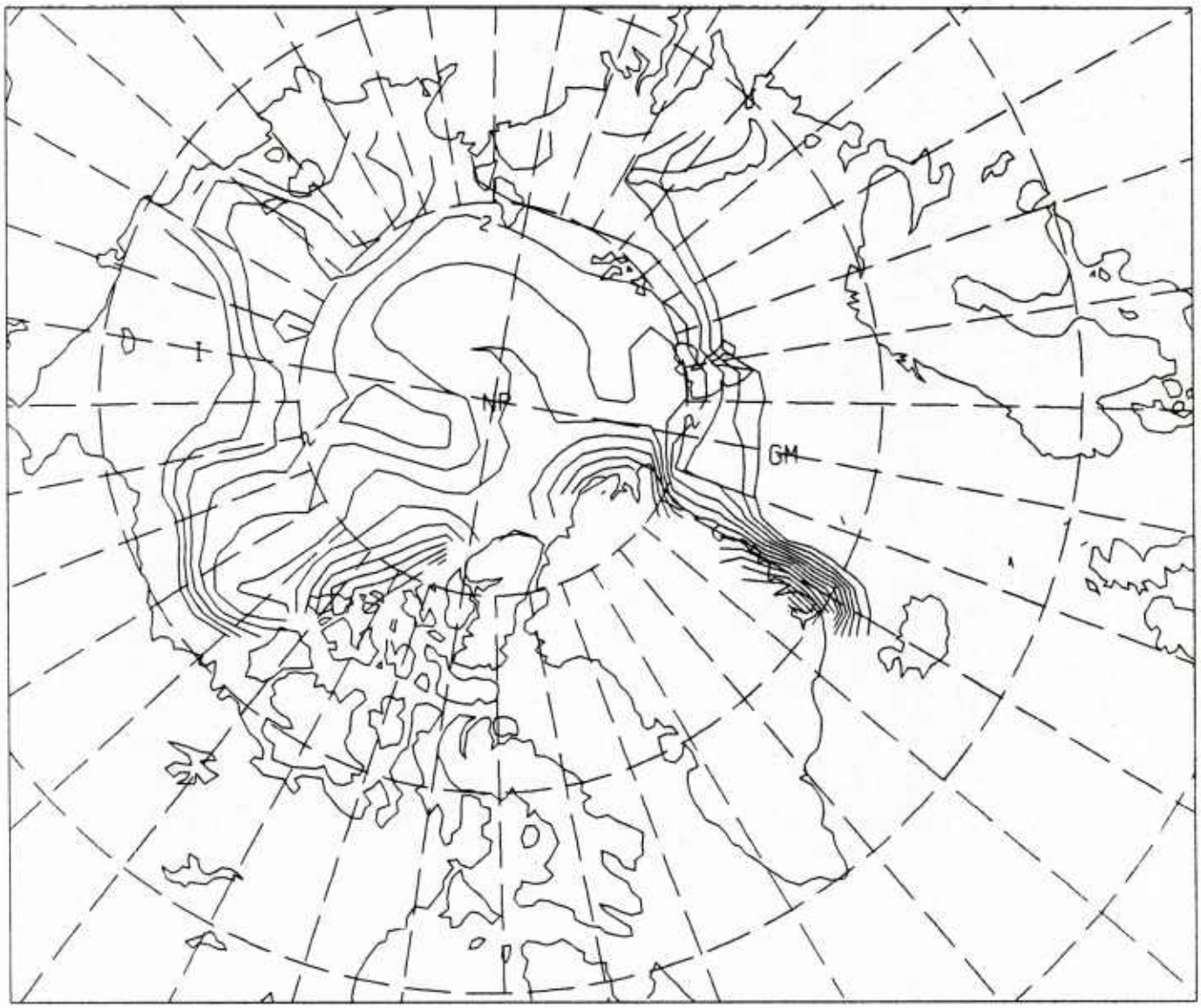

Figure 15. Ice model thickness contours (m) for the PIPS model using the Hibler-Bryan ocean currents August 4, 1983. Contours go from 0-10 m by 0.5 m.

MØNTHLY HEAT FLUX

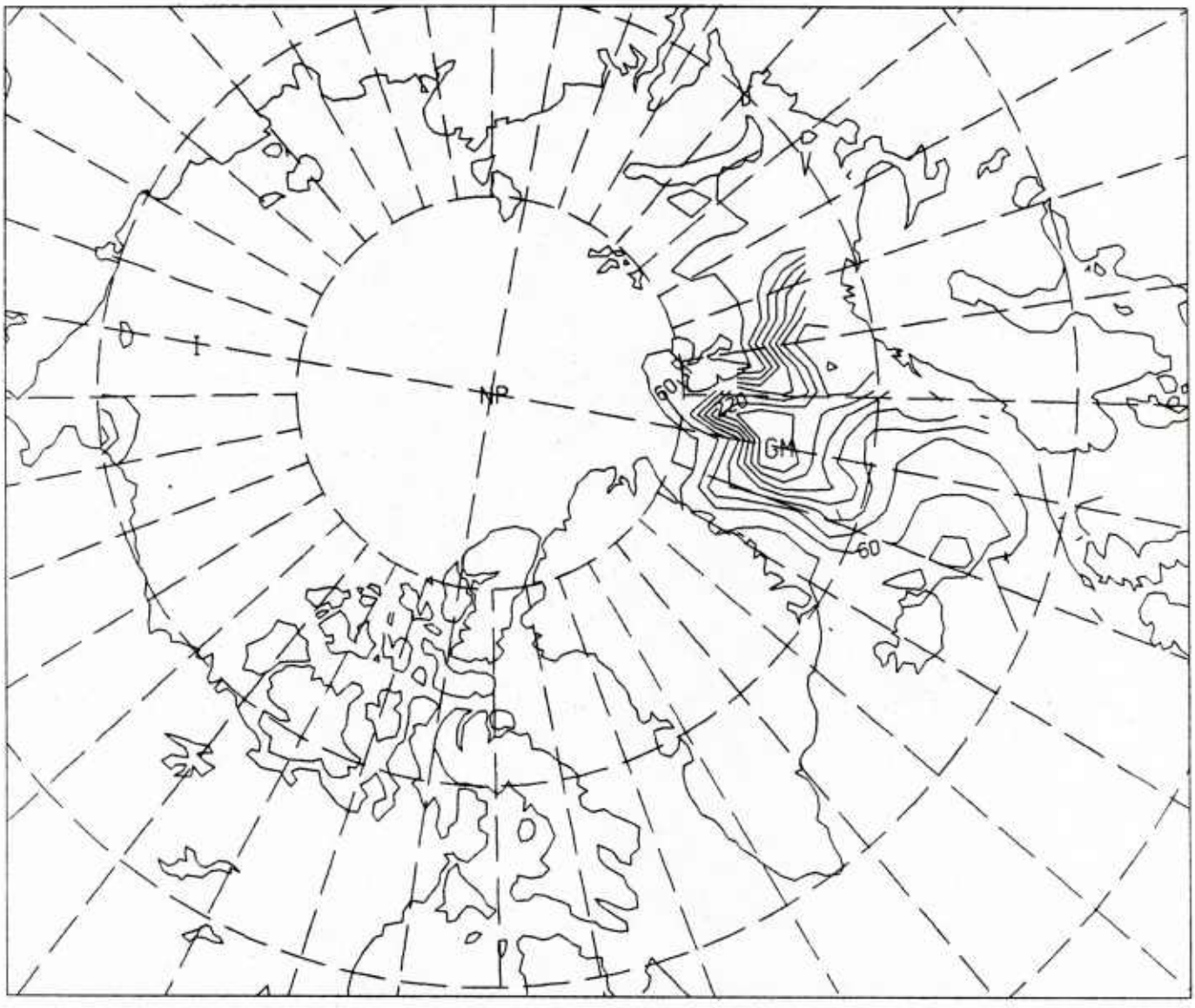

Figure 16a. Hibler-Bryan deep oceanic heat fluxes for March in watts m^{-2}. *Contours go from* -100 *to 340 at intervals of 40. Central Arctic values approximately 2 watts* m^{-2}.

MØNTHLY HEAT FLUX

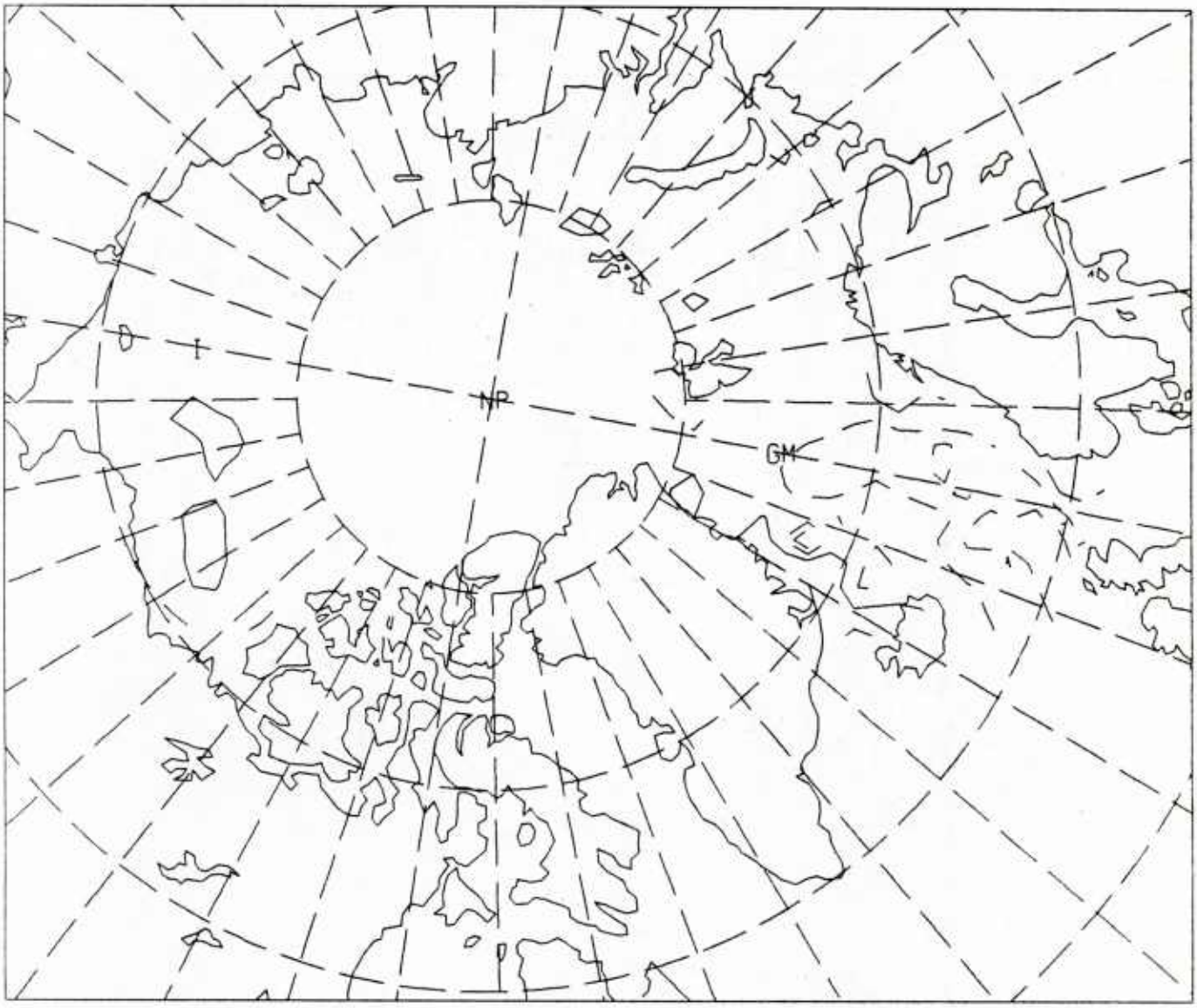

Figure 16b. Hibler-Bryan deep oceanic heat fluxes for September in watts m^{-2}. Contours go from -100 to 340 at intervals of 40. Central Arctic values approximately 2 watts m^{-2}.

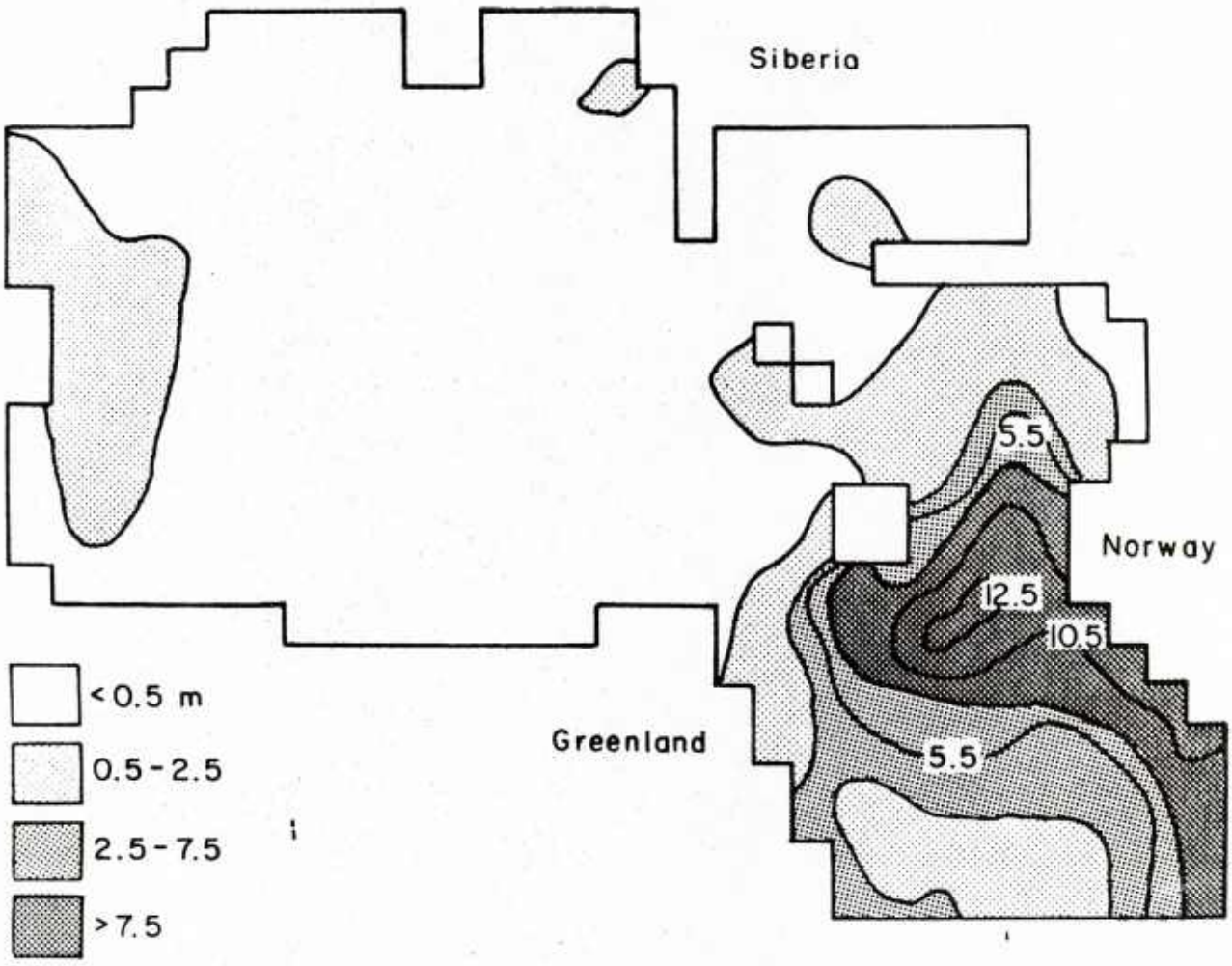

Figure 17. Average annual heat gained by the upper layer of the ocean from the deeper ocean and lateral heat transport. Contours are in capacity of heat to melt meters of ice per year. (1 m/year = 9.57 watts m^{-2}) (from Hibler and Bryan, 1984).

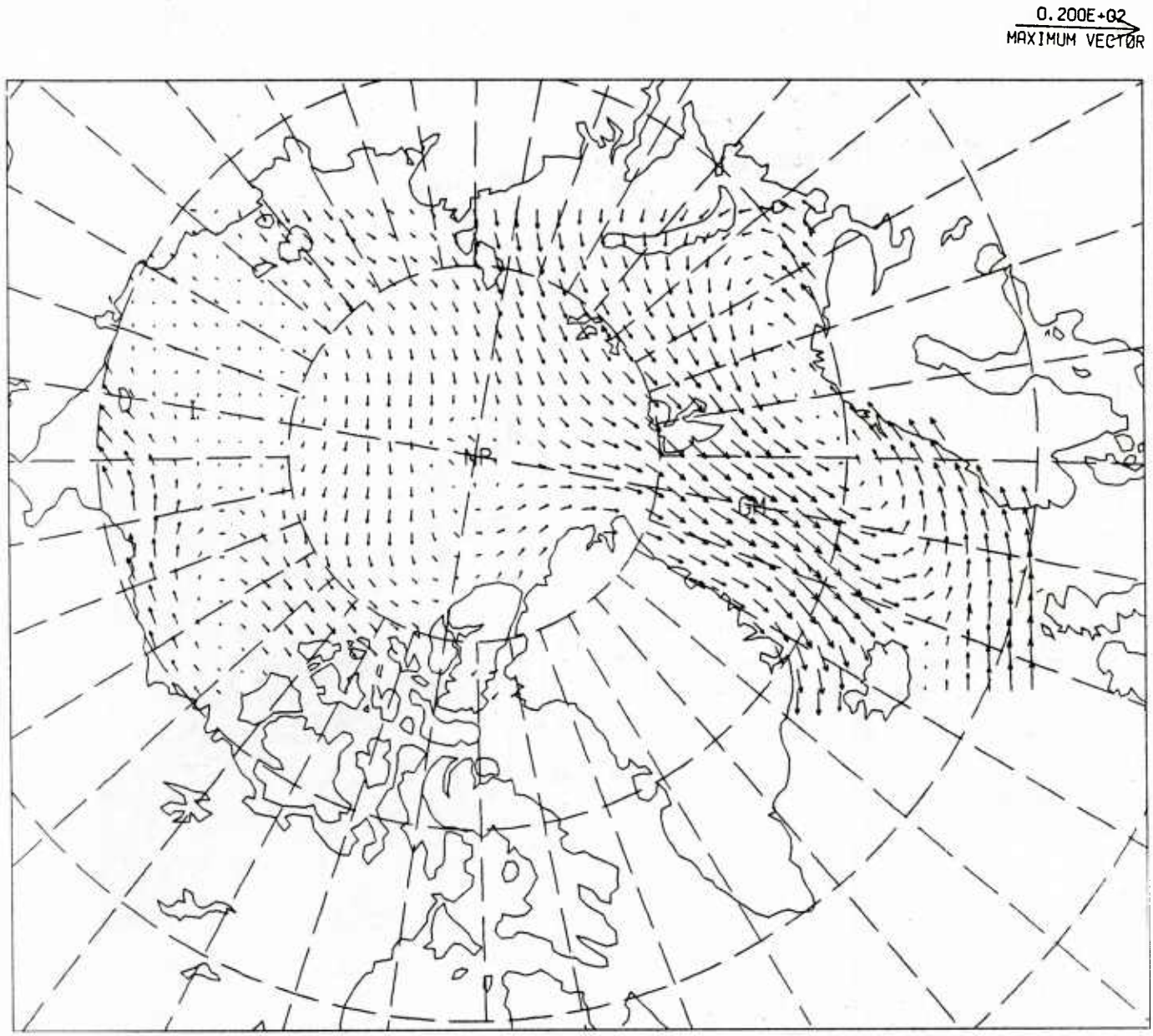

Figure 18a. Third-year averaged solution for the PIPS model, wind velocity—maximum vector 20 m/sec.

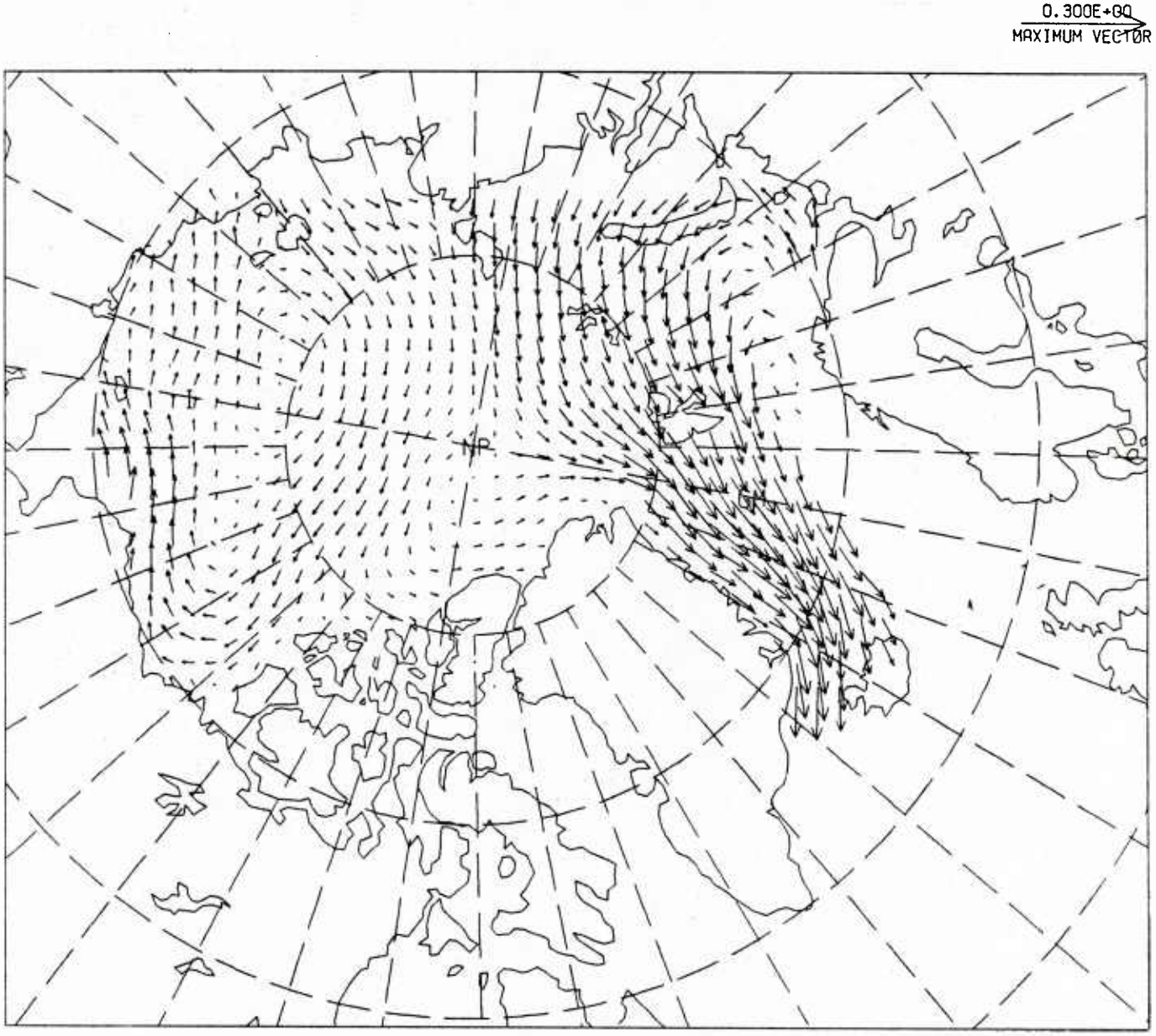

Figure 18b. Third-year averaged solutions for the PIPS model, ice velocity—maximum vector 0.3 m/sec

ICE THICKNESS

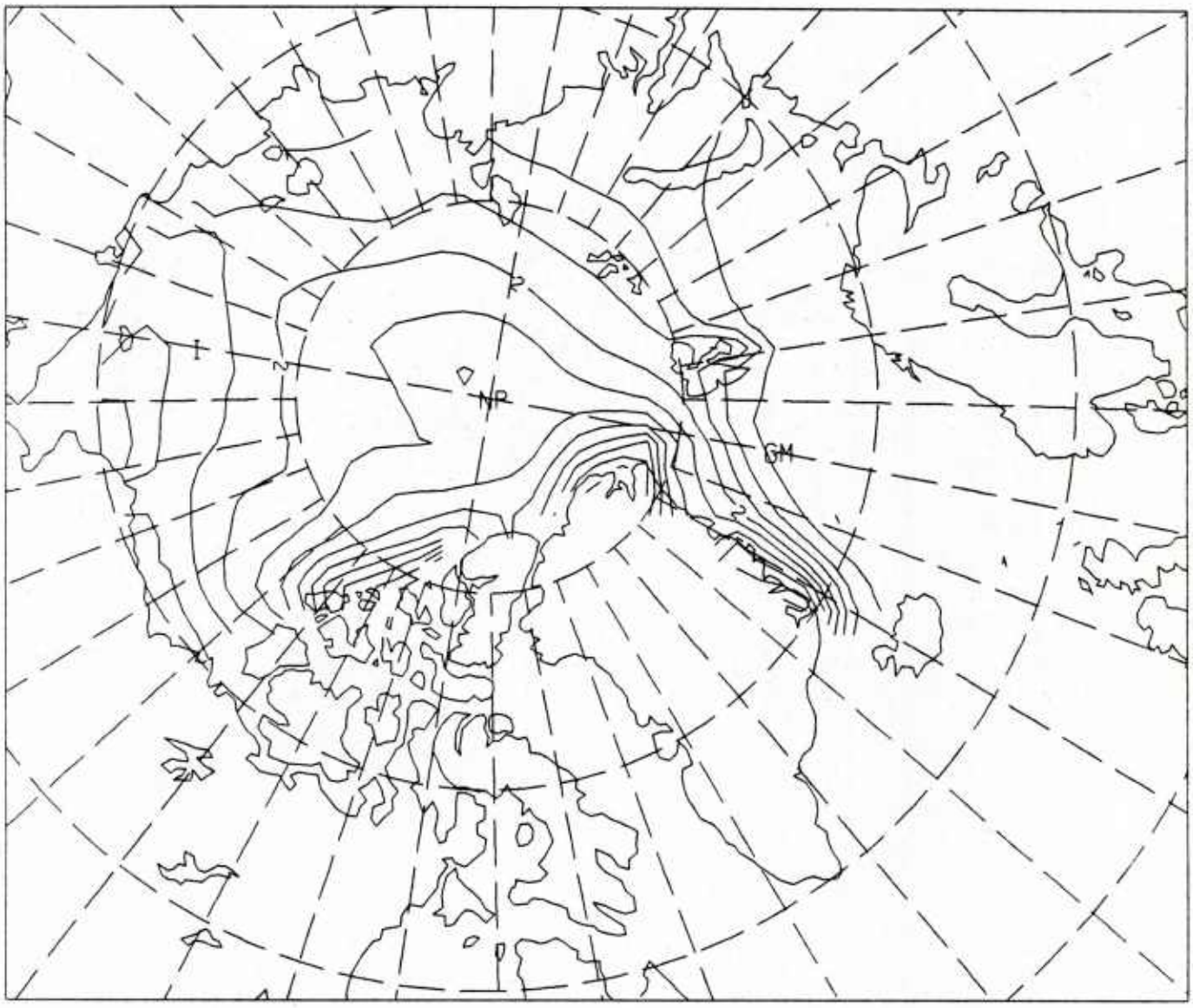

Figure 18c. Third-year averaged solutions for the PIPS model, ice thickness—contours go from 0·10 m by 0.5 m.

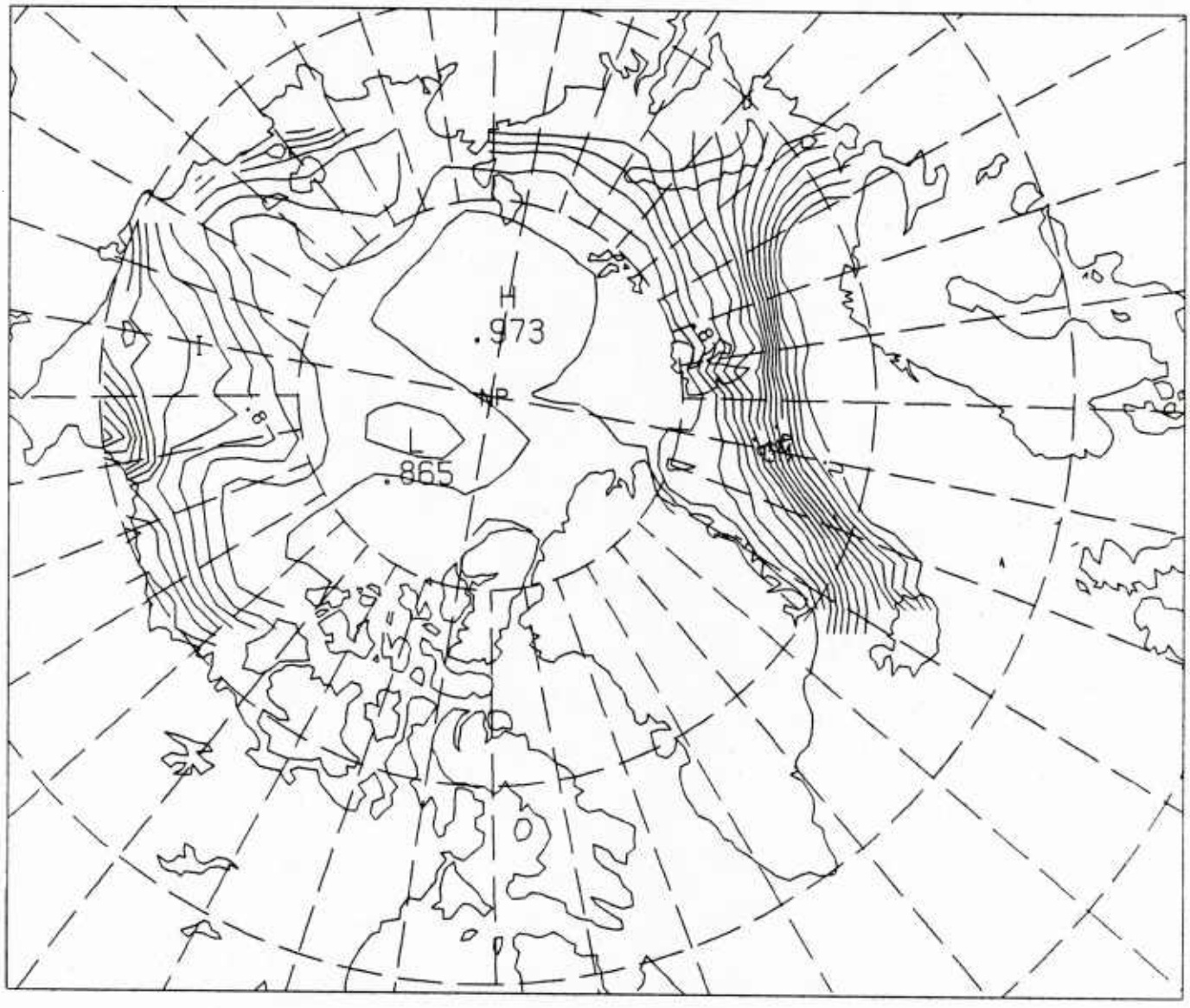

Figure 18d. Third-year averaged solutions for the PIPS model, percentage of ice concentration (compactness) at 5% intervals.

TØTAL GRØWTH ØF ICE

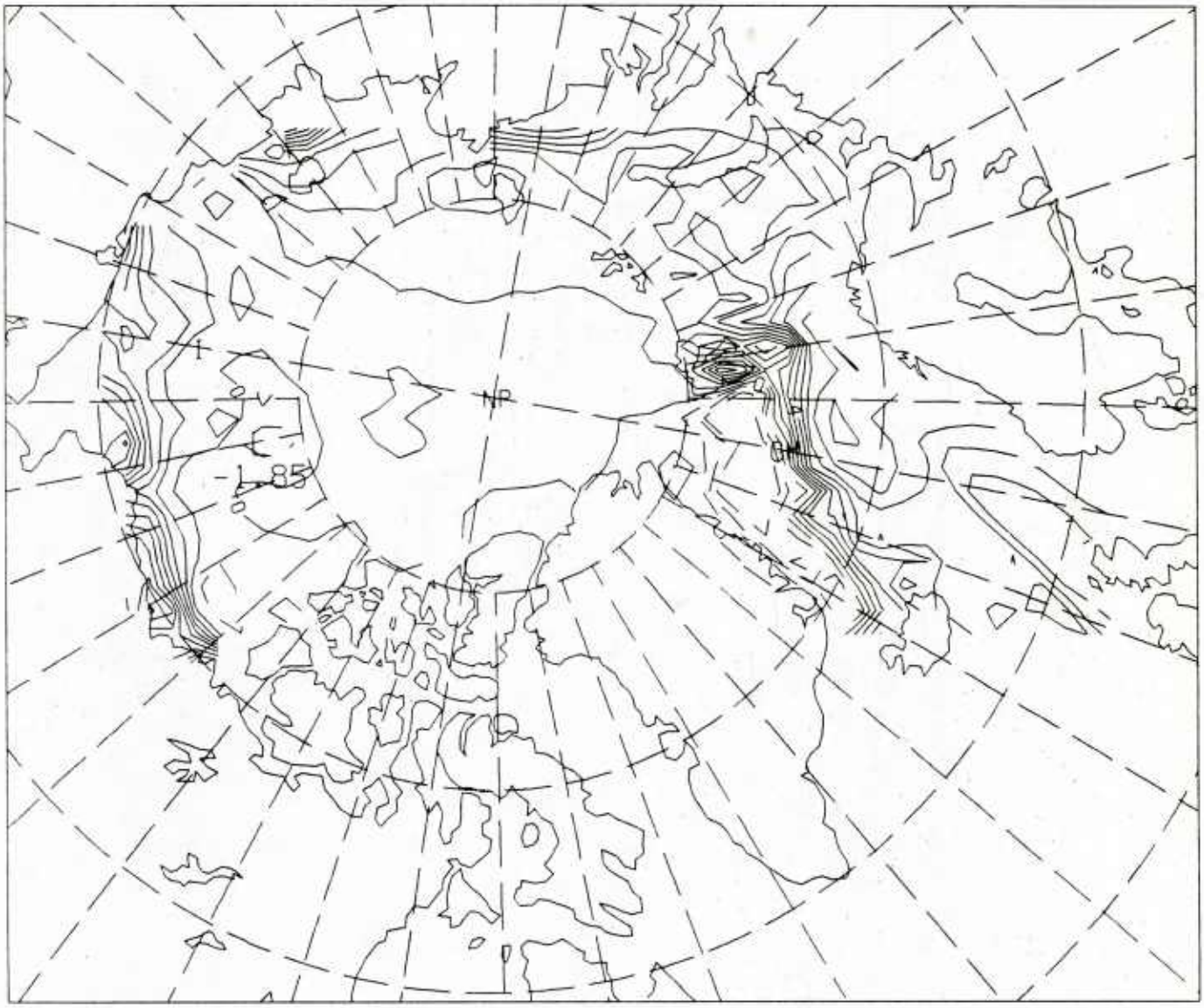

Figure 18e. Third-year averaged solutions for the PIPS model, total growth of ice (thick plus thin minus lateral melt)—contours go from −3 m to 7 m by 1 m.

GRØWTH ØF THICK ICE

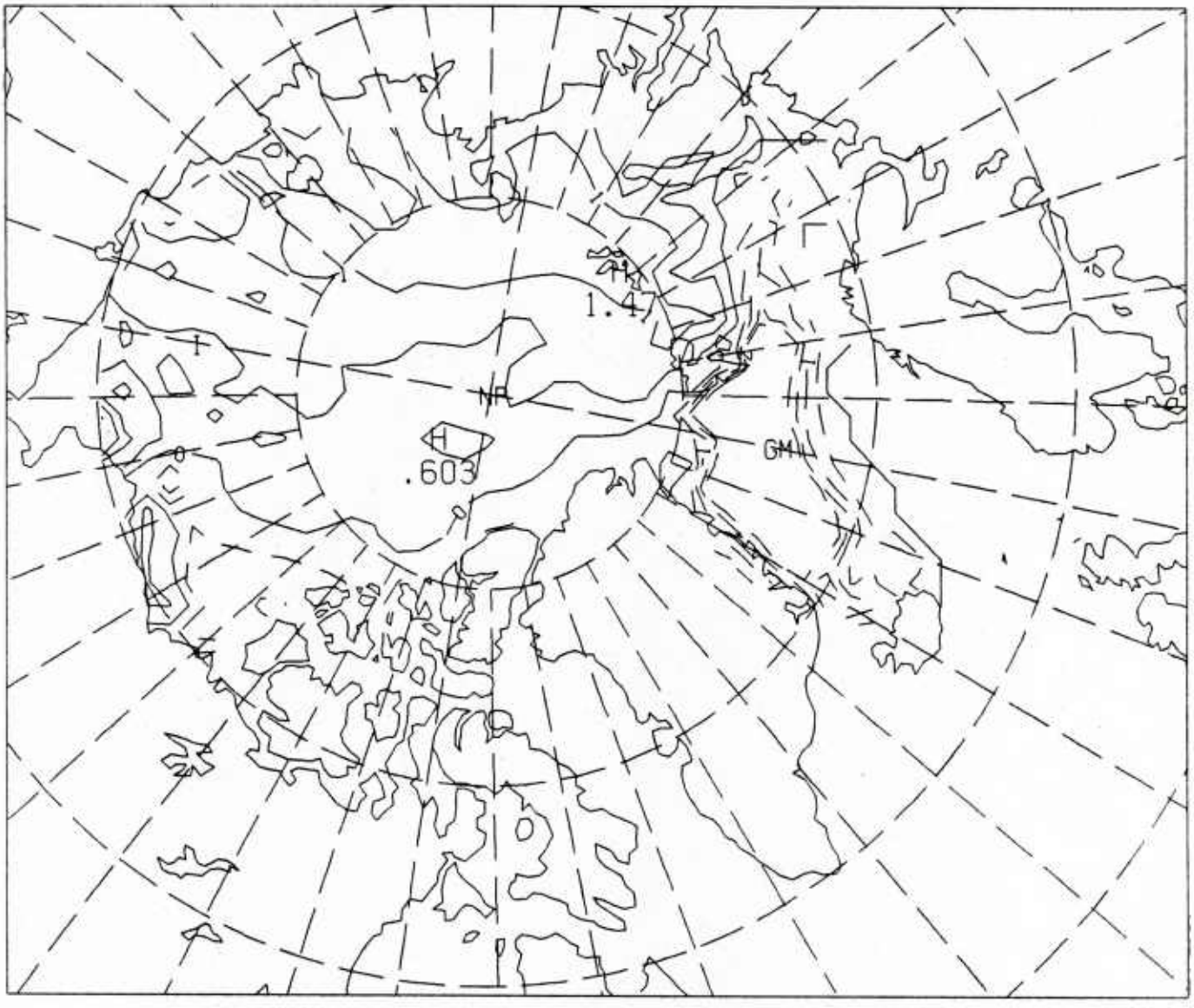

Figure 18f. Third-year averaged solutions for the PIPS model, growth of thick ice—contours go from −2 m to 2 m by 0.5 m.

GRØWTH ØF ICE ØN ØPEN WATER

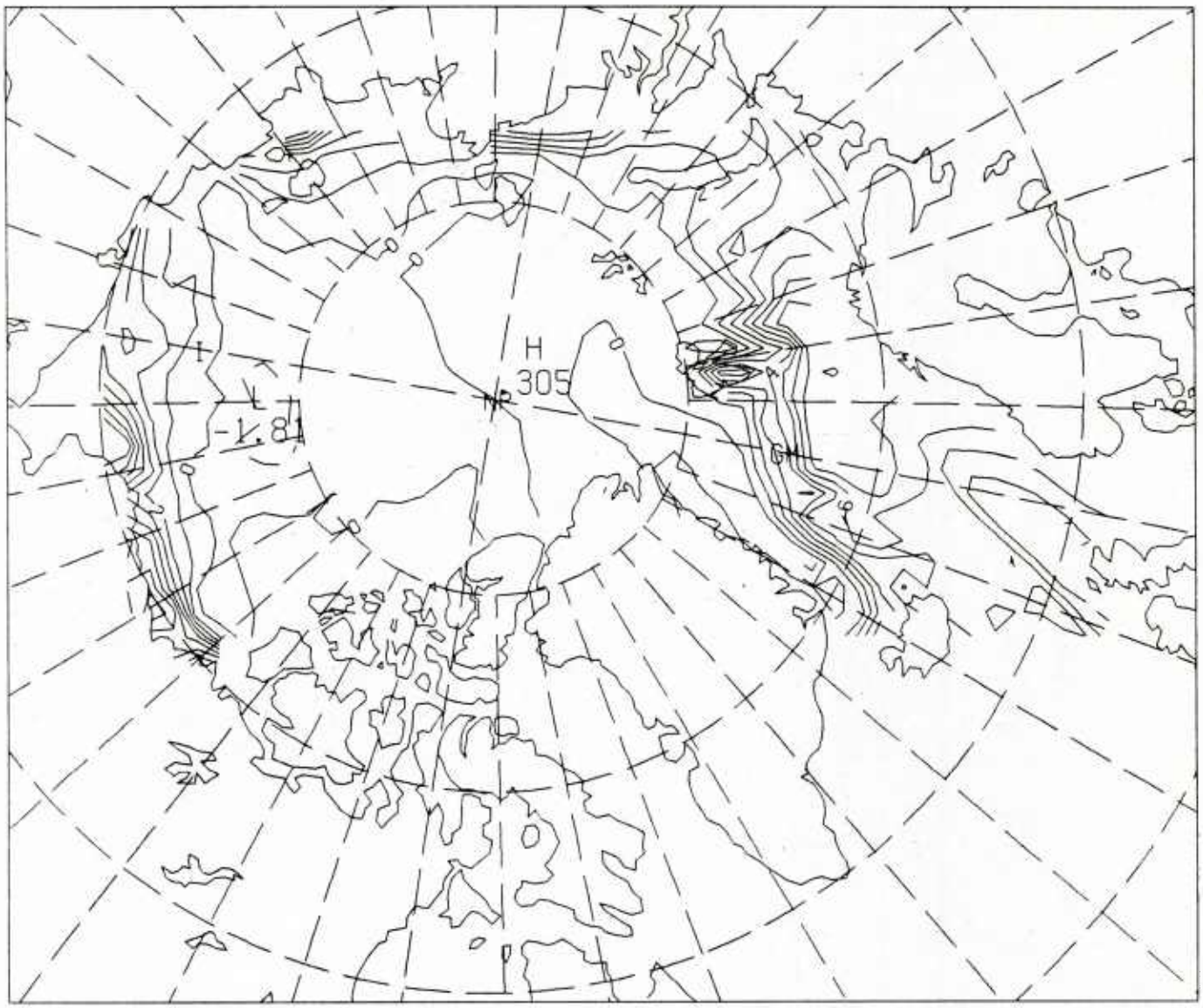

Figure 18g. Third-year averaged solutions for the PIPS model, growth of thin ice or ice on open water without the effects of lateral melt—contours go from −2 m to 7 m by 0.5 m.

ICE STRENGTH

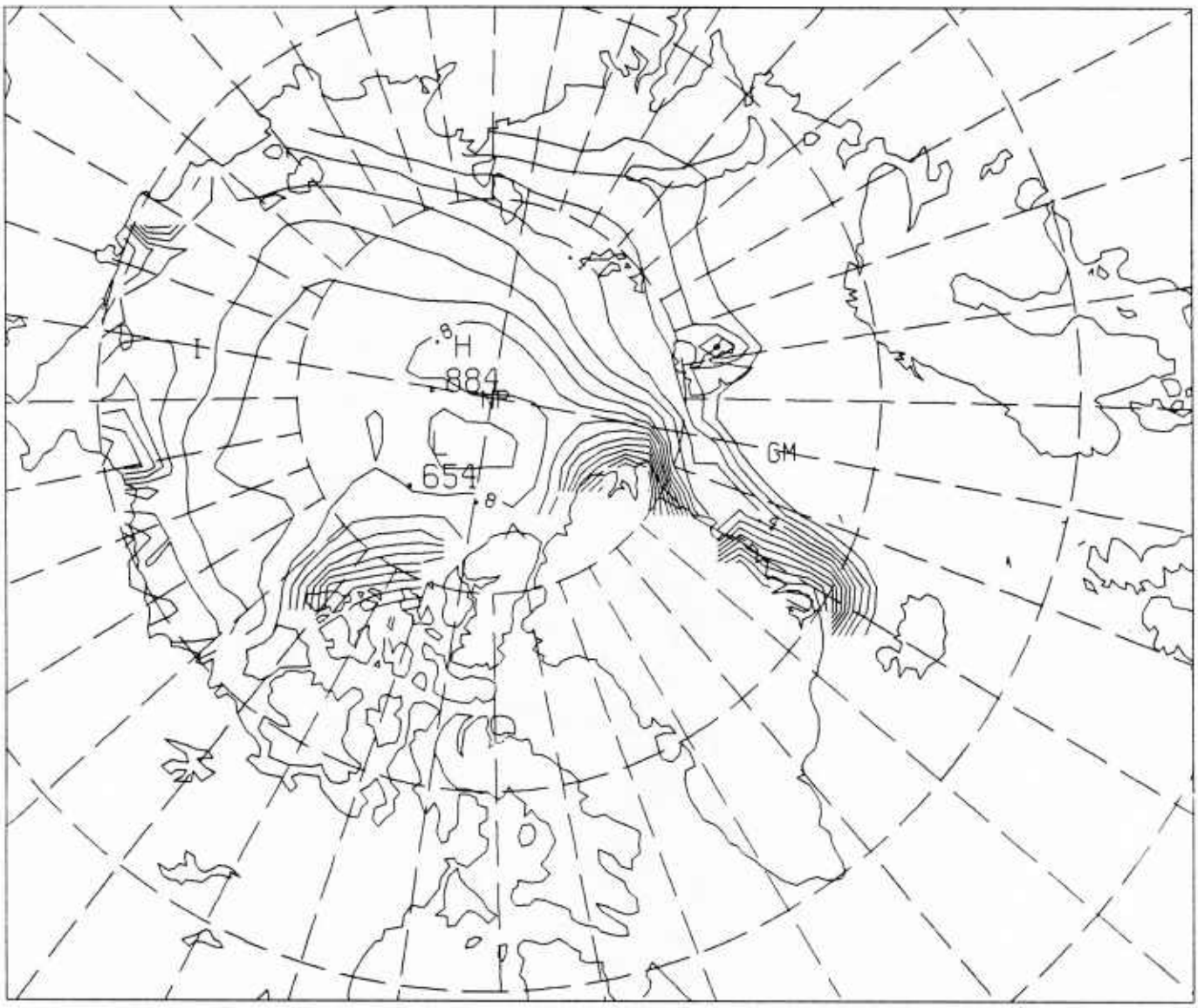

Figure 18b. Third-year averaged solutions for the PIPS model, ice strength or pressure—contours go from 0 to 2 (x 10^{-5}) Nt m^{-2} by 0.1.

ICE DIVERGENCE

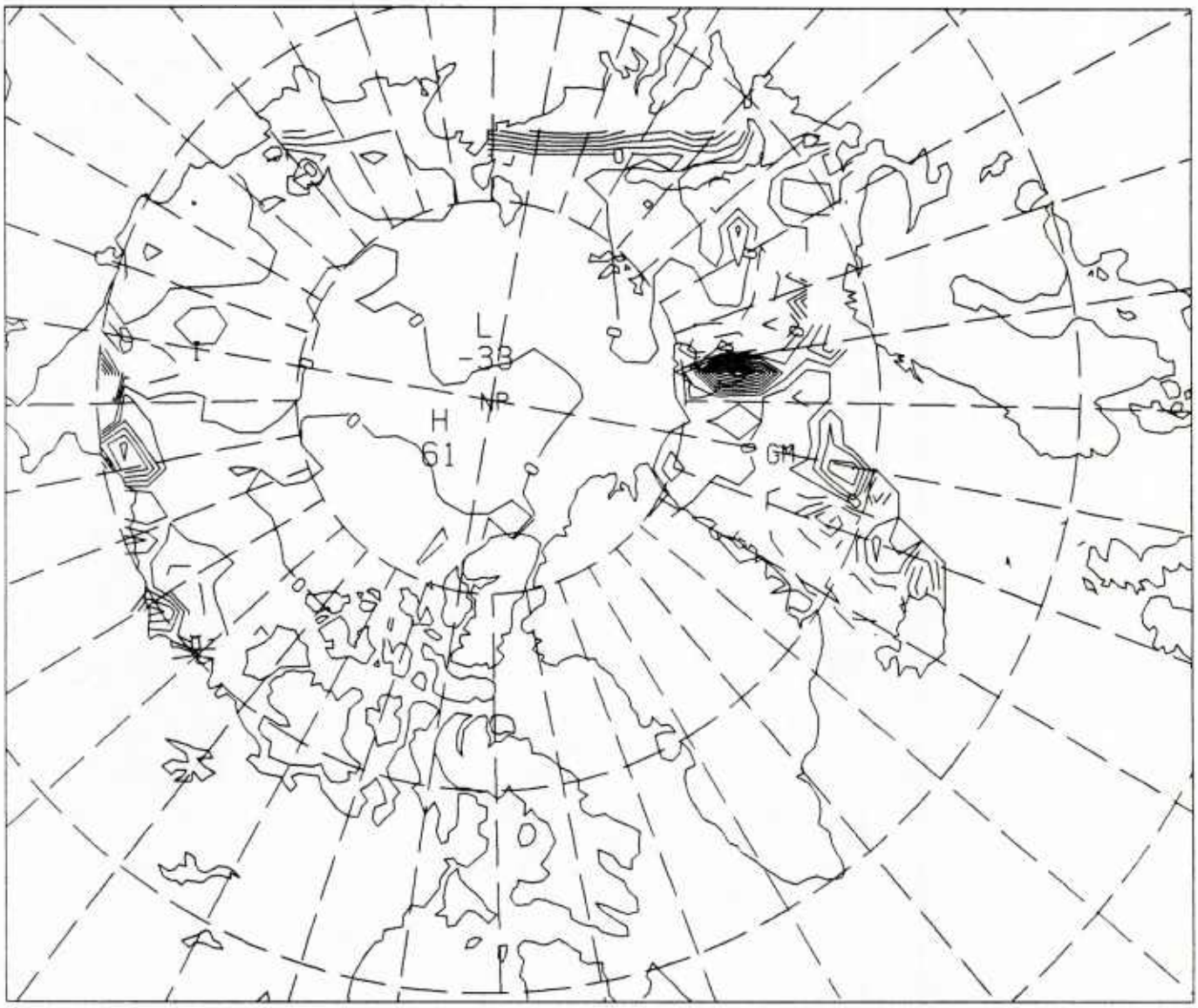

Figure 18i. Third-year averaged solutions for the central Arctic model, ice divergence (x 10^4) in sec^{-1} contours go from -0.008 to 0.009 at intervals of 0.001.

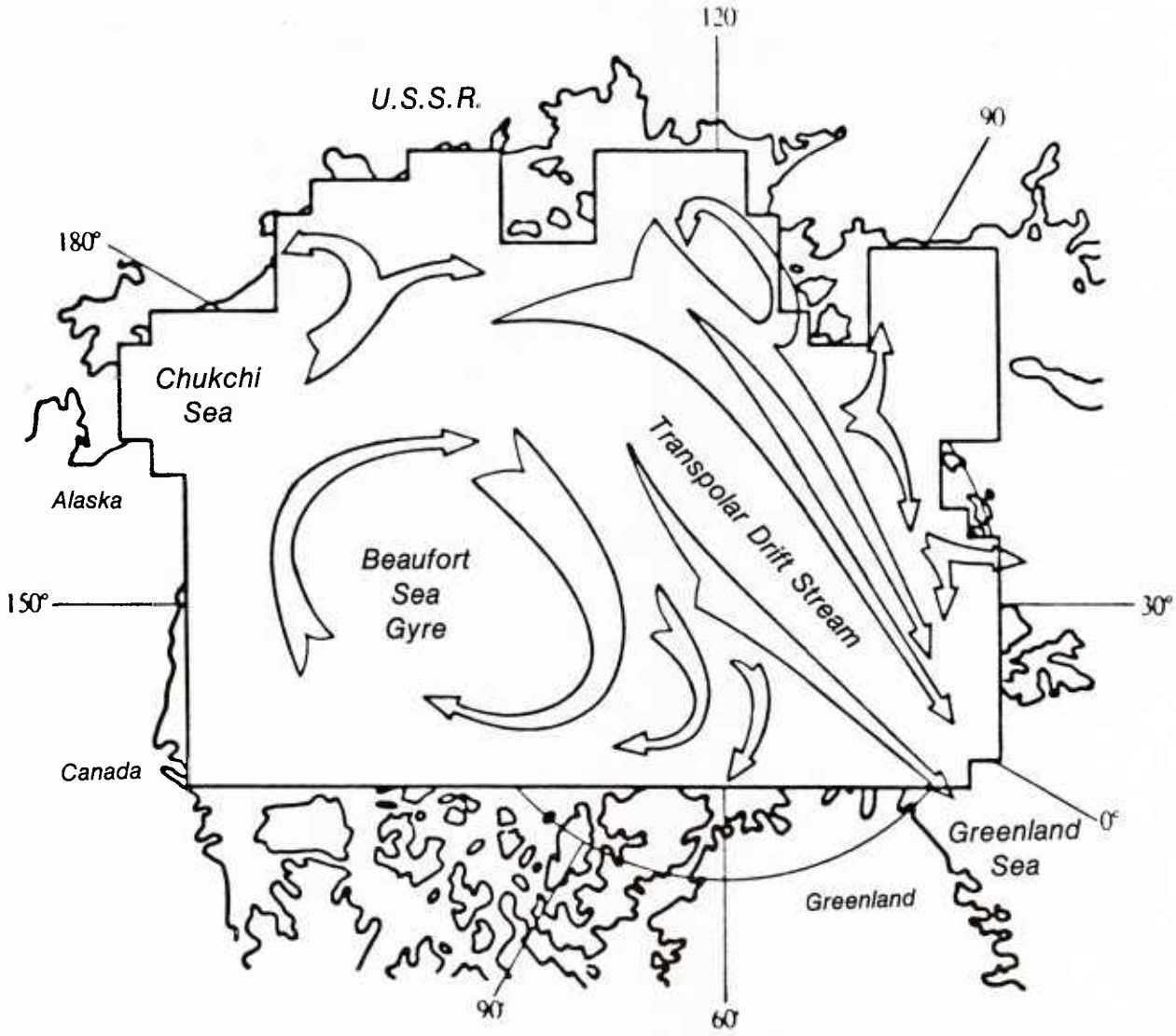

Figure 19. Pattern of mean drift in the Arctic ocean (from Gordienko, 1958).

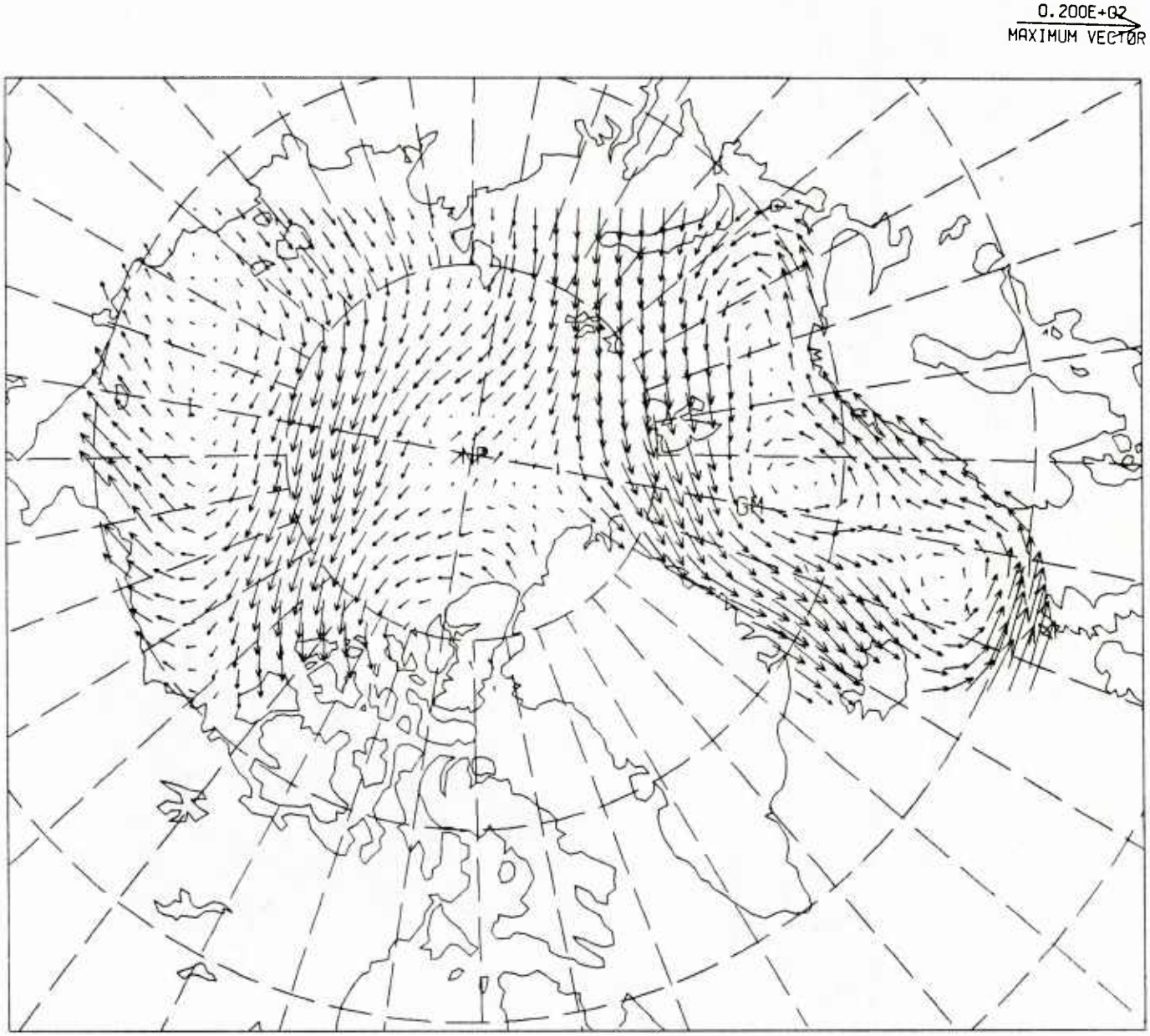

Figure 20a. March mean solutions from the third year of integration of PIPS using both Hibler-Bryan ocean currents and deep oceanic heat fluxes, wind velocities—maximum vector is 20 m/sec.

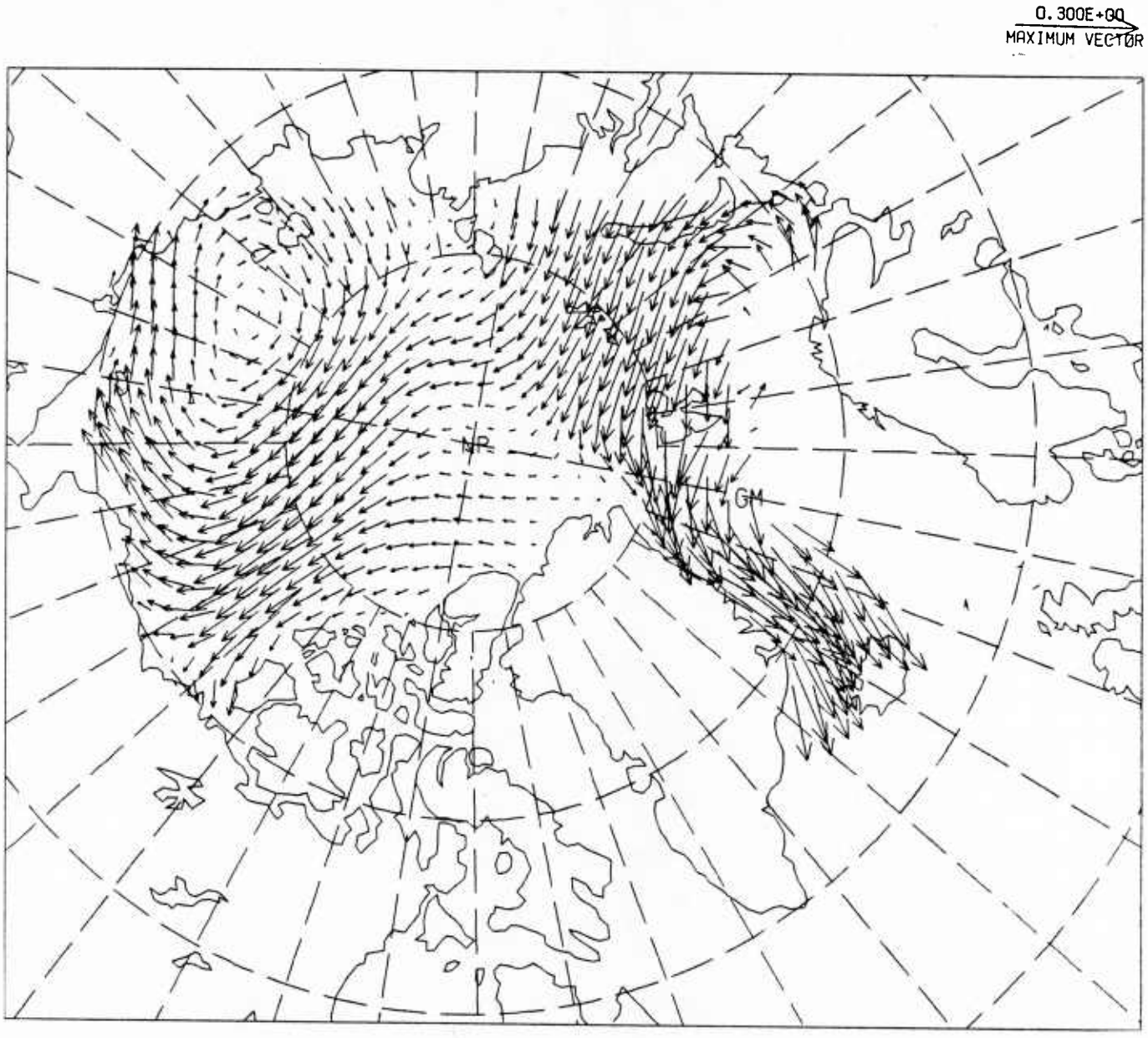

Figure 20b. March mean solutions from the third year of integration of PIPS using both Hibler-Bryan ocean currents and deep oceanic heat fluxes, ice drift velocities—maximum vector is 0.3 m/sec.

ICE THICKNESS

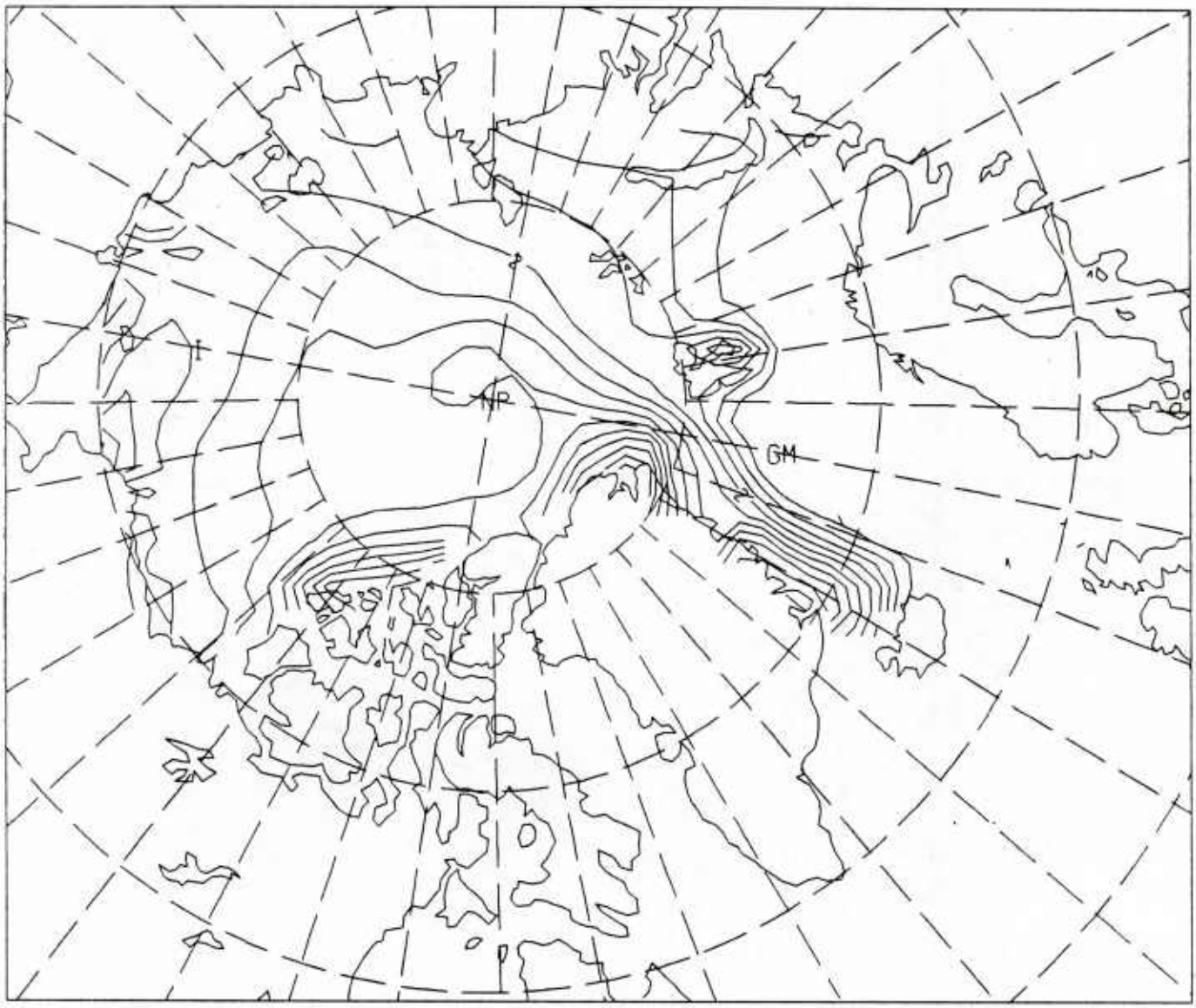

Figure 20c. March mean solutions from the third year of integration of PIPS using both Hibler-Bryan ocean currents and deep oceanic heat fluxes, ice thickness—contours go from 0 to 10 m at intervals of 0.5 m.

ICE CØNCENTRATIØN

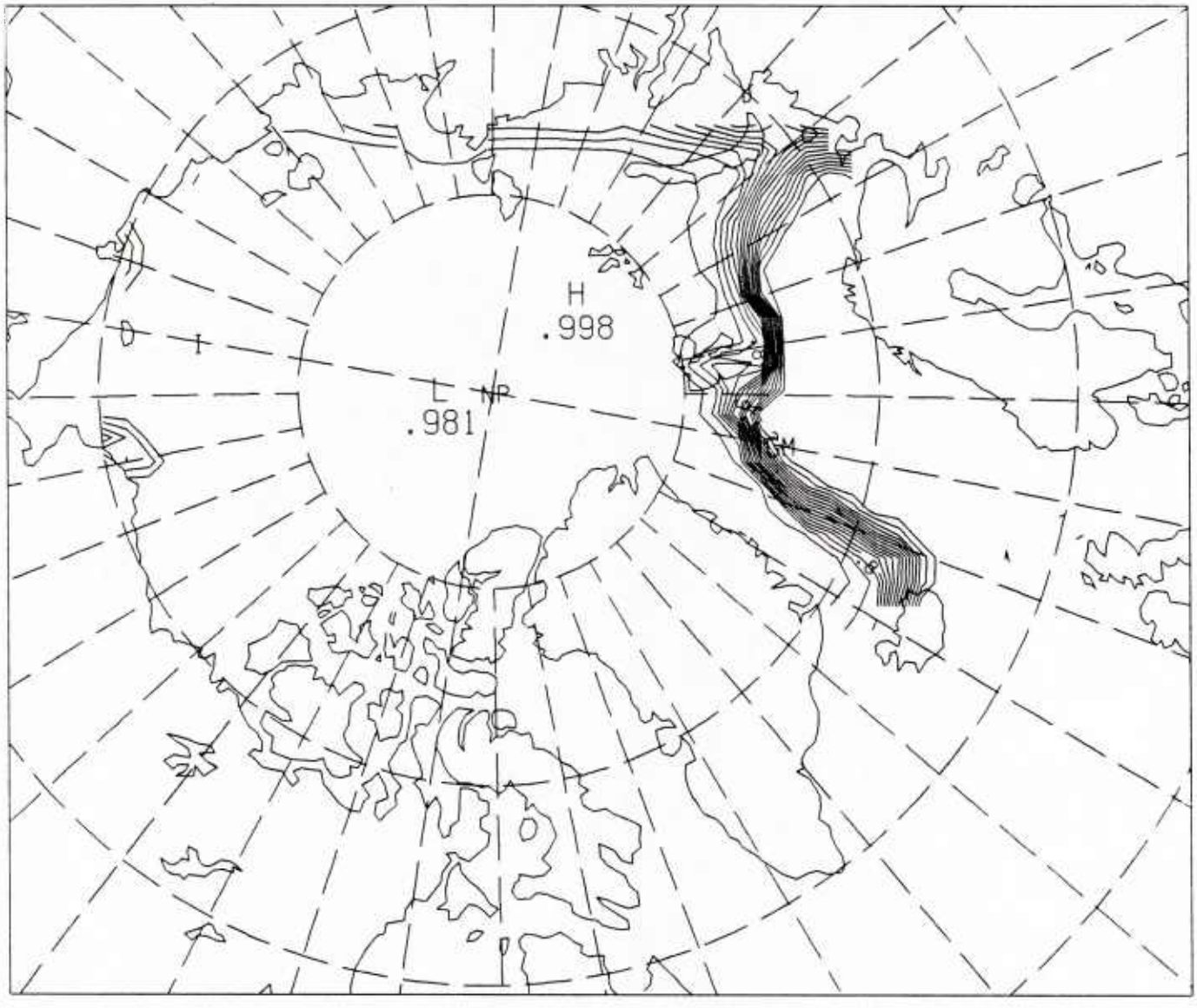

Figure 20d. March mean solutions from the third year of integration of PIPS using both Hibler-Bryan ocean currents and deep oceanic heat fluxes, percentage of ice concentration at 5% intervals.

TØTAL GRØWTH ØF ICE

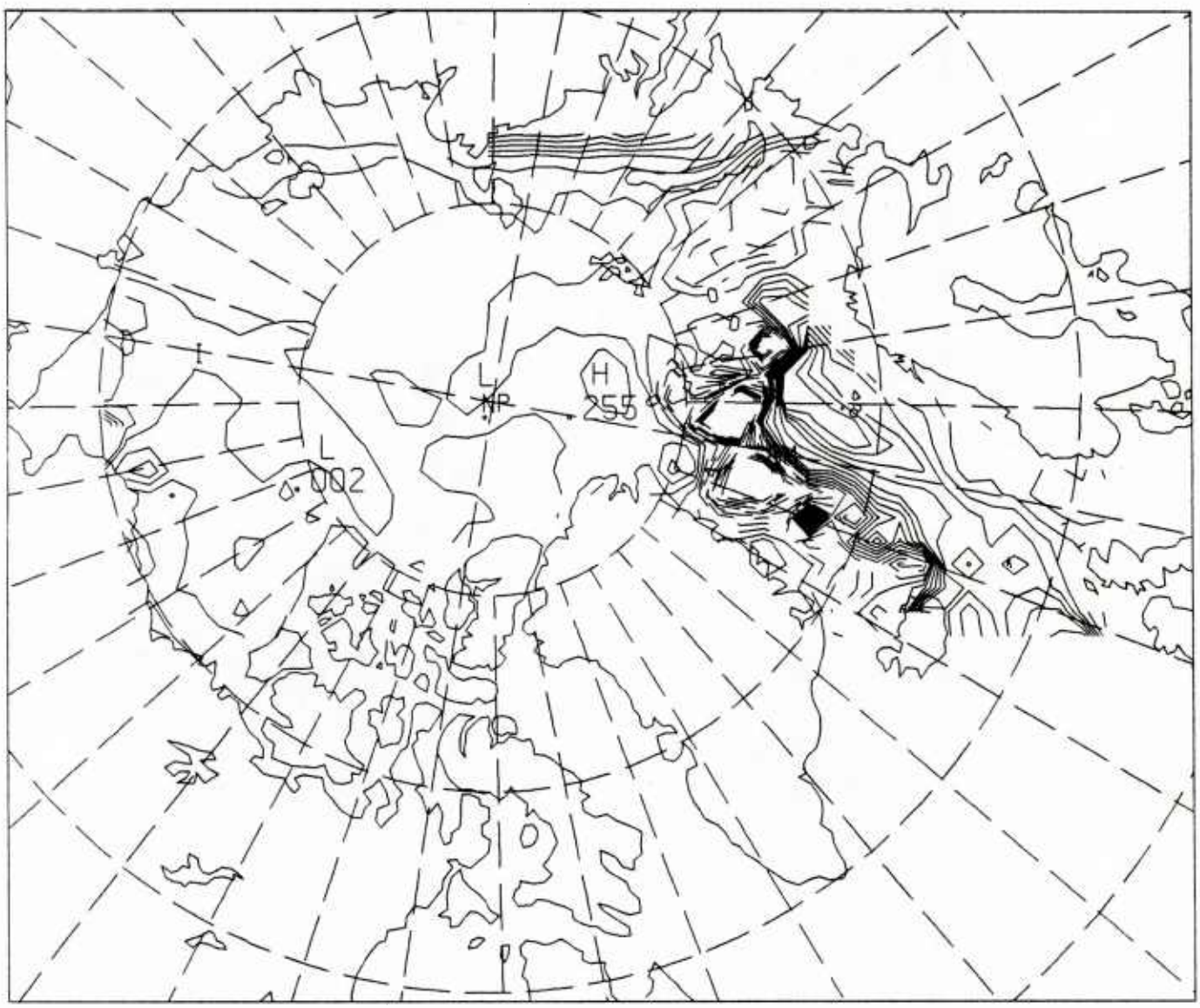

Figure 20e. March mean solutions from the third year of integration of PIPS using both Hibler-Bryan ocean currents and deep oceanic heat fluxes, total growth of ice (thick plus thin without the effects of lateral melt)—contours go from −1 m to 1 m by 0.1 m.

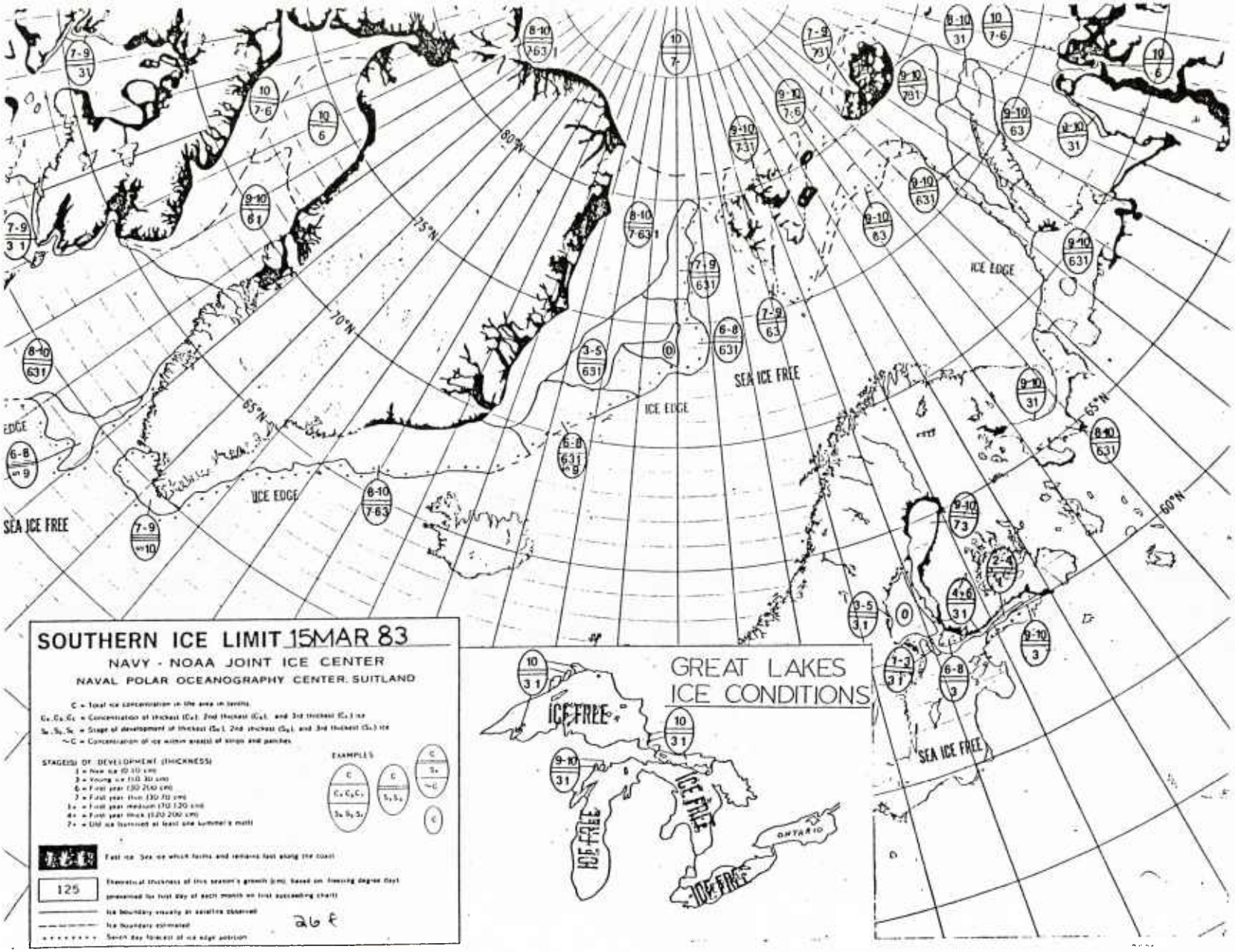

Figure 20f. March mean solutions from the third year of integration of PIPS using both Hibler-Bryan ocean currents and deep oceanic heat fluxes, NPOC southern ice edge—east from 3/15/83.

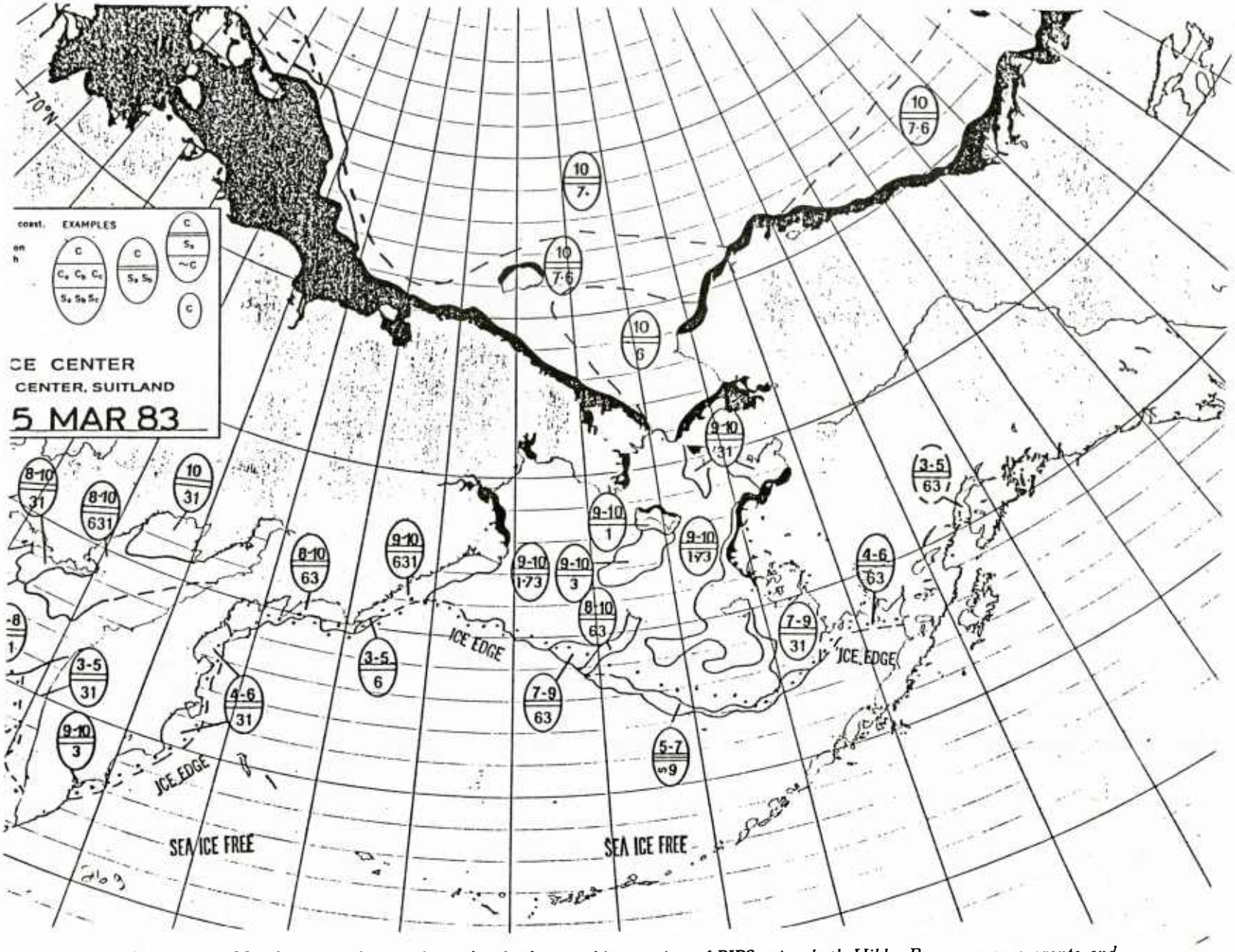

Figure 20g. March mean solutions from the third year of integration of PIPS using both Hibler-Bryan ocean currents and deep oceanic heat fluxes, NPOC southern ice edge—west from 3/15/83.

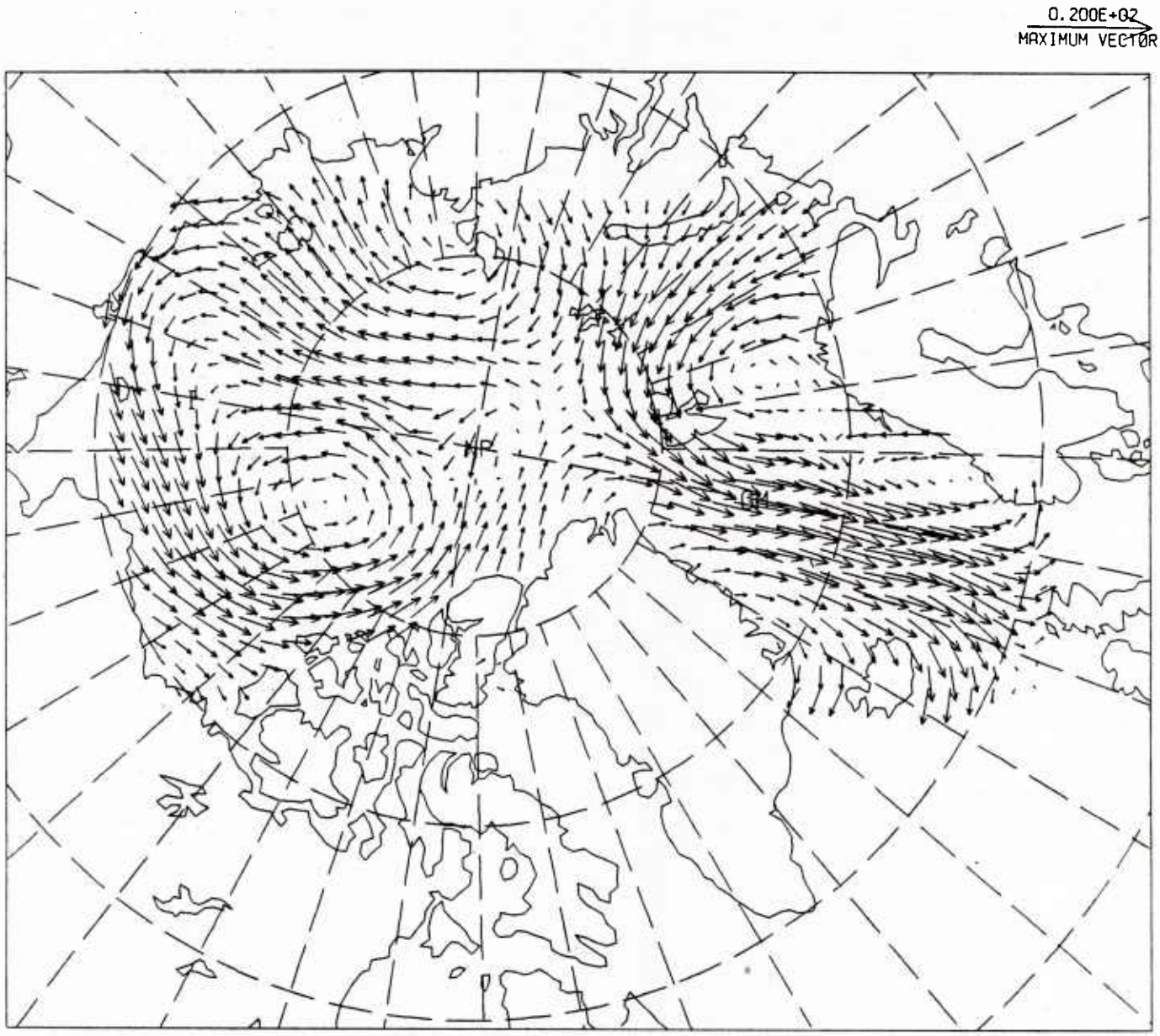

Figure 21a. September mean solutions from the third year of integration of PIPS using both Hibler-Bryan ocean currents and deep oceanic heat fluxes, wind velocities—maximum vecter is 20 m/sec.

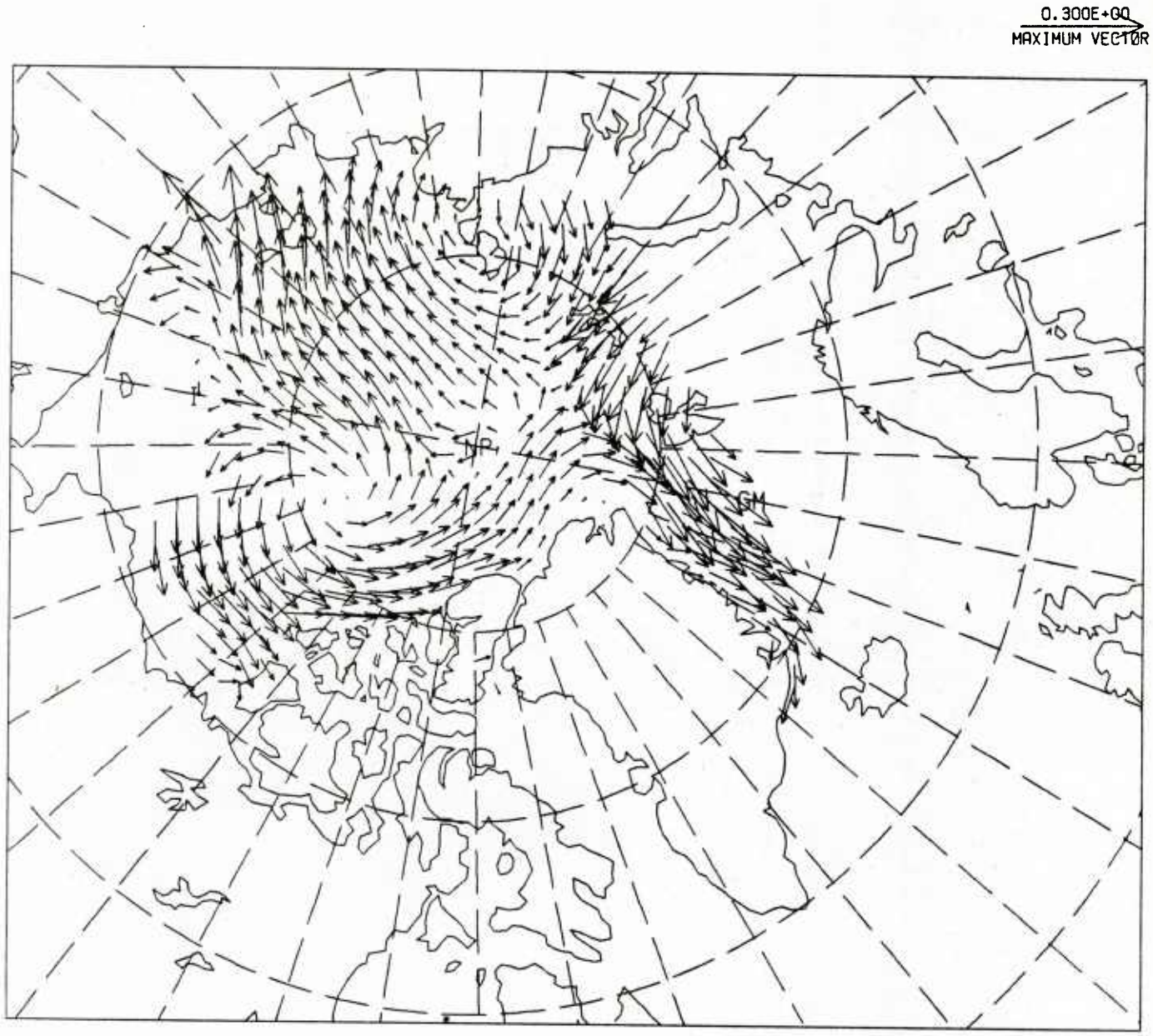

Figure 21b. September mean solutions from the third year of integration of PIPS using both Hibler-Bryan ocean currents and deep oceanic heat fluxes, ice drift velocities—maximum vector is 0.3 m/sec.

ICE THICKNESS

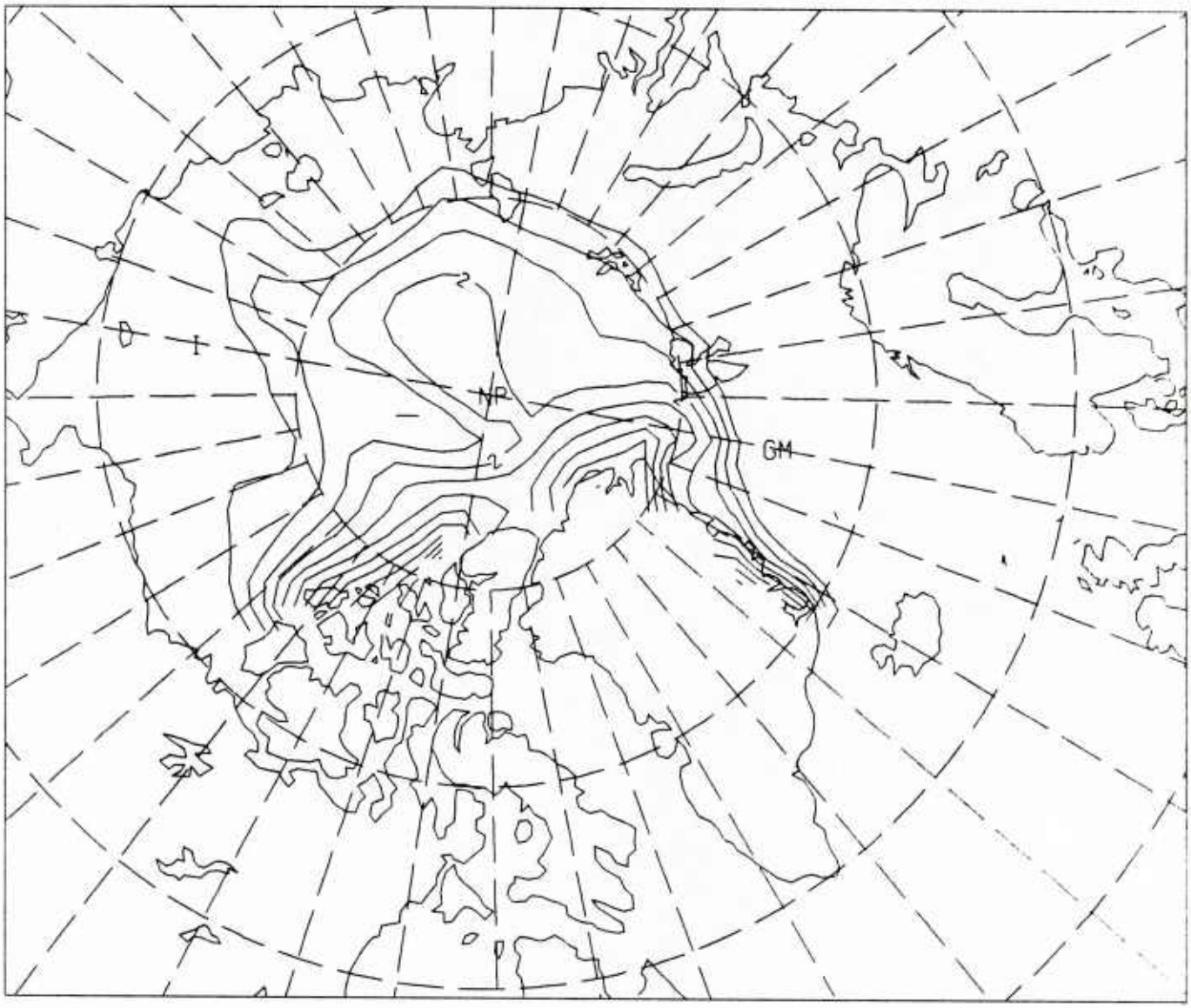

Figure 21c. September mean solutions from the third year of integration of PIPS using both Hibler-Bryan ocean currents and deep oceanic heat fluxes, ice thickness—contours go from 0 to 10 m at intervals of 0.5 m.

ICE CØNCENTRATIØN

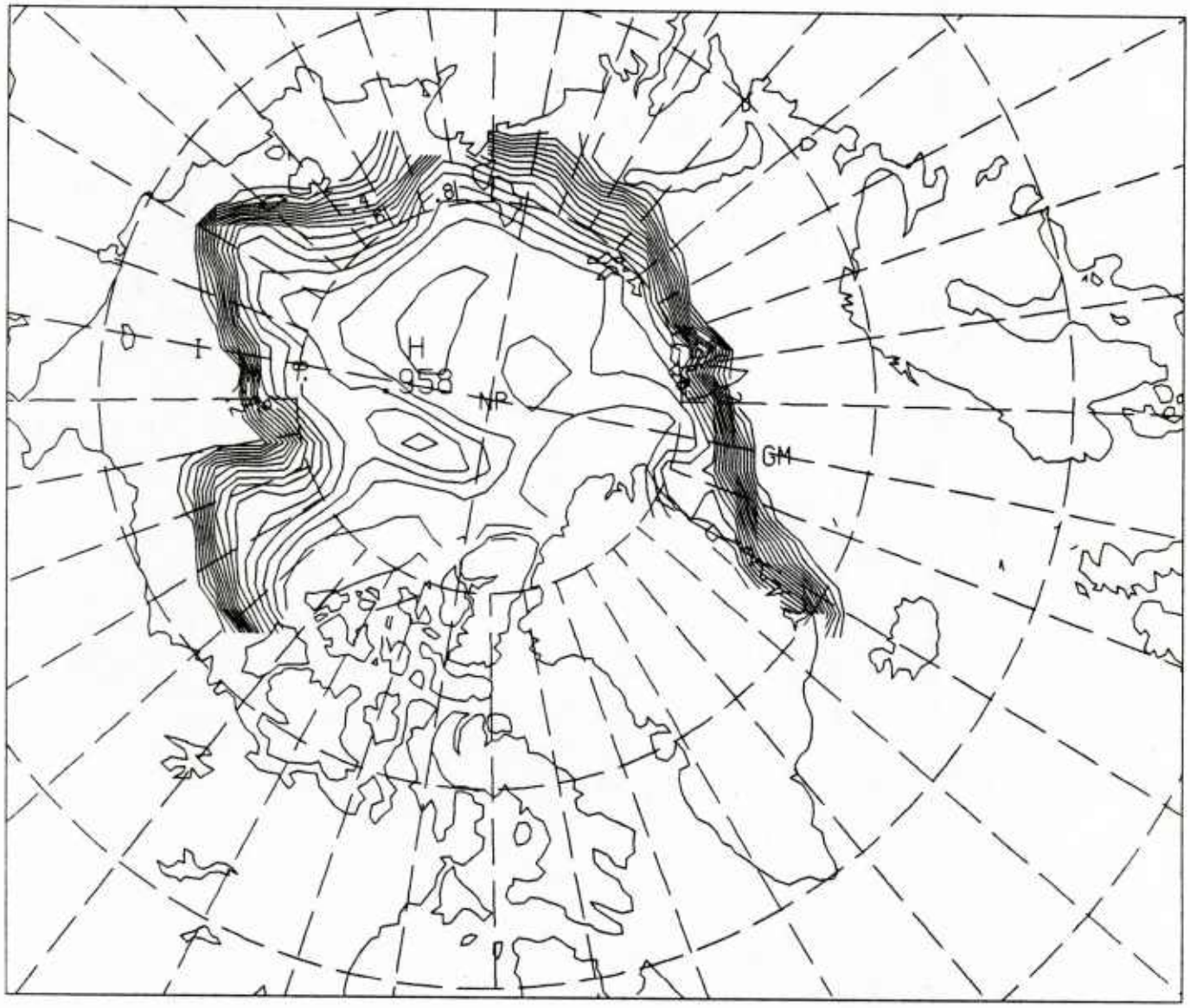

Figure 21d. September mean solutions from the third year of integration of PIPS using both Hibler-Bryan ocean currents and deep oceanic heat fluxes, percentage of ice concentration at 5% intervals.

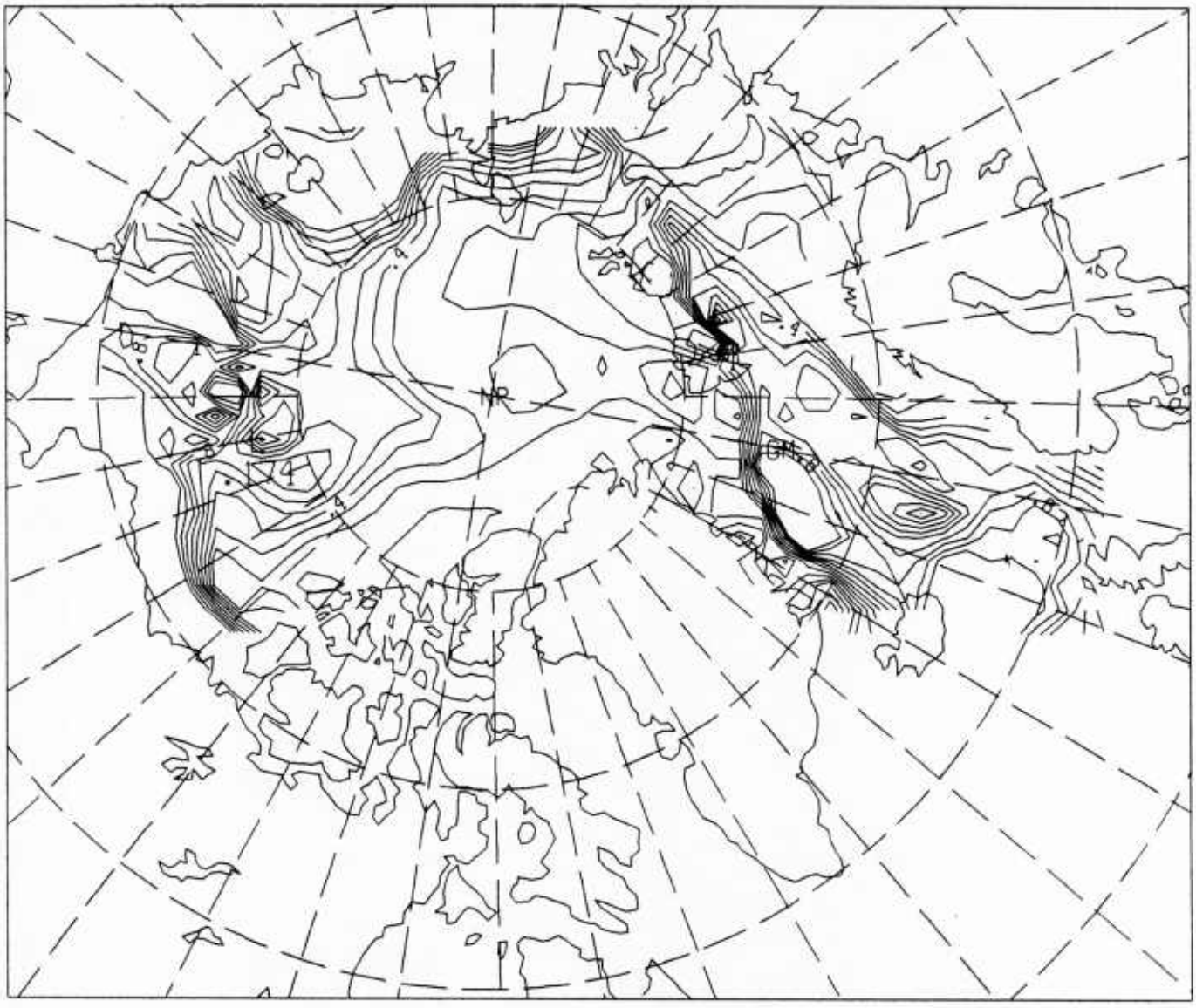

Figure 21e. September mean solutions from the third year of integration of PIPS using both Hibler-Bryan ocean currents and deep oceanic heat fluxes, total growth of ice (thick plus thin without the effects of lateral melt)—contours go from −1 m to 1 m by 0.1 m.

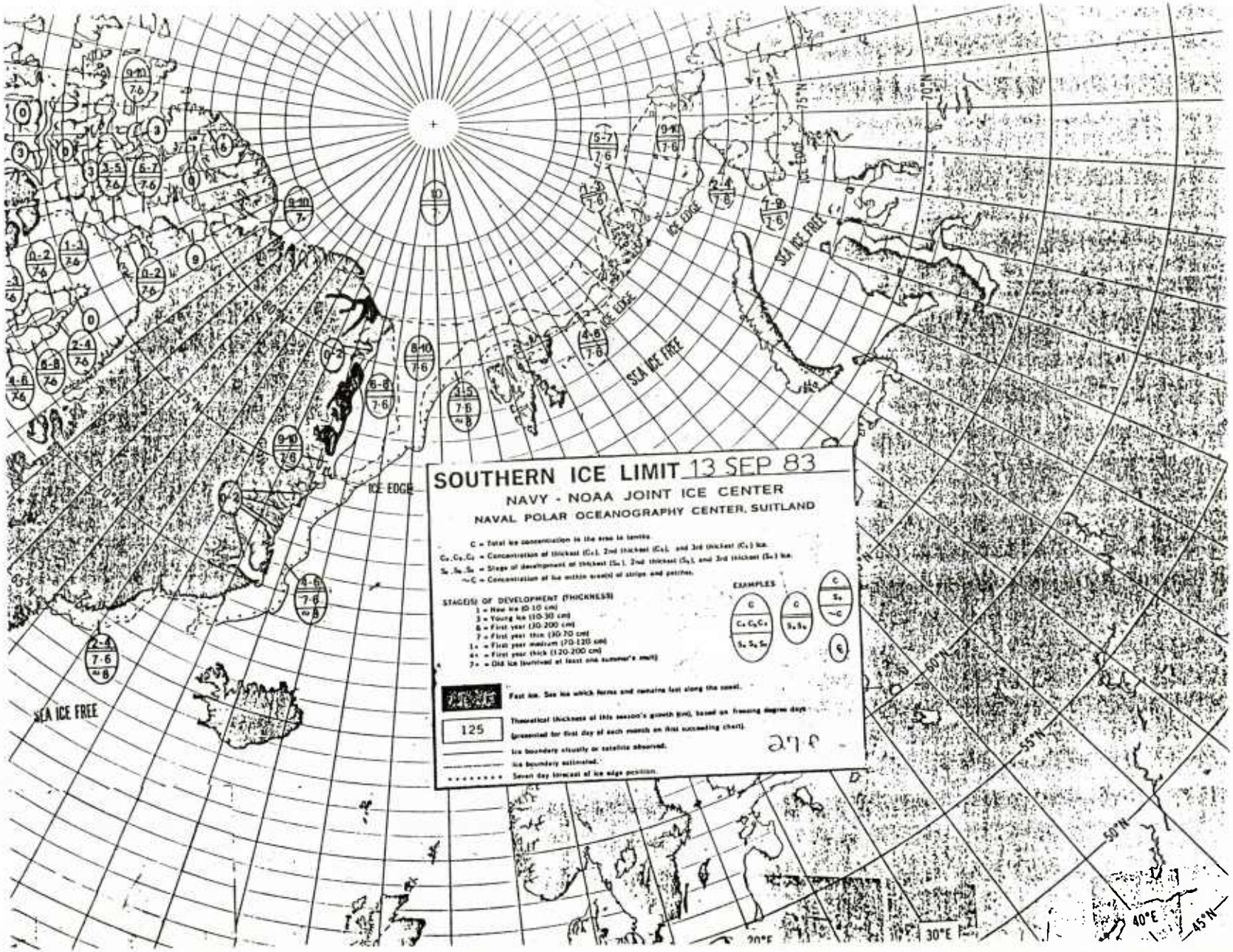

Figure 21f. September mean solutions from the third year of integration of PIPS using both Hibler-Bryan ocean currents and deep oceanic heat fluxes, NPOC southern ice edge—east from 9/13/83.

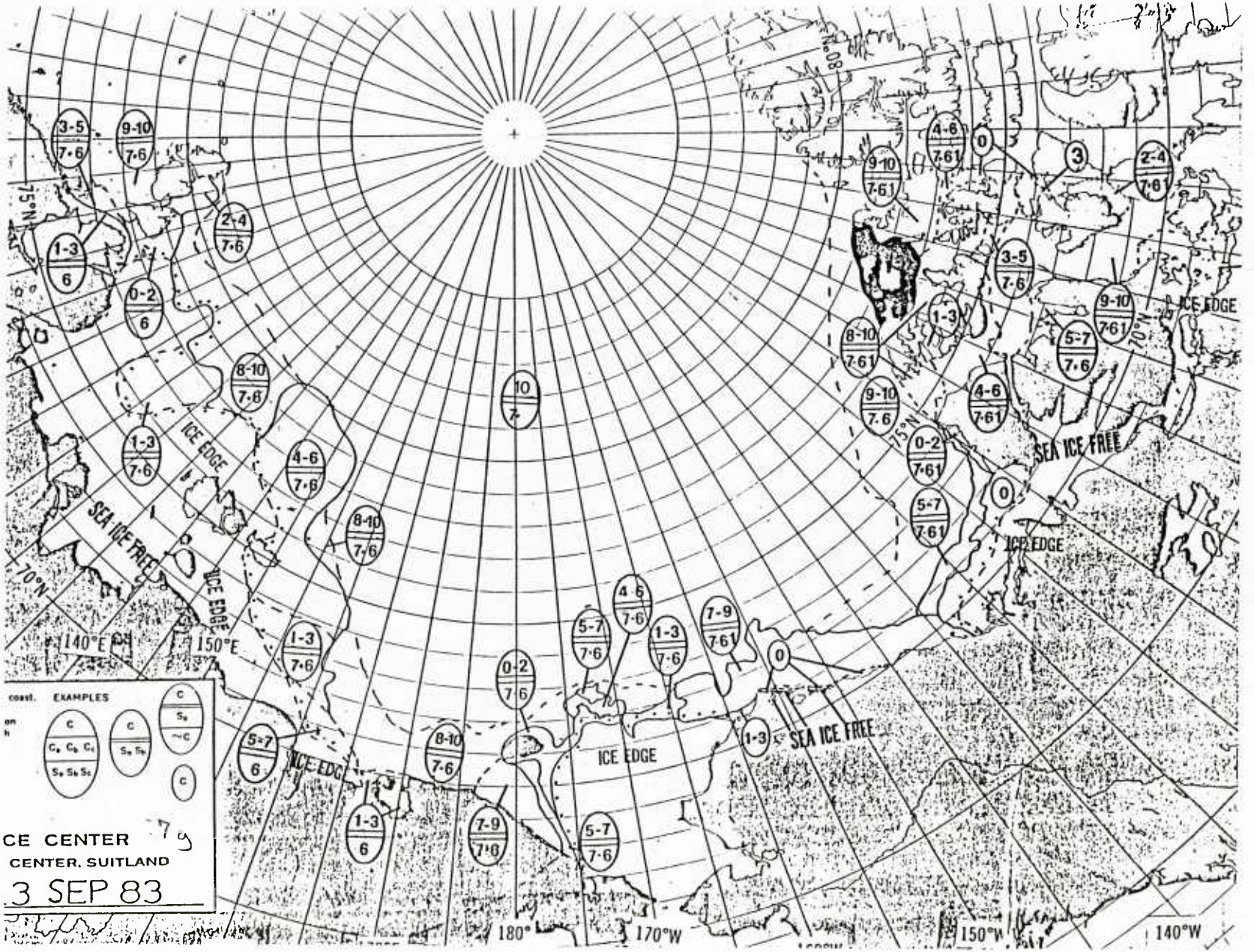

Figure 21g. September mean solutions from the third year of integration of PIPS using both Hibler-Bryan ocean currents and deep oceanic heat fluxes, NPOC southern ice edge—west from 9/13/83.

ICE THICKNESS

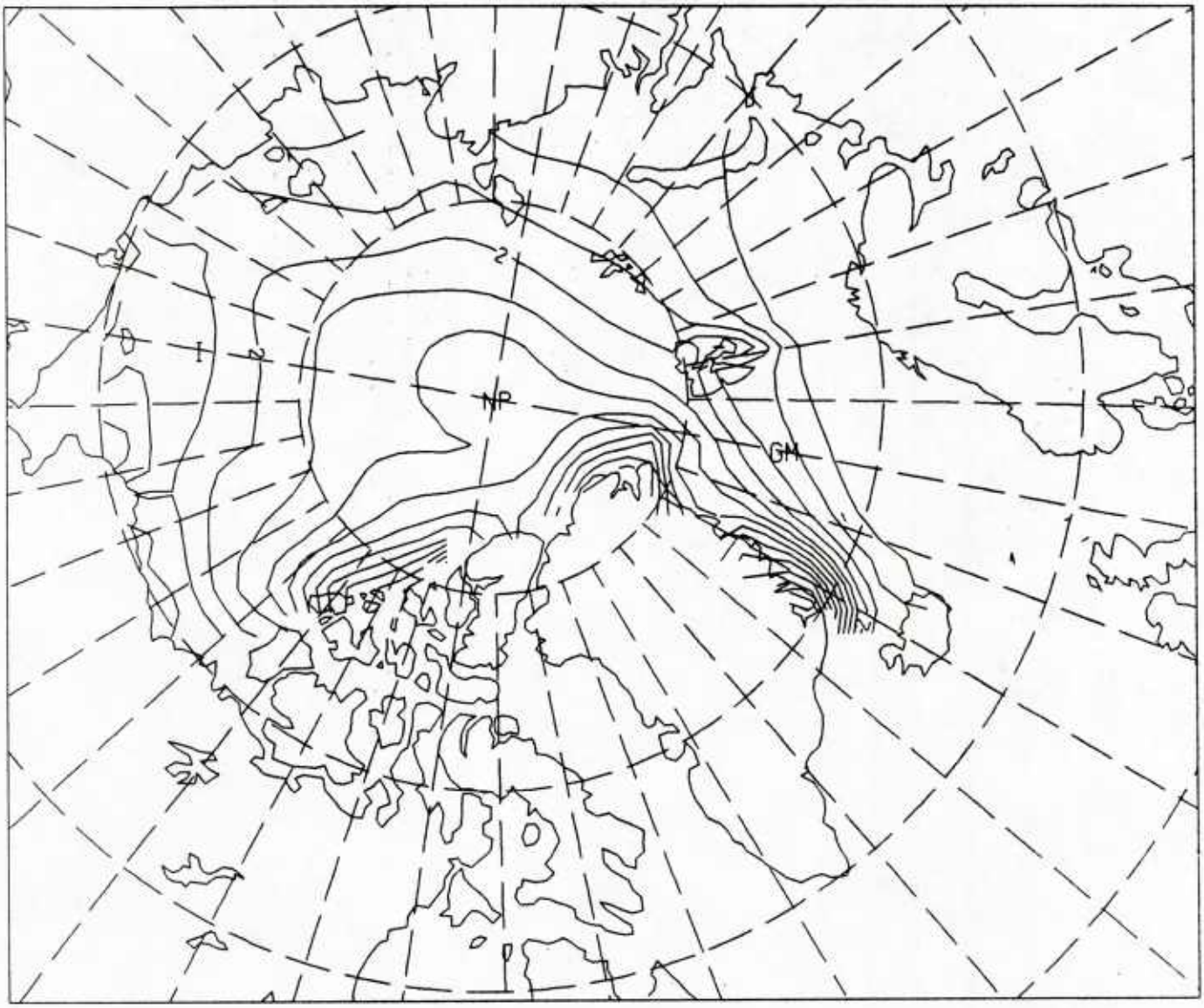

Figure 22. Annual average ice thickness from the third year of an experiment with Hibler-Bryan currents but a constant deep oceanic heat flux – contours go from 0-10 m by 0.5 m intervals.

ICE THICKNESS

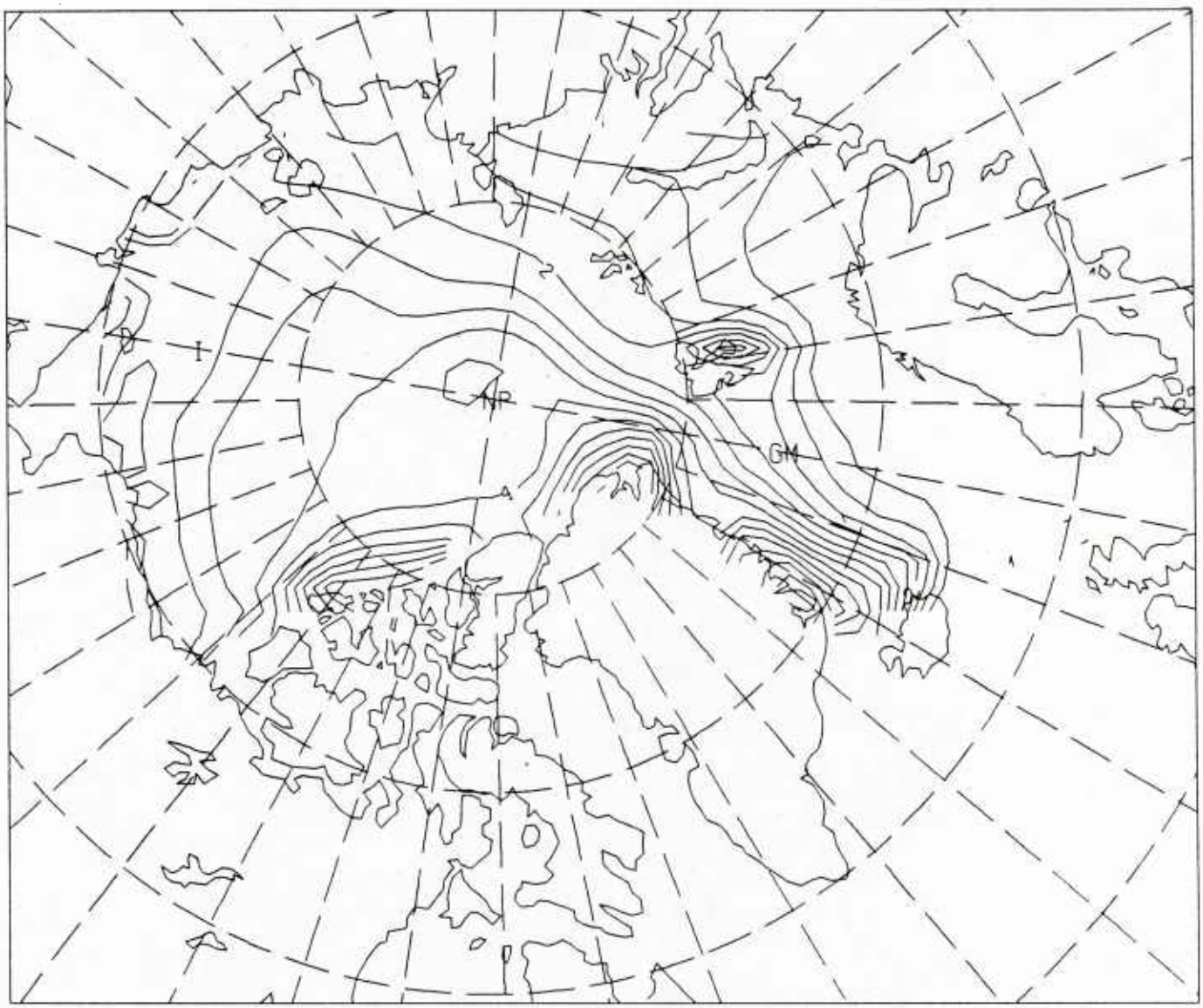

Figure 23. March monthly mean ice thickness from the third year of an experiment with Hibler-Bryan currents but a constant deep oceanic heat flux—contours go from 0·10 m by 0.5 m intervals.

ICE THICKNESS

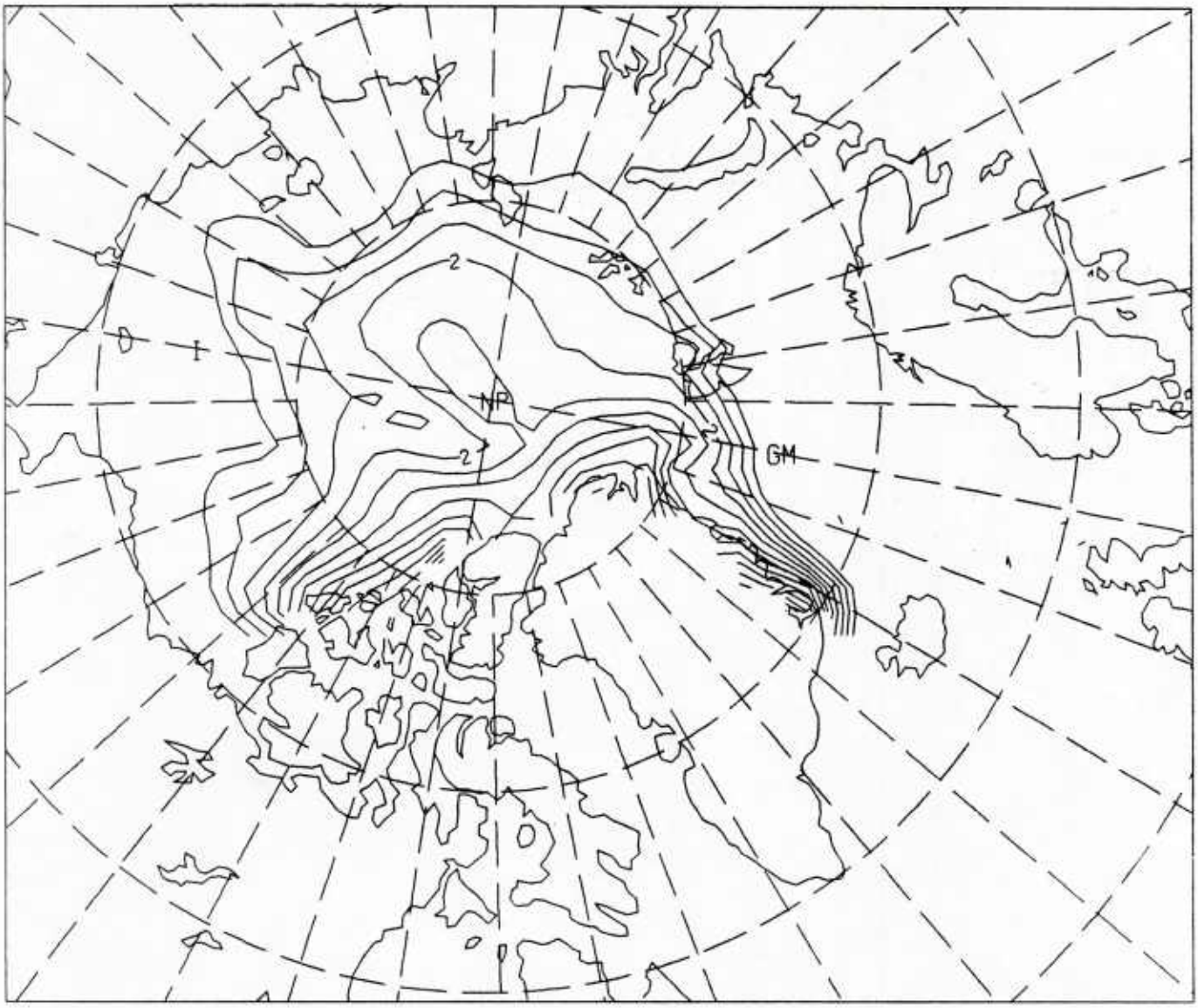

Figure 24. September monthly mean ice thickness from the third year of an experiment with Hibler-Bryan currents but a constant deep oceanic heat flux—contours go from 0·10 m by 0.5 m intervals.

Distribution List

Department of the Navy
Asst Secretary of the Navy
(Research Engineering & System)
Washington DC 20350

Department of the Navy
Chief of Naval Operations
ATTN: OP-951
Washington DC 20350

Department of the Navy
Chief of Naval Operations
ATTN: OP-952
Washington DC 20350

Department of the Navy
Chief of Naval Operations
ATTN: OP-987
Washington DC 20350

Department of the Navy
Chief of Naval Material
Washington DC 20360

Commander
Naval Air Development Center
Warminster PA 18974

Commander
Naval Air Systems Command
Headquarters
Washington DC 20361

Commanding Officer
Naval Coastal Systems Center
Panama City FL 32407

Commander
Naval Electronic Systems Com
Headquarters
Washington DC 20360

Commanding Officer
Naval Environmental Prediction
Research Facility
Monterey CA 93940

Commander
Naval Facilities Eng Command
Headquarters
200 Stovall Street
Alexandria VA 22332

Commanding Officer
Naval Ocean R & D Activity
ATTN: Codes 100/105/110/111/112/113
115/125L/125P/200/300
NSTL MS 39529

Commanding Officer
Naval Research Laboratory
Washington DC 20375

Commander
Naval Oceanography Command
NSTL MS 39529

Commanding Officer
Fleet Numerical Ocean Cen
Monterey CA 93940

Commanding Officer
Naval Oceanographic Office
NSTL MS 39522

Commander
Naval Ocean Systems Center
San Diego CA 92152

Commanding Officer
ONR Branch Office LONDON
Box 39
FPO New York 09510

Officer in Charge
Office of Naval Research
Detachment, Pasadena
1030 E. Green Street
Pasadena CA 91106

Commander
Naval Sea System Command
Headquarters
Washington DC 20362

Commander
DWTaylor Naval Ship R&D Cen
Bethesda MD 20084

Commander
Naval Surface Weapons Center
Dahlgren VA 22448

Commanding Officer
Naval Underwater Systems Center
ATTN: NEW LONDON LAB
Newport RI 02841

Superintendent
Naval Postgraduate School
Monterey CA 93940

Project Manager
ASW Systems Project (PM-4)
Department of the Navy
Washington DC 20360

Department of the Navy
Deputy Chief of Naval Material
for Laboratories
Rm 866 Crystal Plaza Five
Washington DC 20360

Officer in Charge
Naval Underwater Sys Cen Det
New London Laboratory
New London CT 06320

Defense Technical Info Cen
Cameron Station
Alexandria VA 22314

Director
Chief of Naval Research
ONR Code 420
NSTL MS 39529

Director, Liaison Office
Naval Ocean R & D Activity
800 N. Quincy Street
Ballston Tower #1
Arlington VA 22217

Department of the Navy
Office of Naval Research
ATTN: Code 102
800 N. Quincy Street
Arlington VA 22217

Director
Woods Hole Oceanographic Inst
86-96 Water St.
Woods Hole MA 02543

Director
University of California
Scripps Institute of Oceanography
P. O. Box 6049
San Diego CA 92106

Working Collection
Texas A & M University
Department of Oceanography
College Station TX 77843

Wayne Worsely
McDonald-Douglass Corp.
5301 Boloa Avenue
Huntington Beach CA 92647

P. Vidmar
Applied Research Laboratories
University of Texas
Austin TX 78712